Development of Thermodynamic Cycles for Sodium-Cooled-Fast Reactors

by

Alexey Dragunov

A Thesis Submitted in Partial Fulfillment
of the Requirements for the Degree of

Master of Applied Science

in

Nuclear Engineering

The Faculty of Energy Systems and Nuclear Science

University of Ontario Institute of Technology

December, 2013

© Alexey Dragunov, 2013

CONTENTS

LIST OF TABLES

LIST OF FIGURES

ABSTRACT

Currently, one engineering challenge is designing Generation IV (GEN-IV) Nuclear Power Plants (NPPs) with significantly higher thermal efficiencies compared to current NPPs, and to match, or at least to be close to, the thermal efficiencies reached by fossil-fired power plants, which are currently at the level of 40-62%.

As there are six GEN-IV nuclear-reactor concepts and the performance of these reactors-concepts depends on their design, it is reasonable to start with all GEN-IV reactor concepts and investigate the coolants and their characteristics in these concepts. For this objective, main thermophysical, corrosion, and neutronic properties of coolants of the GEN-IV reactors within the proposed temperature range of operation were investigated. Heat Transfer Coefficients (HTCs) for the coolants of the GEN-IV concepts were also calculated and compared to typical HTCs published in the open literature for coolant candidates.

Based on a comparison of properties and HTCs, a Sodium-cooled Fast Reactor (SFR) - one of the six concepts considered under the Generation IV International Forum (GIF), was selected because it is the most experienced reactor technology among all of the proposed GEN-IV reactor concepts. Moreover, with depleting uranium resources, there is an interest to design reactors that operate on a closed fuel cycle, and SFR is one of the potential options. A BN-600 reactor is a sodium-cooled fast-breeder reactor built at the Beloyarsk NPP in Russia, and it is in operation since 1980. On the secondary side it utilizes a subcritical-pressure Rankine-steam cycle with heat regeneration. The power-conversion system is presented, and calculations of thermal efficiency of this scheme have been performed and analyzed.

To achieve higher thermal efficiency of the plant, one of the possibilities is to increase thermal efficiency of the turbine cycle. Two main approaches for the SFR in terms of the power-conversion cycle were investigated: supercritical-pressure Rankine-“steam” cycle and supercritical-pressure CO_2 Brayton-gas-turbine cycle. The feasibility of these options is discussed. The thermal efficiencies of ideal and non-ideal CO_2 Brayton gas-turbine cycles were optimized by varying CO_2 pressures and

temperatures at the outlet of Na-CO_2 heat exchanger.

ACKNOWLEDGEMENTS

There are several people I would like to acknowledge for the attention and help they gave me during the preparation of my thesis.

First of all, I would like to acknowledge my supervisor Dr. Igor Pioro for providing me with a unique opportunity to work in this research area, for his ideas, cooperation and support through my graduate studies. I benefited from his advice; his positive outlook and confidence always inspired me during my research. I would like to sincerely thank Dr. Pioro for everything he has done for me during my graduate studies.

I would like to acknowledge the work and thank for the contributions of Eugene Saltanov, for his help, advices and encouragement during my studies at UOIT.

I would like to express my warm gratitude to my wife Ksenia for her continued support, patience and encouragement.

I would like to express my deepest thankfulness to my mom Irina and all of my family members who have supported me through my graduate studies.

For reviewing and editing a portion of the thesis that was used in referred papers, I gratefully thank Dr. Brian Ikeda, Dr. Glenn Harvel and Dr. Rachid Machrafi.

Also, financial support from the NSERC Discovery Grant, MRI International Strategic Opportunities Program, FedDev Grant on Small Modular Reactors and the Ontario Research Fund on Clean Hydrogen Production is gratefully acknowledged.

DEFINITIONS

Below are the definitions of special terms, and expressions used in the thesis.

Critical point (also called a *critical state*) is a point in which the distinction between the liquid and gas (or vapour) phases disappears, i.e., both phases have the same temperature, pressure and density. The *critical point* is, therefore, characterized by these phase state which have unique values for each pure substance.

Pseudocritical point is a point at a pressure above the critical pressure and at a temperature above the critical temperature that corresponds to the maximum value of the specific heat for this particular pressure.

Supercritical fluid is a fluid at pressures and temperatures that are higher than the critical pressure and critical temperature.

Superheated steam is steam at pressures below the critical pressure, but at temperatures above the critical temperature.

Critical temperature of a substance is the temperature at and above which vapor of the substance cannot be liquefied, no matter how much pressure is applied.

Critical pressure of a substance is the pressure required to liquefy a gas at its critical temperature.

NOMENCLATURE

A	area, m^2
a	ratio of power removed to required circulation power
c_p	specific heat at constant pressure, J/kg K
D	diameter, mm
G	mass flux, $kg/m^2 \cdot s$
$H,(h)$	specific enthalpy, J/kg
htc	heat-transfer coefficient, $W/m^2 \cdot K$
k	thermal conductivity, W/m·K
$\dot{m}$	mass-flow rate, kg/s
P	pressure, MPa
P	perimeter, m
q	heat added (to the cycle), kJ/kg
q''	heat flux, kW/m^2
$\dot{Q}$	power or heat-transfer rate, W
s	specific entropy, kJ/kg·K
T	temperature, °C
W	circulation power, W
x	steam extraction

Greek letters

α	relative consumption of steam
Δ	difference

ρ	density, kg/m^3
μ	dynamic viscosity, Pa·s
η	theoretical efficiency

Non-dimensional Numbers

Nu	Nusselt number $\left(\frac{htc \cdot D_{hy}}{k}\right)$
$\overline{\mathbf{Pr}}$	Average Prandtl number $\left(\frac{\mu}{k} \cdot \frac{h_w - h_b}{T_w - T_b}\right)$
Pr	Prandtl number $\left(\frac{\mu \cdot c_p}{k}\right)$
Re	Reynolds number $\left(\frac{4\dot{m}}{\mu\pi D_{hy}} = \frac{G \cdot D_{hy}}{\mu}\right)$

Subscripts

add	(heat) addition
b	bulk-fluid
c	condenser (Rankine cycle diagrams)
c	compressor (Brayton cycle diagrams)
comp	compressor (Brayton cycle calculations)
cr	critical
el	electrical
fl	flow
fw	feedwater
hy	hydraulic

max	maximal
in	inlet
s	surface
sat	saturation (temperature)
se	steam extraction
th	thermal
w	wall
wet	wetted (perimeter)

Abbreviations and Acronyms

ABWR	Advanced Boiling Water Reactor
AECL	Atomic Energy of Canada Limited
AGR	Advanced Gas-cooled Reactor
AES	Atomic Electrical Station (Nuclear Power Plant in Russian)
Ave	Average
BN	Fast Neutrons (in Russian abbreviation)
BWR	Boiling Water Reactor
CANDU	CANada Deuterium Uranium reactor
CP	Circulation Pump
Cyl	Cylinder
DOE	Department Of Energy (USA)
EGP	Energy Heterogeneous Loop reactor (in Russian abbreviation)
GCHP	Gas Cooler of High Pressure
GCLP	Gas Cooler of Low Pressure
GCR	Gas-Cooled Reactor

GEN-IV	Generation IV
GFR	Gas-cooled Fast Reactor
GIF	Generation IV International Forum
GT	Gas Turbine
H	Heater
HDI	Human Development Index
HP	High Pressure
HPH	High Pressure Heater
HPT	High Pressure Turbine
HTC	Heat Transfer Coefficient
HX	Heat Exchanger
ID	Internal Diameter
IHX	Intermediate Heat exchanger
IP	Intermediate Pressure
IPT	Intermediate Pressure Turbine
LBE	Lead-Bismuth Eutectic
LFR	Lead-cooled Fast Reactor
LGR	Light-water Graphite-moderated Reactor
LMFBR	Liquid-Metal Fast-Breeder Reactor
LMZ	Russian manufacturer of power turbines for electric power stations
LNG	Liquefied Natural Gas
LP	Low Pressure
LPH	Low Pressure Heater
LPT	Low Pressure Turbine
LWR	Light Water Reactors

MSR	Molten Salt Reactor
NPP	Nuclear Power Plant
NRC	National Regulatory Commission (USA)
OD	Outside Diameter
PCh	Pressure Channel
PHWR	Pressurized Heavy Water Reactor
PT	Pressure Tube
PV	Pressure Vessel
PP	Power Plant
PWR	Pressurized Water Reactor
RPV	Reactor Pressure Vessel
RBMK	Reactor of Large Capacity Channel type (in Russian abbreviations)
SC	SuperCritical
SCC	Stress Corrosion Cracking
SCP	SuperCritical-pressure
SCW	Supercritical Water
SCWR	SuperCritical-Water-cooled Reactor
SG	Steam Generator
SFR	Sodium-cooled Fast Reactor
TDr	Turbine Drive
ThPP	Thermal Power Plant
T-S	Temperature – Entropy
U	Uranium
UK	United Kingdom
USA	United States of America

VHTR	Very-High-Temperature Reactor
VVER	Water-cooled Water-moderated Power Reactor (in Russian abbreviations)

CHAPTER 1. INTRODUCTION

Most of the current nuclear power reactors operate on thermal neutrons. This leads to a decrease of the resources of ^{235}U on the Earth. It is well known that uranium resources are limited - the world's present estimated resources of uranium, used only in conventional reactors, are enough to last for approximately 80 years (World Nuclear Association, 2012). Eventually, Generation III and III+ conventional reactor designs, which are all more efficient than their precursors, will stay as the major source of nuclear power over the next decades. Therefore, there is need to compare the designs, specifics and efficiencies of the current Generation II, III and III+ reactors and thermal power plants.

However, in the near future (beyond 2030-2040), Generation IV (GEN-IV) reactors are going to take over the place and show an advanced step forward in the development of reactor technology, once implemented. Most of the GEN-IV reactor designs are fast-neutron reactors; they can utilize the ^{238}U, which has a natural abundance of 99.27%. Also, there are 1.2 million tonnes of depleted uranium left after uranium enrichment around the world (World Nuclear Association, 2013), which also might be used as fuel for fast-neutron reactors. Reactors are called “breeder reactors” if they convert non-fissile ^{238}U to fissile ^{239}Pu or ^{241}Pu; this allows an increase of utilization of uranium resources by 50 times. This unique option among all mineral resources offers some sort of “insurance” against a shortage of resources in future.

It is reasonable to start with all GEN-IV reactor concepts and investigate coolants of all the reactor designs. For this purpose, there is need to perform an analysis of the main thermophysical, corrosion, and neutronic properties of coolants of the GEN-IV reactors within the proposed temperature range of operation. This objective also includes calculations of Heat Transfer Coefficients (HTCs) of the GEN-IV coolant candidates and comparison of these HTCs with the typical HTCs published in the open literature.

A comparison of all the coolants of the GEN-IV nuclear power reactors in Chapter 3 shows that a Sodium-cooled Fast Reactor (SFR) is the only GEN-IV nuclear power reactor which has a well-proven technology (more than 40 years of operating

experience with sodium as a coolant in power generation in Russia and Japan). Liquid sodium has been used in numerous experimental reactors, in a number of power reactors, and is currently being used in BN-600 reactor in Russia. Its predecessor, BN-350 first produced electricity in 1973; it was an SFR located at the Aktau Nuclear Power Plant (NPP) in Kazakhstan (see Figure 1.1). Sodium as a coolant was also used in the Monju reactor in Japan (Figure 1.2).

Figure 1.1 Reactor hall of the BN-350 reactor (Wikimedia Commons, 2012a)

SFRs are already included in the long-term energy plans in countries such as Russia and India. Moreover, development of more advanced SFR technology is proposed by the Russian nuclear agency "Rosatom" – a BN-800 reactor is currently being built at the Beloyarsk NPP site. Also, the BN-1200 reactor project is currently in its last stage of the design. The SFR concept is also on the priority list for the US DOE (Generation IV reactor concepts, DOE).

For the BN-600 SFR, relatively high outlet temperatures of sodium coolant allow achieving high power-conversion side temperatures of ~505°C. Due to this, it is necessary to investigate different power conversion cycles for modern nuclear and fossil-fired power plants (PPs), determine inlet parameters of steam going to the

turbine, reheat steam pressure and temperature in each turbine cycle and compare them to SFR.

Figure 1.2 View of the Monju NPP in Japan (Wikimedia Commons, 2012b).

At this moment only one type of transformation of thermal energy to mechanical is realized in the BN-600 and Monju SFRs – a heat exchanger (steam generator) operating on a subcritical Rankine steam cycle. As parameters of steam in the current SFRs are subcritical, to improve the efficiency of the cycle the possibility of utilizing SuperCritical (SC) Rankine-"steam"-cycle should be considered. The SC Rankine "steam" cycle has been utilized for more than 50 years in thermal power plants around the world and can be "connected" to an SFR. Recent investigations on SC Rankine "steam" cycles were performed by Lizon-A-Lugrin et al. (2012) and Naidin et al. (2009) but they applicable for the outlet temperatures of a Supercritical Water-Cooled Reactor (SCWR), not for the outlet temperature of the secondary sodium in the SFR, which is lower than that of water in SCWR.

It is well known that utilizing sodium as a coolant requires very complex technologies. A number of research and power reactors have been shut down due to fires on site – this happened in the case of the Monju reactor in Japan in 1995 when, after a non-radioactive secondary sodium leak, sodium contacted with oxygen in air

and caused a major fire. As a result, the reactor was shut down. Therefore, to improve safety and avoid possible reaction of sodium with air and water, other option in terms of the power-conversion should be investigated. It is well known that liquid sodium is more compatible with SC CO_2 than with water. Nowadays, the USA and other countries are developing a SC CO_2 Brayton-gas-turbine cycle as a power-conversion cycle for an SFR. Applications of SC CO_2 Brayton-gas-turbine cycles for Gen-IV reactors have been previously investigated by Dostal et al. (2004), Hejzlar et al (2005), and others, but not for SFRs that operate at outlet temperatures of CO_2 of 505°C at the outlet of a Na-CO_2 heat exchanger. This temperature of 505°C is the actual outlet temperature of the fluid in the current power-conversion cycle currently utilized at the BN-600 NPP.

Therefore, it is necessary to investigate different power-conversion cycles applicable to an SFR (such as Subcritical-pressure and SC-pressure Rankine "steam" cycles, and ideal and non-ideal Brayton gas-turbine cycles), calculate their thermal efficiencies, and discuss their advantages and disadvantages.

Therefore, the main objectives of the thesis are:

1. To make a comprehensive literature review and compare the designs, specifics and efficiencies of the current Generation II, III and III+ reactors and thermal power plants.

2. To perform an analysis of the main thermophysical, corrosion, and neutronic properties of coolants of the GEN-IV reactors within the proposed temperature range of operation. This objective also includes calculations of Heat Transfer Coefficients (HTCs) for the GEN-IV coolant candidates and comparison of these HTCs with the typical HTCs published in the open literature.

3. To investigate different power conversion cycles for modern nuclear and fossil-fired power plants (PPs), determine inlet parameters of steam going to the turbine, reheat steam pressure and temperature in each turbine cycle and compare them to SFR.

4. To investigate different power-conversion cycles applicable to an SFR (such as Subcritical-pressure and SC-pressure Rankine "steam" cycles, ideal and non-ideal

Brayton gas-turbine cycles), calculate their thermal efficiencies, and discuss their advantages and disadvantages

Chapter 2 of this thesis presents the literature review of current energy generation sources in the world with an emphasis on NPPs. Review and analysis of thermophysical, corrosion and nuclear properties of coolants of GEN-IV reactors with calculations of HTCs of the reactors coolants are presented in Chapter 3. Chapter 4 is devoted to an analysis of current Generation III and III+ nuclear power reactors and their power-conversion cycles with corresponding temperature – entropy (T-S) diagrams. Analysis of the secondary side of the actual BN-600 SFR and proposed SC Rankine "steam" and SC CO_2 Brayton-gas-turbine cycles for SFR with calculated thermal efficiencies are presented in Chapter 5. Conclusions are summarized in Chapter 6. Ideas for future work are presented in Chapter 7.

CHAPTER 2. CURRENT STATUS OF ELECTRICITY GENERATION IN THE WORLD

2.1 INTRODUCTION

Today, electrical-power production is a key factor for the development of any industry. Level of living also depends on the power generation, it is clearly seen from the Table 2.1 that a high electrical-energy consumption per capita in developed countries correlates with a high Human Development Index (HDI) achieved by the individual country (Pioro, 2012).

It is well known that electrical power (see Figure 2.1a) can be produced by:

- non-renewable-energy sources such as coal, natural gas, oil, and nuclear; and
- renewable-energy sources such as hydro, wind, solar, biomass, geothermal and marine (tidal power and wave energy).

While principally, the main sources for power generation are as follows (Figure 2.1):

1. thermal - primary coal and secondary natural gas;
2. “large” hydro;
3. nuclear.

As seen from Figure 2.1c,e, the rest of the energy sources might have a noticeable impact just in some countries. Besides, a renewable-energy source such as wind (Figure 2.2) requires special conditions, such as a minimum wind speed to generate electricity, and maximum wind speed to avoid damage to the turbine blades. Solar generation depends on various factors including location, time of year or day, and light levels (Figure 2.3). Also, relative costs of electricity generated by these and some other renewable-energy sources, except large hydro-electric power-generating plants, can be much higher than the cost of electricity generated by non-renewable sources. Due to this, wind, solar and some other renewable-energy sources aren’t

reliable or applicable for industrial-power generation.

Table 2.1 Electrical energy consumption per capita in some countries (Wikipedia, 2013: http://en.wikipedia.org/wiki/List_of_countries_by_Human_Development_Index; and http://en.wikipedia.org/wiki/List_of_countries_by_electricity_consumption; Pioro, 2012).

No.	Country	Population, millions	Energy consumption		Year	HDI* (2012)	
			TW h/year	W/Capita		Rank	Value
1	Norway	5	116	2,603	2013	1	0.955
2	Australia	23	225	1,114	2013	2	0.938
3	USA	316	3,886	1,402	2012	3	0.937
5	Germany	80	607	822	2009	5	0.920
6	New Zealand	4.5	38	976	2013	6	0.919
10	Japan	127	860	774	2012	10	0.912
11	Canada	33	550	1,871	2011	11	0.911
12	S. Korea	50	455	1,038	2012	12	0.909
20	France	65	461	804	2012	20	0.893
27	United Kingdom	63	345	622	2011	26	0.875
55	Russia	143	1,017	808	2013	55	0.788
79	Ukraine	45	182	461	2012	78	0.740
101	China	1,354	4,693	395	2012	101	0.699
139	India	1,210	959	90	2011	136	0.554

* The HDI is a comparative measure of life expectancy, literacy, education and standards of living for countries worldwide. It is used to distinguish whether the country is a developed, a developing or an under-developed country. It is also used to measure the influence of economics on quality of life. Countries are divided into 4 wide human-development categories, each of which includes about 42 countries: 1) Very high – 42 countries; 2) high – 43; 3) medium – 42; and 4) low – 42.

Table 2.2 lists the 10 top largest power plants of the world by installed capacity, and Table 2.3, the largest power plants of the world by energy source.

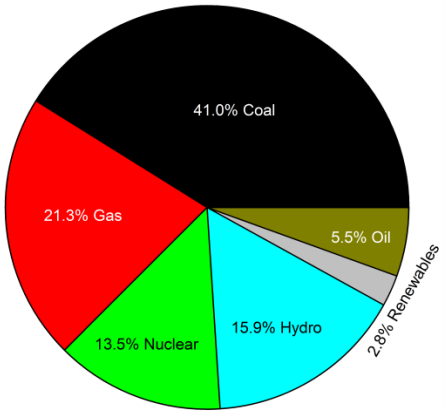

(a) World (2008), in total: 20,183 TWh (based on data from www.environment.nationalgeographic.com)

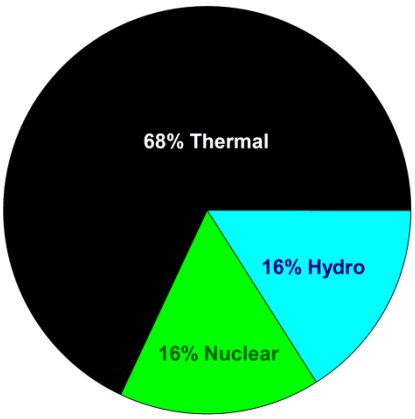

(b) Russia

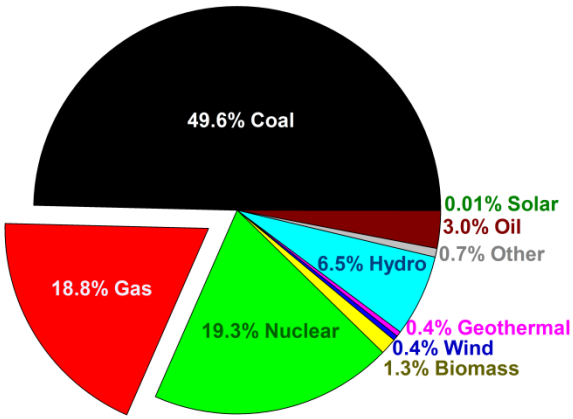

(c) USA

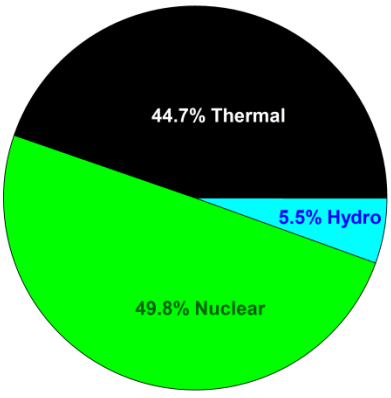

(d) Ukraine

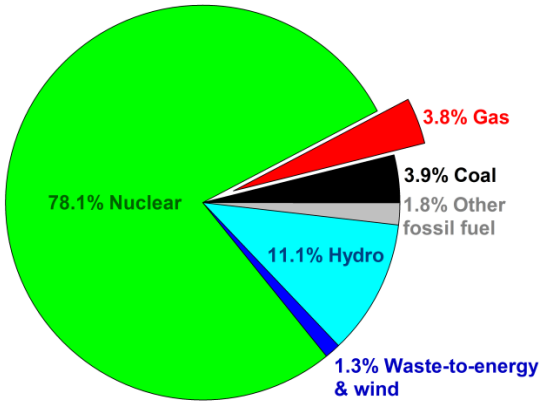

(e) France

Figure 2.1 Electricity generation by energy source in the world and in selected countries (Wikipedia, 2012; Pioro, 2012).

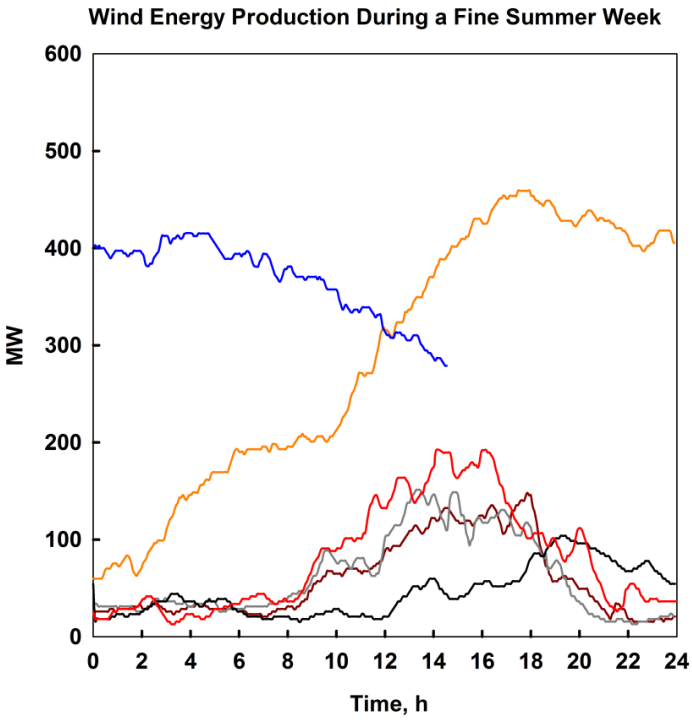

Figure 2.2 Power generated by 650-MW_{el} wind turbines in the Western Part of Denmark (based on data from www.wiki.windpower.org/index.php/variations_in_energy): Shown a summer week (6 days with different colours) of wind-power generation (Pioro, 2012).

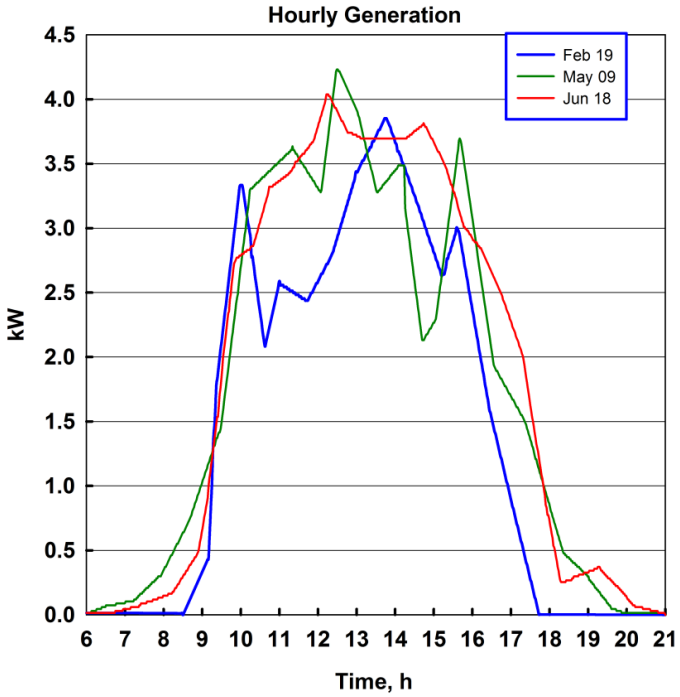

Figure 2.3 Power generated by photovoltaic system in New York State (USA) (based on data from www.burningcutlery.com/solar): Shown three mostly sunny days: February 19th; May 9th and June 18th (Pioro, 2012).

Table 2.2 Ten top power plants of the world by installed capacity (Pioro, 2012).

Rank	Plant	Country	Capacity, MW_{el}	Ave. annual generation, TWh	Plant type
1	Three Gorges Dam	China	21,000[1]	84.5	Hydro
2	Itaipu Dam	Brazil/Paraguay	14,000[2]	94.7	Hydro
3	Guri Dam	Venezuela	10,235	53.4	Hydro
4	Kashiwazaki-Kariwa NPP	Japan	8,212[3]	24.6	Nuclear
5	Tucurui Dam	Brazil	8,125[4]	21.4	Hydro
6	Bruce NPP	Canada	7,276[5]	35.3	Nuclear
7	Grand Coulee Dam	United States	6,809	21.0	Hydro
8	Longtan Dam	China	6,426	-	Hydro
9	Uljin NPP	South Korea	6,157	48.0	Nuclear
10	Krasnoyarsk Dam	Russia	6,000	20.4	Hydro
10	Zaporizhzhia NPP	Ukraine	6,000	40.0	Nuclear

[1] – another 1,500 MW under construction;

[2] – the maximum number of generating units allowed to operate simultaneously cannot exceed 18 (12,600 MW);

[3] – 4,912 MW are operational, 3 units (3,300 MW) have not been restarted since the 2007 Chūetsu offshore earthquake;

[4] – another 245 MW under construction;

[5] – currently, the largest fully operating NPP in the world.

It should be noted that two parameters are essential characteristics of any power plant:

1. Overall (gross) or net efficiency of a plant. Gross efficiency of a unit during a given period of time is the ratio of the gross electrical energy generated by the unit to the energy consumed during the same time by the same unit. The difference between gross and net efficiencies is internal needs for electrical energy of a power plant;

2. Capacity factor of a plant - the net capacity factor of a power plant is the ratio of the actual output of a power plant over a period of time and its potential

output in the case it operates at full declared capacity for the entire time. In order to calculate the capacity factor, take the total amount of energy a power plant generated over a period of time and divide it by the amount of energy the plant would have produced if operated at full capacity. Capacity factors can vary significantly depending on the type of a plant.

Some power-plant efficiencies will be discussed in the next sections for thermal and nuclear power plants. Average capacity factors of various power plants are listed in Table 2.4.

Table 2.3 Largest power plants of the world (based on installed capacity) by energy source (Pioro, 2012).

Rank	Plant	Country	Capacity, MW_{el}	Plant type
1	Three Gorges Dam Power Plant	China	21,000	Hydro
2	Kashiwazaki-Kariwa NPP	Japan	8,210	Nuclear
3	Taichung Power Plant	Taiwan	5,780	Coal
4	Surgut-2 Power Plant	Russia	5,600	Fuel oil
5	Futtsu Power Plant	Japan	5,040	Natural gas
6	Eesti Power Plant	Estonia	1,615	Oil shale
7	Shatura Power Plant	Russia	1,020	Peat
7	Alta Wind Energy Center	United States	1,020	Wind
9	Hellisheiði Power Plant	Iceland	303	Geothermal
10	Alholmens Kraft Power Plant	Finland	265	Biofuel
11	Sihwa Lake Tidal Power Plant	South Korea	254	Tidal
12	Charanka Solar Park	India	214	Solar
13	Vasavi Basin Bridge Diesel Power Plant	India	200	Diesel
14	Aguçadoura Wave Farm	Portugal	2	Marine (wave)

In the Province of Ontario, Canada, various energy sources generate electricity in a grid (see Figure 2.4): (a) shows installed capacity and (b) - electricity generation by the energy source. Figure 2.5 shows the power generated by different energy sources

and their capacities as of June, 2012. Figure 2.4a shows that in Ontario the significant installed capacities are nuclear (31%), gas/oil (mainly natural gas) (24%), coal (17%), hydro (21%) and renewables (7%), and in Figure 2.4b, electricity is principally generated by nuclear (55%), hydro (25%), gas/oil (mainly natural gas) (10%), coal (7%) and renewables (3%)(Pioro, 2012).

Table 2.4 Typical average capacity factors of various power plants (Pioro, 2012).

No.	Power plant type	Location	Year	Capacity factor, %
1	Nuclear	USA	2010	91
		UK	2011	66
2	Combined-cycle	UK	2011 2007-2011	48 62
3	Coal-fired	UK	2011	42
4	Hydroelectric	UK	2011	39
		World (average)	-	44
		World (range)	-	10-99
5	Wind	UK	2011	30
		World	2008	20-40
6	Wave	Portugal	-	20
7	Concentrated-solar thermal	USA California	-	21
8	Photovoltaic solar	USA Arizona	2008	19
		USA Massachusetts	-	12-15
		UK	2011 2007-2011	5.5 8.3

Figure 2.5 shows the power generated by various energy sources in the Province of Ontario, Canada, on June 19, 2012 (hot summer day, when many air-conditioning systems were needed) and Figure 2.6 shows corresponding capacity factors of these energy sources. The analysis of Fig. 2.5 shows that electricity from midnight until 3 A.M. that day was mainly generated by nuclear, hydro, gas, wind, "other" and coal. After 3 A.M., wind power began to decrease due to external factors, but electricity

consumption began to rise. “Fast-response” gas-fired power plants and later on, hydro

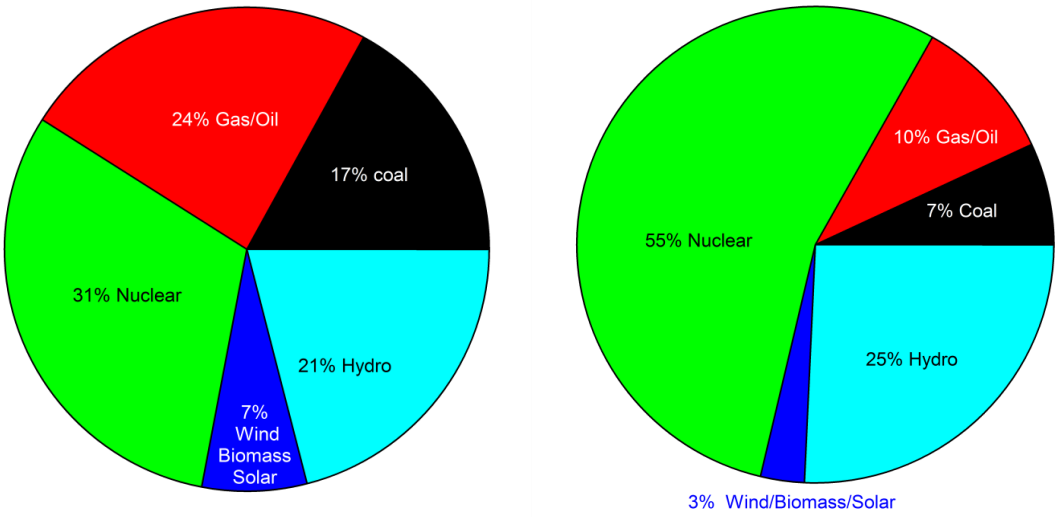

(a) Installed capacity by energy source

(b) Electricity generation by energy source

Figure 2.4 Installed capacity (a) and electricity generation (b) by energy source in the Province of Ontario in Canada in 2010 (Pioro, 2012 (based on data from Yatchew and Baziliauskas, 2011)).

and coal-fired power plants plus “other” power plants began to increase electricity generation to compensate for the decreasing wind power and the increasing demand for electricity. After 6 P.M. energy consumption in the province dropped slightly, and at the same time, wind power began to increase by external factors. Gas-fired, hydro and “other” power plants decreased energy generation accordingly (“other” plants dropped power quite abruptly), but their role in the total energy generation was very small. After 10 P.M. energy consumption began to drop even more, and coal-fired power plants, as the most “dirty” plants, abruptly decreased electricity generation followed by gas-fired and hydro plants.

This example shows that if the grid has NPPs and/or renewable-energy sources the grid must include “fast-response” power plants such as gas- and coal-fired and/or large hydro power plants.

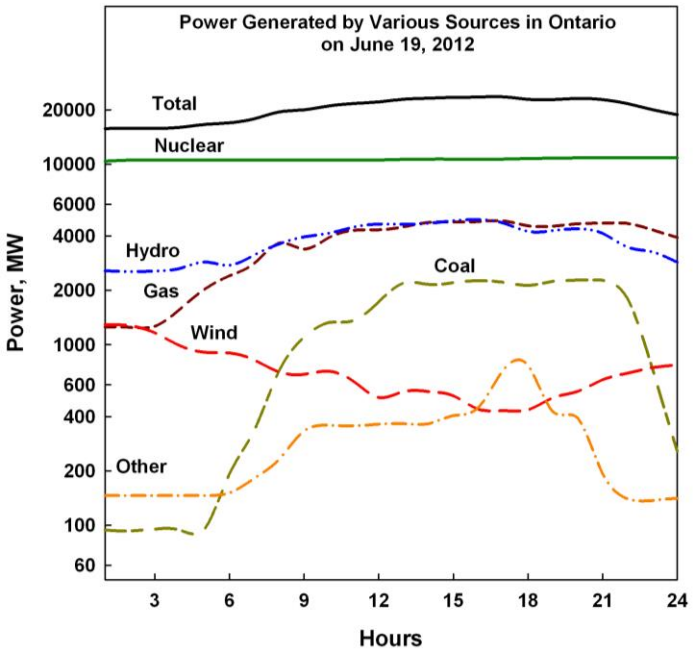

Figure 2.5 Power generated by various energy sources in the Province of Ontario, Canada, on June 19, 2012 (plotted based on the data from http://ieso.ca/imoweb/marketdata/genEnergy.asp).

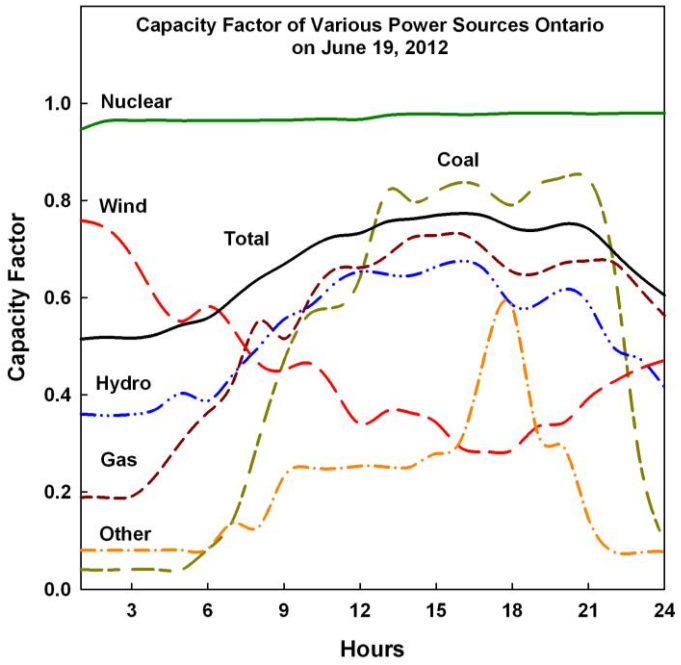

Figure 2.6 Capacity factors of various energy sources in the Province of Ontario, Canada, on June 19, 2012 (plotted based on the data from http://ieso.ca/imoweb/marketdata/genEnergy.asp).

2.2 CURRENT STATUS OF ELECTRICITY GENERATION AT THERMAL POWER PLANTS

All thermal power plants utilize one of the following five types of power-conversion cycles (Pioro, 2012; Cengel and Boles, 2011):

- Rankine steam-turbine cycle (the most utilized in various power plants);
- Brayton gas-turbine cycle (the second most utilized in power industry);
- combined cycle, which is a combination of Brayton and Rankine cycles in one power plant;
- Diesel internal-combustion-engine cycle which is used in Diesel generators;
- Otto internal-combustion-engine cycle.

In general, the term "thermal power plants" includes the following types of power-plants:

1. solid-fuel-fired power plants based on Rankine steam-turbine cycle with fuels such as coal, lignite, peat, oil-shale and others;
2. gas-fired power plants;
3. geothermal power plants;
4. biofuel thermal power plants;
5. Diesel- and Otto-cycle-generators power plants;
6. concentrated-solar thermal power plants; and
7. recovered-energy generation thermal power plants.

The primary driving force for all advances in thermal power plants is to improve thermal efficiency of the plant (Cengel and Boles, 2011). Ranges of thermal efficiencies of modern thermal power plants are listed in Table 2.5.

Table 2.5 Typical ranges of gross thermal efficiencies of modern thermal power plants (Pioro, 2012).

No.	Type of power plant	Gross efficiency, %
1	Combined-cycle power plant (Brayton gas-turbine cycle (utilized fuel is natural or Liquefied Natural Gas (LNG); combustion-products parameters at the gas-turbine inlet: $T_{in} \approx 1650$°C) and Rankine steam-turbine cycle (steam parameters at the turbine inlet: $T_{in} \approx 620$°C (T_{cr} = 374°C)).	Up to 62
2	Supercritical-pressure (SCP) coal-fired ThPP (new plants) (Rankine-cycle steam inlet turbine parameters: $P_{in} \approx 25 – 38$ MPa (P_{cr} = 22.064 MPa), $T_{in} \approx 540$ - 625°C (T_{cr} = 374°C) and $T_{reheat} \approx 540$ - 625°C).	Up to 55
3	Internal-combustion-engine generators (Diesel cycle and Otto cycle with natural gas utilized as a fuel).	Up to 50
4	Subcritical-pressure coal-fired thermal power plant (older plants) (Rankine-cycle steam: $P_{in} \approx 17$ MPa, $T_{in} \approx$ 540°C (T_{cr} = 374°C) and $T_{reheat} \approx 540$°C).	Up to 40
5	Concentrated-solar thermal power plants with heliostats, a solar receiver (heat exchanger) on a tower and molten-salt heat-storage system: molten salt maximum temperature is about 565°C; Rankine steam-turbine power cycle utilized.	Up to 20

2.2.1 Coal-fired thermal power plants

For thousands of years mankind have been using wood and coal for heating purposes. For around one hundred years coal has been used for generating electrical power at coal-fired Thermal Power Plants (ThPPs) worldwide. All coal-fired power plants use the Rankine steam-turbine cycle, which can be organized at two ranges of pressures (Pioro, 2012):

1. Older or smaller-capacity power plants that operate at steam pressures no greater than 16 – 17 MPa;

2. Recent large-capacity power plants that operate at SC pressures from 23.5 MPa and higher.

Supercritical pressures are the pressures above the critical pressure of water – 22.064 MPa. From thermodynamics it is known that higher thermal efficiencies of the plant correspond to the higher temperatures and pressures at the turbine inlet (listed in Table 2.5). Most of the subcritical-pressure power plants have thermal efficiencies in the order of 34 – 40% and recent SC-pressure plants – 45 – 55%. Steam-generator outlet temperatures or steam-turbine inlet temperatures reached the level of 625°C (and even greater) at pressures of about 25 – 30 MPa and more. However, a general range of temperature is about 535 – 585°C at pressures of 23.5 – 25 MPa (Pioro and Duffey, 2007).

Selected data on Genesee Power Plant (Alberta, Canada) is provided below. An EPCOR coal-fired power plant with two units at subcritical pressures and 1 unit at SC pressures (Kindzierski, 2007). The EPCOR coal-fired power plant consists of three power-generating units:

- units G1 and G2 each of 381 MW_{el} net or 410 MW_{el} gross (built in 1989 and 1994 respectively);

- unit G3 is the SC-pressure coal-fired power plant unit which is the only one of its kind in Canada. The power is 450 MW_{el} net or 490 MW_{el} gross, meaning that the internal needs are 40 MW_{el} or 8.2% from gross power.

Below are the operating design parameters of the unit G3:

- normal net annual production is 3,745 GWh;

- the unit annually requires 1.8 million tonnes of coal;

- ash production is about 41 tonnes per hour which is the equivalent of ~360,000 tonnes annually;

- unit G3 utilizes supercritical-boiler technology;
- combustion-chamber temperatures of SC-pressure boiler reaches range of about 1,300-1,400°C; and
- boiler of the unit G3 produces steam at 26 MPa, what is higher than the pressures in units G1 and G2.

Below is some information on recent Hitachi turbines: power of 495 MW, TCDF-40, 3600 rpm, primary steam – 24.1 MPa and temperatures 566°C are of the main "steam" and the reheat steam.

Regardless of advances in coal-fired power-plant designs and operation worldwide, they are still considered to be not environmentally clean as they produce carbon-dioxide emissions as a result of the combustion process, ash, slag and even acid rain (Kruglikov et al., 2009). It should be noted that known resources of coal in the world are greater than that of other fossil fuels such as oil and natural gas.

2.2.2 Combined-cycle thermal power plants

Natural gas is considered to be relatively "clean" fossil fuel compared to coal and oil, but it still emits carbon dioxide due to combustion process when it used for electrical power generation. The most efficient modern ThPPs with thermal efficiencies in the range of 50 – 62%, are combined-cycle power plants (utilize natural gas as a fuel).

Notwithstanding advances in ThPPs design and their operation, they still emit carbon dioxide into the environment, which is currently considered as one of the primary causes for climate changes. In addition, all fossil-fuel resources are being depleted quite quickly. Due to this, a new reliable and environmental friendly source for the power generation should be considered (Pioro, 2012).

2.3 CURRENT STATUS OF ELECTRICITY GENERATION AT NUCLEAR POWER PLANTS

Nuclear power is also a non-renewable-energy source as fossil fuels, but nuclear resources can be used for a significantly longer time than some fossil fuels. Also, it is well known that nuclear power does not emit carbon dioxide into the atmosphere. However, NPPs create radioactive waste, and there is a problem with reprocessing and ultimate safe storage of nuclear waste, which should be resolved. Currently, nuclear power generally is considered as the most viable source of power for electrical-power production for the period of next 50 – 100 years.

The first success of use of nuclear power for electrical production was accomplished in the 1950-s. Nowadays, most of the nuclear-power reactors, which operate around the world, are Generation II and III. Generally, definitions of nuclear-reactor generations (Pioro, 2012) are as follows:

1. Generation I (1950 – 1965) – early prototypes of nuclear-power reactors;
2. Generation II (1965 – 1995) – mostly commercial nuclear-power reactors;
3. Generation III (1995 – 2010) – modern reactors (pressurized-water-cooled NPPs with thermal efficiencies of 30 – 36%; carbon-dioxide-cooled NPPs with thermal efficiencies up to 42% and sodium-cooled NPPs with the thermal efficiencies up to 40%) and Generation III+ which are more recent reactors with improved parameters, which are evolutionary design improvements (water-cooled NPPs with thermal efficiencies up to 38%);
4. Generation IV (2025 – …) – reactors in principle with new parameters – NPPs with thermal efficiencies of about 43 – 50% and higher. Several classifications of NPPs are listed in a paper by Pioro (2012).

Operating and planned nuclear-power reactors in the world as per April, 2013 listed in Table 2.6. It is seen that the majority of reactors are Pressurized Water Reactors (PWRs), while the least common are Liquid-Metal Fast-Breeder Reactors (LMFBRs). Table 2.7 shows nuclear-power reactors by nation as of April, 2013.

Table 2.6 Operating and forthcoming nuclear-power reactors as of April 2013 (Pioro, 2012; Nuclear News, 2013); (*in Italic mode*) - number of nuclear power reactors before the Japan earthquake and tsunami disaster in 2011 (Nuclear News, 2011).

Type of reactor	Number of current units	Number of forthcoming units
Pressurized Water Reactors	271 (251 GW_{el})	85 (89 GW_{el}).
Boiling Water Reactors (BWRs) or Advanced BWRs (ABWRs)	83 (78 GW_{el});	6 (8 GW_{el})
Pressurized Heavy Water Reactors (PHWRs)	48 (24 GW_{el})	7 (4 GW_{el})
Gas Cooled Reactors (GCRs)	48 (24 GW_{el})	0
Light-water, Graphite-moderated Reactors (LGRs)	15 (10 GW_{el})	0
LMFBR	1 (0.6 GW_{el})	4 (1.5 GW_{el}).

Table 2.7 Current nuclear power reactors by nation as of April 2013 (Pioro, 2012; Nuclear News, 2013); (*in Italic mode*) - number of nuclear power reactors before the Japan earthquake and tsunami disaster in spring of 2011) (Pioro, 2012; Nuclear News, 2011).

No	Nation	Number of units	Net GW_{el}	Changes in number of reactors from 2011
1	USA	103 (104)	103 (103)	Decreased by1 reactor
2	France	58	63	- No changes
3	Japan	50 (54)	44 (47)	Decreased by 4 reactors
4	Russia	33 (32)	24 (23)	Increased by 1 reactor
5	S. Korea	23 (20)	21 (18)	Increased by 3 reactors
6	Canada	19 (22)	13 (15)	Decreased by 3 reactors
7	Ukraine	15	13	No changes
8	Germany	9 (*17*)	12 (*20*)	Decreased by 8 reactors
9	China	15 (13)	12 (10)	Increased by 2 reactors
10	UK	16 (19)	9 (10)	Decreased by 3 reactors

From Table 2.7 it is seen that number of current reactors in Germany and Japan decreased by 8 and 4 units respectively over the period of 2 years. In the Table 2.8 some selected Generation III+ reactors with deployment of 5 to 10 years are listed. It shows how many Generation III+ reactors are planned to be built.

Table 2.8 Selected Generation III+ reactors with the deployment in 5–10 years (Pioro, 2012).

Reactors	Design, Deployment
ABWR	Toshiba, Mitsubishi Heavy Industries and Hitachi-GE, Japan-USA - the only one Generation III+ reactor design already implemented in the power industry
Advanced CANDU Reactor (ACR-1000)	AECL, Canada
Advanced Plant (AP-1000)	Toshiba-Westinghouse, Japan-USA; 6 under construction in China, 6 planned to be built in China and 6 – in the USA
Advanced PWR (APR-1400)	South Korea - 4 under construction in S. Korea and 4 planned to be constructed in United Arab Emirates
European Pressurized-water Reactor (EPR)	AREVA, France - 1 should be put into operation in Finland, 1 under construction in France and 2 - in China, and 2 planned to be built in USA
ESBWR (Economic Simplified Boiling Water Reactor)	GE-Hitachi, USA-Japan
VVER (designs:Atomic Electrical Station (AES) - 2006 or VVER-1200 with ~1200 MW_{el})	GIDROPRESS, Russia- 2 under construction in Russia and several more planned to be built in various countries

In Table 2.9 some reference parameters for the Russian Generation III+ Water-cooled Water-moderated Power Reactor (in Russian abbreviation – VVER) NPP are listed (Ryzhov et al., 2010). The declared thermal efficiency of the Generation III+ VVER NPP is 36%. The expected NPP service life is 50 years, while the expected main

equipment service life is 60 years.

Table 2.9 Reference parameters of Generation III+ VVER (Ryzhov et al., 2010).

Parameter	Value
Thermal power, MW_{th}	3200
Electric power, MW_{el}	1160
Thermal efficiency of a NPP, %	36
Coolant pressure, MPa	16.2
Steam-generator steam pressure, MPa	7.0
Coolant temperature at reactor inlet, ^{o}C	298
Coolant temperature at reactor outlet, ^{o}C	329
Service life of an NPP, years	50
Main equipment service life, years	60
Replaced equipment service life, years	≥30
Capacity factor, %	up to 90
Equipment availability factor	99
Length of fuel cycle, years	4 - 5
Frequency of re-fuelling, months	12 - 18
Fuel assembly maximum burn-up, MW day/kgU	up to 60 - 70
Inter-repair period length, years	4 – 8
Annual average length of scheduled shut-downs (for re-fuelling, scheduled maintenance work), days/year	16 - 40
Refueling length, days per year	≤16
Number of unscheduled reactor shutdowns/year	≤1
Frequency of severe core damage, 1/year	$<10^{-6}$
Frequency of limiting emergency release, 1/year	$<10^{-7}$
Efficient time of passive safety and emergency control system operation without operator's action and power supply, hour	≥24
Compliance with EUR requirements, yes/no	Yes

The basic features of a typical Russian VVER NPP (ROSENERGOATOM, 2004) are:

- uranium-dioxide (UO_2) fuel;

- fuel enrichment about 4%;
- indirect cycle with a steam generator (also, a pressurizer required), double flow circuit (double loop);
- Reactor Pressure Vessel (RPV) with vertical fuel rods, assembled in bundle strings and cooled with upward flow of light water;
- reactor coolant and moderator are the same fluid;
- reactor coolant outlet parameters: Pressure 15 – 16 MPa (T_{sat} = 342 – 347°C) and temperatures inlet / outlet 290 – 325°C; and
- power-conversion cycle is subcritical-pressure regenerative Rankine steam cycle with implemented steam reheat (working fluid is light water, turbine steam inlet parameters: saturation pressure 6 – 7 MPa and saturation temperature 276 – 286°C).

On Figure 2.7 a schematic of a typical BWR NPP is shown. Some specifics of BWR reactors are:

- enriched UO_2 fuel (about 3%);
- direct cycle with steam separator (steam generator and pressurizer are eliminated), single-flow circuit (single loop);
- RPV with vertical fuel rods (elements) assembled in bundle strings cooled with upward flow of light water (water and water-steam mixture);
- reactor coolant, moderator and power-cycle working fluid are the same fluid;
- reactor coolant outlet parameters: pressure about 7 MPa and saturation temperature at this pressure is about 286°C; and
- power cycle is subcritical-pressure regenerative Rankine steam-turbine cycle with steam reheat.

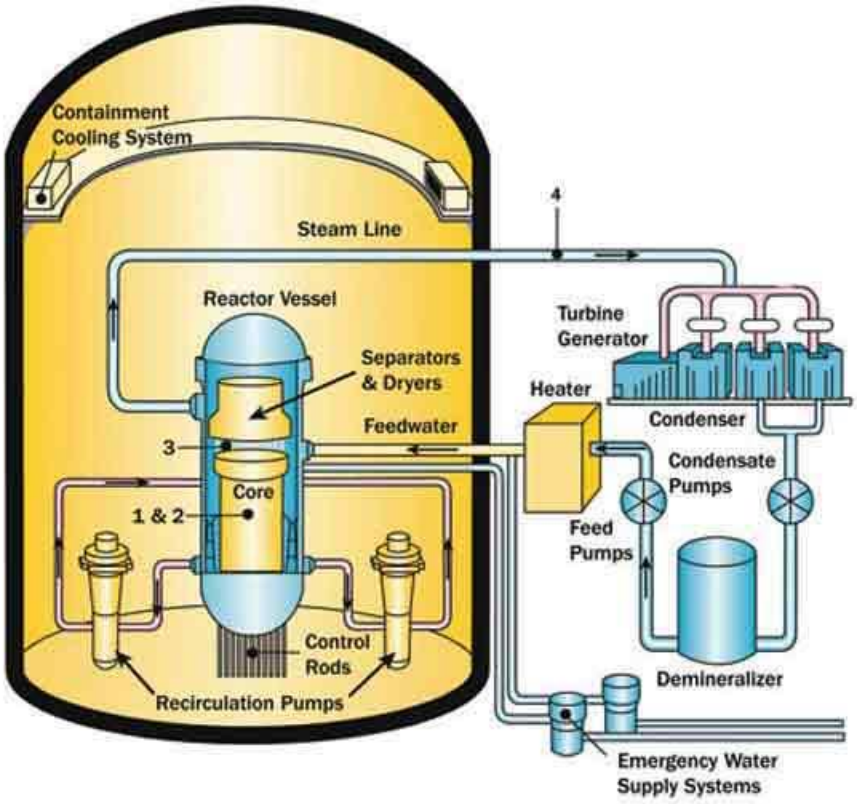

Figure 2.7 Scheme of a typical BWR NPP (Pioro, 2012; courtesy of National Regulatory Commission (NRC), USA).

A schematic of a CANDU-6 PHWR NPP (courtesy of AECL) is presented in Figure 2.8. General specifics of the reactor are:

- natural UO_2 fuel (fuel enrichment is about 0.7%);
- indirect cycle with steam generator, double-flow circuit (double loop);
- pressure-channel design: calandria vessel with horizontal fuel channels;
- reactor coolant and moderator separated, but both are heavy water;
- reactor coolant outlet parameters: pressure about 9.9 MPa and temperature close to saturation (310°C);

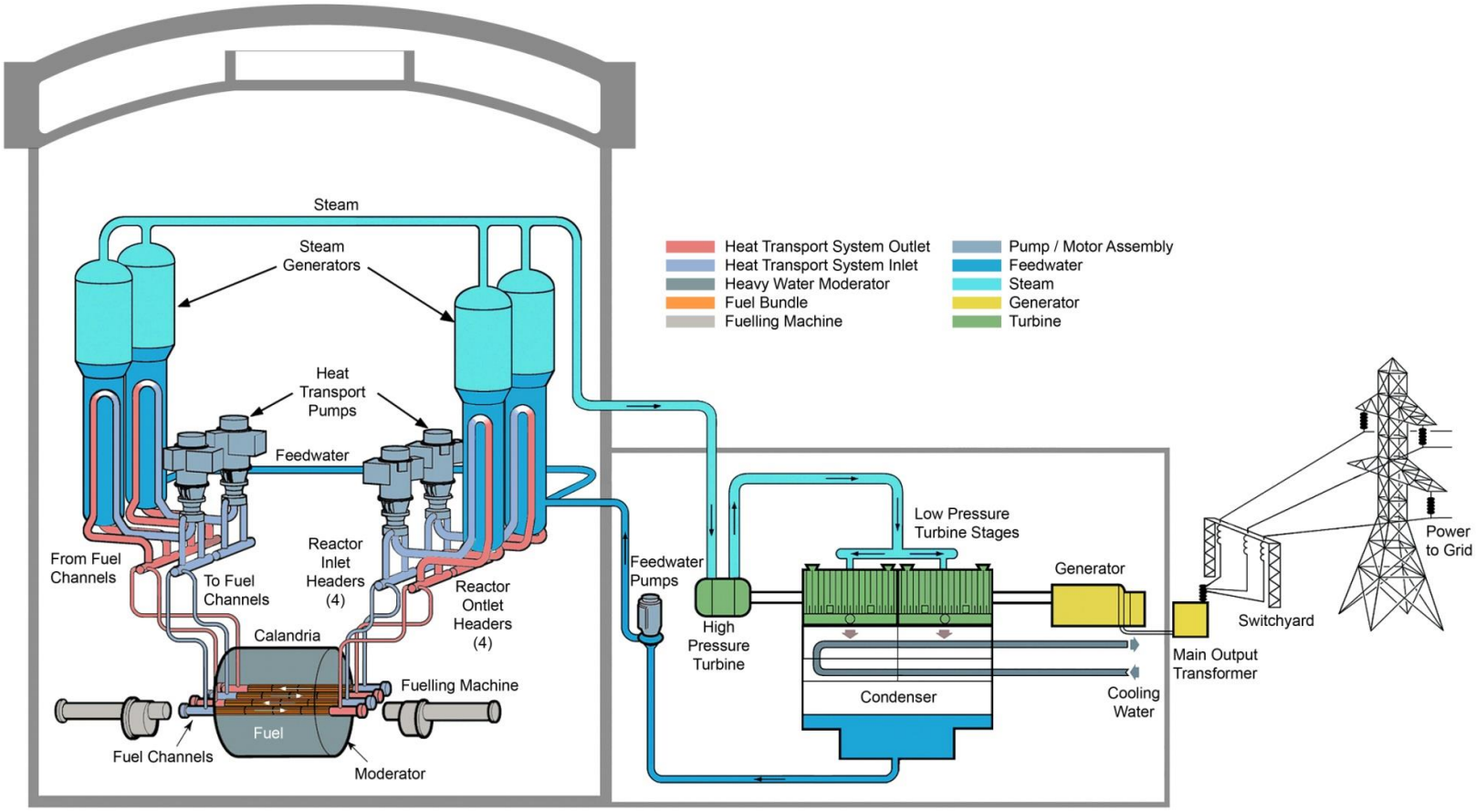

Figure 2.8. Scheme of CANDU-6 reactor NPP (Pioro, 2012; courtesy of AECL).

- reactor moderator temperature is about 70°C;
- possibility of on-line refuelling; and
- power cycle is a subcritical-pressure regenerative Rankine steam-turbine cycle with steam reheat (working fluid - light water, turbine steam inlet parameters: saturation pressure of about 4.6 MPa and saturation temperature of 259°C).

The major features of Russian RBMK-1000 (Reactor of Large Capacity Channel type) LGR NPP (courtesy of ROSENERGOATOM, 2004) are:

- enriched UO_2 fuel (enrichment is about 2%);
- direct cycle with steam separator (steam generator and pressurizer are eliminated), single-flow circuit (single loop);
- pressure-channel design (vertical fuel channels);
- light-water reactor coolant and graphite moderator;
- reactor coolant outlet parameters: pressure about 6.9 MPa and temperature close to saturation, i.e. ~284°C);
- possibility of on-line re-fuelling; and
- power-conversion cycle is subcritical-pressure regenerative Rankine steam-turbine cycle with steam reheat (working fluid light water, turbine steam inlet parameters: saturation pressure of ~6.6 MPa and saturation temperature of ~280°C).

A Russian BN-600 SFR NPP began operation in 1980 at the Beloyarsk NPP as unit number 3. Isotopes of ^{238}U and ^{232}Th can be used in the fuel cycle. Purity of sodium should be about 99.95% (courtesy of ROSENERGOATOM, 2004).

Major parameters of Russian nuclear power-reactors are presented in Table 2.10.

Table 2.10. Major parameters of Russian nuclear-power reactors (Grigoryev and Zorin, 1989).

Parameter	VVER-440	VVER-1000	EGP*-6	RBMK-1000	BN-600
Thermal power, MW_{th}	1375	3000	62	3200	1470
Electrical power, MW_{el}	440	1000	12	1000	600
Thermal efficiency, %	32.0	33.3	19.3	31.3	40.0
Coolant pressure, MPa	12.3	15.7	6.2	6.9	~0.1
Coolant mass flow rate, t/s	1.3	23.6	0.17	13.3	6.9
Coolant inlet/outlet *T*, °C	270/298	290/322	265	284	380/550
Steam mass flow rate, t/s	0.75	1.6	0.026	1.56	0.18
Steam pressure, MPa	4.3	5.9	6.0	6.6	14.0
Steam temperature, °C	256	276	-	280	505
Reactor core: Diameter/Height, m	3.8/11.8	4.5/10.9	-	11.8/7	2.1/0.75
Fuel enrichment, %	3.6	4.3	3.0-3.6	2.0-2.4	17-33
No. of fuel bundles	349	163	273	1580	369

*EGP - Energy Heterogeneous Loop reactor (in Russian abbreviation)

Major parameters of a typical Boiling Water Reactor (BWR) are also presented in Table 2.11.

Table 2.11. Parameters of a typical US BWR (Shultis and Faw, 2008).

Parameter	Value
Thermal output, MW_{th}	3830
Electrical output, MW_{el}	1330
Thermal efficiency, %	34
Power density, kW/L	56
Average linear heat flux, kW/m	20.7
Fuel-rod heat flux average/max, MW/m^2	0.51/1.12
Length of the core, m	3.76
Outside Diameter (OD) of the core, m	4.8
Coolant pressure, MPa	7.17
Core mass-flow rate, kg/s	14,167
Core void fraction average/max	0.37 / 0.75
Feedwater inlet temperature, °C	216
Steam outlet temperature, °C	290
Steam outlet mass flow rate, kg/s	2083
Inside Diameter (ID) of RPV, m	6.4
Height of RPV, m	22.1
Wall thickness of RPV, m	0.15
Fuel pellets	UO_2
Fuel Pellet OD, mm	10.6
Fuel rod OD, mm	12.5
Zircaloy sheath (cladding) thickness, mm	0.86

The UK CO_2-cooled reactors mainly presented in two designs (Hewitt and Collier, 2000):

1. Older design – Magnox reactor (only one in operation);

2. Newer design – Advanced Gas-cooled Reactor (AGR).

The Magnox design of CO_2-cooled reactors is a natural-uranium graphite-moderated reactor with the parameters listed in Table 2.12.

Table 2.12. Typical parameters of Magnox reactors.

Parameter	Value
Coolant	CO_2
Coolant pressure, MPa	2
Inlet/outlet temperatures, °C	250/414
Core diameter, m	~14
Core height, m	8
Sheath material and type	Magnesium-alloy sheath with fins
Thermal efficiency	~32%

Parameters of AGR reactors are listed in Table 2.13.

Table 2.13. Typical parameters of AGR reactors.

Parameter	Value
Coolant	CO_2
Coolant pressure, MPa	4.1
Inlet/outlet temperatures, °C	292/650
Secondary-loop pressure of water, MPa	17
Secondary-loop temperature of water, °C	560
Fuel enrichment, %	2.3
Sheath material and type	Stainless-steel sheath with ribs and hollow fuel pellets
Thermal efficiency	~42%

It worth mentioning that the thermal efficiency of AGR reactors is about 42%, which is currently the highest thermal efficiency achieved in nuclear-power industry. However, neither Magnox nor AGR designs will be built anymore. They will just continue to operate until the end of their expected life and then they will be shut down. The same applies to Russian EGPs and RBMKs.

From the data provided in Table 2.6 it is seen that:

1. The majority of nuclear-power reactors are water-cooled reactors – 96% of all nuclear power reactors: PWR design – 63%, BWR design – 19%, PHWR (mainly CANDU-type) design – 11% and LGR design – 3%.

2. The majority of water-cooled reactors are pressure-vessel type: PWRs and BWRs – 85%, pressure-channel- or pressure-tube-type reactors: PHWR, RBMK and EGP – 15%.

3. Only reactors built in UK are of the gas-cooled type: Magnox and AGR designs – 3% of all nuclear power reactors,

4. One reactor in Russia utilizes liquid sodium as a coolant.

Installed capacities of nuclear power reactors range from 11 MW_{el} to 1500 MW_{el} (Figure 2.9). It is seen that 30% of all reactors (131 units) have installed capacities in a range of 1000 – 1500 MW_{el}. 24% percent of all power-reactors (106 units) have installed capacities in the range of 900 – 1000 MW_{el}. The largest power reactors are located in France (2 units with up to 1500 MW_{el}), Germany and Sweden (6 units with up to 1400 MW_{el}).

From the data shown in Table 2.8 it is seen that Generation III+ nuclear power reactors often are quite large units with the installed capacity in the range of 1200 – 1400 MW_{el}. An EPR has an installed capacity of 1600 MW_{el}.

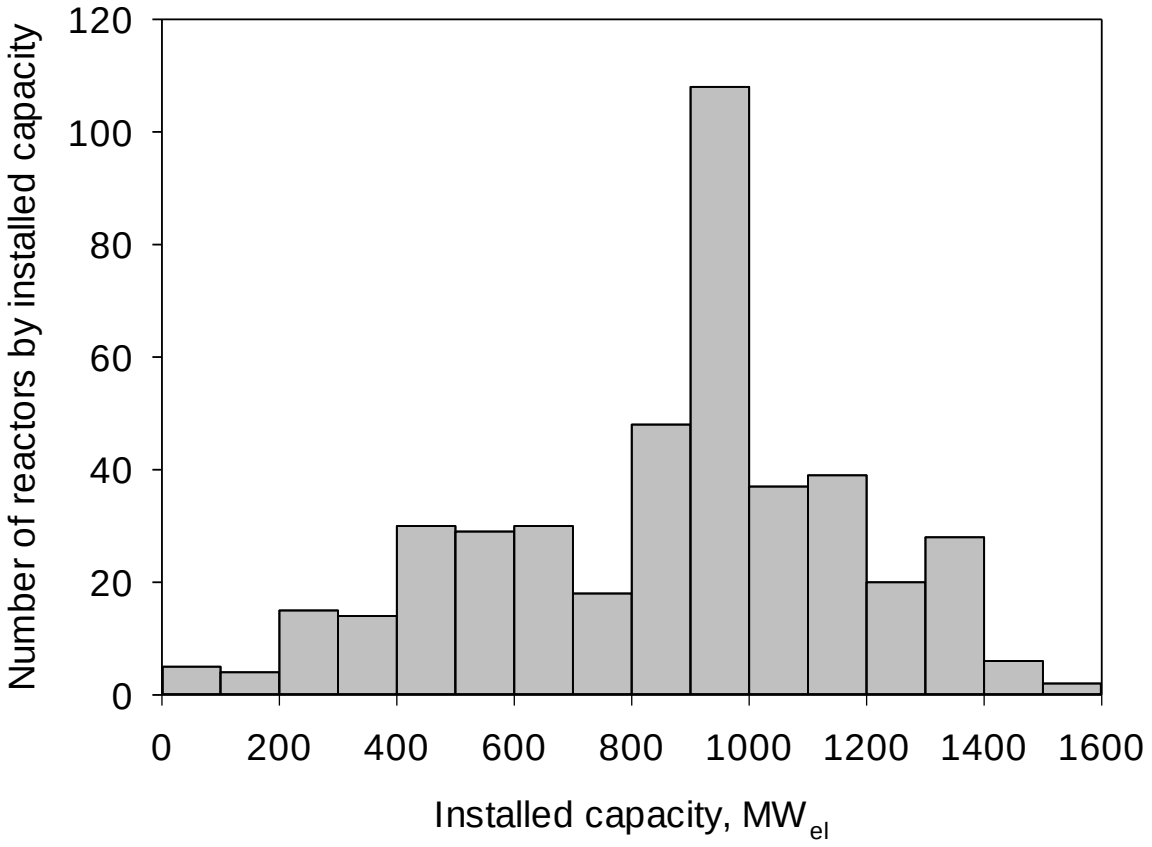

Figure 2.9. Number of nuclear power reactors in the world by installed capacity (based on data in Nuclear News, 2013).

2.4 CONCLUSIONS

Nuclear power is a non-renewable source as are the fossil fuels, with the difference that nuclear resources can be used for a much longer time than some fossil fuels. It should also be mentioned that coal-fired power plants require millions of tons of coal annually. Also, NPPs do not emit CO_2 in large quantities into the atmosphere, but create radioactive waste. Currently, nuclear energy is considered as the most viable source of power for electricity generation for the next 50 – 100 years.

The primary driving force for all advances in thermal and nuclear power plants is thermal efficiency. Ranges of gross thermal efficiencies for modern power plants are:

- combined-cycle thermal power plants – up to 62%;
- supercritical-pressure coal-fired thermal power plants – up to 55%;
- carbon-dioxide-cooled reactor NPPs – up to 42%;
- sodium-cooled fast reactor NPP – up to 40%; and
- modern water-cooled reactors – 30 – 36%.

It can be seen that all current Generation II, III and oncoming Generation III+ NPPs are not very competitive with modern ThPPs in terms of the thermal efficiency. The difference in values of thermal efficiencies between ThPPs and NPPs can be up to 20 – 25%. Hence, new Generation IV of NPPs with thermal efficiencies within a range of 45 – 50% at least to be close to those of modern ThPPs, should be designed and constructed in the nearest future. Also, the problem with reprocessing and ultimate safe storage of nuclear wastes should be resolved.

CHAPTER 3. INVESTIGATION OF THERMOPHYSICAL AND NUCLEAR PROPERTIES OF PROSPECTIVE COOLANTS FOR GENERATION-IV NUCLEAR REACTORS

Recently, a group of countries initiated an international collaboration, the Generation IV International Forum (GIF), to develop the next-generation nuclear reactors (GIF, 2002). The GIF program has narrowed the design options of nuclear reactors to the following six concepts:

- SuperCritical-Water-cooled Reactor (SCWR);
- Sodium-cooled Fast Reactor;
- Lead-cooled Fast Reactor (LFR);
- Molten Salt Reactor (MSR);
- Gas-cooled Fast Reactor (GFR); and
- Very-High-Temperature Reactor (VHTR).

The purpose of this chapter is to compare main thermophysical, corrosion, and neutronic properties of the Generation-IV (GEN-IV) reactors' coolants within the proposed temperature range of operation. This comparison wasn't done before in the open literature for all the coolants and on the one place.

3.1 INTRODUCTION

A group of countries has recently initiated an international collaboration to develop the next-generation nuclear reactors. Research and development of the next-generation nuclear systems is being conducted in the areas of advanced structural materials, coolants, and fuels. The GIF program has selected six GEN-IV reactor concepts. They are discussed below.

The first concept is the SCWR – one of the most promising reactor concepts currently being developed. There is no need for the steam generators and moisture separators used in Light-Water Reactors (LWRs), it allows for reducing dimensions of and decreasing operational cost of the reactor.

The second concept is the SFR. The inlet and outlet temperatures considered for primary-coolant sodium are around 370 and 550°C, respectively. SuperCritical water (SCW) and SC carbon dioxide are considered as the most promising working fluids for power conversion in an SFR.

The LFR is another prospective concept that falls into the class of liquid-metal-cooled reactors. It has a coolant with inlet and outlet coolant temperatures of around 420 and 540°C, respectively, although the mean-core outlet temperature for a large power-plant concept was decreased to 480°C because of corrosion difficulties by lead caused by rapid increasing of temperature (GIF, 2002). The estimated thermal efficiency of the LFR is around 42%.

The MSR has the fuel dissolved in a fluoride-salt coolant. MSRs promise attractive safety features such as large negative-temperature and void-reactivity coefficients.

High outlet temperature of the helium coolant used in the GFR concept makes it possible to achieve high thermal efficiency for the plant. There is no need for an intermediate loop in GFR, because there is no low-pressure exothermally reacting coolant. However, high operational pressures are required (around 9 MPa).

Another example of a helium-cooled reactor is the VHTR. This is a graphite-moderated reactor with an expected core outlet temperatures of up to 1,000°C. Such high temperatures lead to very high thermal efficiency of the plant, which is estimated to be up to 55%. The primary pressure of helium is 7 MPa. Inlet temperature of helium in both VHTR and GFR concepts is proposed to be 490°C.

To investigate the advantages and limitations of GEN-IV nuclear reactors it is important to compare their coolants. The properties of the coolants for the above mentioned reactor concepts will be discussed in the following sections.

3.2 COOLANTS FOR GEN-IV REACTORS

It follows from the discussion in introduction that the following coolants are proposed for the GEN-IV reactor concepts are:

- *supercritical water* in SuperCritical-Water-cooled Reactor;
- *sodium* in a Sodium-cooled Fast Reactor;
- *lead or Lead-Bismuth Eutectic* (LBE) in a Lead-cooled Fast Reactor;
- *fluoride-salt coolant* in a Molten Salt Reactor; and
- *helium* in both Gas-cooled Fast Reactor and Very-High-Temperature Reactor.

SCW is the coolant in the SCWR and has an operating pressure of 25 MPa, and reactor inlet and outlet temperatures of 350°C and 625°C, respectively. Beyond the critical point (22.064 MPa and 373.95°C), water does not undergo a phase change, which is the case for subcritical water.

The second considered coolant is sodium, which is used in the SFR. Sodium is well known because of its high thermal conductivity and low neutron-absorption cross-section. The high boiling point (882.8°C) of sodium allows the reactor to operate at relatively low pressures (less than 1 MPa). It is important to note that melting point of sodium is ~97°C. Sodium reacts chemically with air and water. Therefore, to improve safety, a secondary sodium loop is utilized, which acts as a buffer between the radioactive sodium in the first loop and the water in the third loop.

Lead is proposed to for use in the LFR at low pressures (less than 1 MPa). Lead has a very high melting point (327.5°C) what impacts the reactor operation.

LBE is a eutectic alloy of lead (44.5%) and bismuth (55.5%), and it is being considered as an option for the LFR. One of the main advantages of LBE is its melting point, of 123.5°C, which is relatively low compared to that of lead. Neither lead nor LBE react readily with water or air, in contrast to sodium, which allows for the elimination of the

intermediate-coolant system used in SFRs. Moreover, LBE is not a new technology – it has been proven by years of reliable service as a coolant in nuclear-power submarines operated in the Soviet Union since 1970's. The chemical properties of LBE are similar to those of its constituents (Gerasimov and Monachov, 1982).

The helium coolant at high outlet temperatures of 850°C and 1,000°C (in the GFR and VHTR respectively) makes it possible to achieve very high thermal efficiencies of the plant. Helium has less neutron absorption and moderation than some other coolants. Helium has some requirements, such as sheath surface roughening and high operational pressure.

It is reasonable to compare the GEN-IV coolants with current Generation III reactor-system coolants used in the most efficient reactor system (AGR, efficiency up to 42%, coolant – CO_2 under pressure of 4 MPa) and the most common reactor system worldwide (PWR, coolant – water with pressure of 15.5 MPa, T_{in}/T_{out} – 292°C/329°C). Therefore, for comparison purposes in this chapter subcritical water and subcritical CO_2, utilized in PWRs and AGRs respectively, also will be considered.

Carbon dioxide in the subcritical state is currently being used in the most efficient nuclear reactors – AGRs. CO_2 is not a strong absorber of thermal neutrons and does not become extremely radioactive. Other advantages of CO_2 are its chemical stability in the range of expected operating temperatures (292 – 650°C) and the fact that it does not react with either the moderator or fuel (Lamarsh and Baratta, 2001).

In the next section a comparison of the main thermophysical properties for all the coolants mentioned above will be conducted. The range of investigated temperatures covers the operating temperature ranges of the corresponding reactor concepts. Basic averaged parameters of each of the proposed reactor concepts are listed in Table 3.1.

Table 3.1. Basic averaged parameters of selected current Generation III and Generation IV nuclear power reactors (Dragunov et al. 2013a).

Reactor	Neutron spectrum	Core design		Reactor coolant	Moderator	Reactor cycle	No of circuits	*P*	*T*
								MPa	°C
PWR	Thermal	Heterogeneous	PV	Water		Indirect	2	15.5	292 – 329
AGR	Thermal	Heterogeneous	PV*	CO_2	Graphite	Indirect	2	4	292 – 650
SFR	Fast	Heterogeneous	PV	Sodium	–	Indirect	3	~0.1	370 – 550
GFR	Fast	Heterogeneous	PV	Helium	–	Direct	1	9	490 – 850
						Indirect	2		
VHTR	Thermal	Heterogeneous	PV	Helium	Graphite	Direct	2	7	490 – 1000
						Indirect			
LFR	Fast	Heterogeneous	PV	Lead/ or Lead-Bismuth	–	Indirect	2	~0.1	550 – 800 (420 – 540)
MSR	Epithermal	Homogeneous	PV	Sodium fluoride with dissolve uranium	Graphite	Indirect	3	~0.1	T_{out} = 700 – 800
MSFR	Fast	Homogeneous	PV	Sodium fluoride with dissolve uranium	–	Indirect	3	~0.1	T_{out} = 700 – 800
SCWR	Thermal	Heterogeneous	PV	Water	Water	Direct	1	25	300 – 625
			PCh (PT)		Heavy water	Indirect	2		
	Fast		PV	Water	–	Direct	1		300 – 625
			PCh (PT)			Indirect	2		

* Though coolant flows through individual channels inside graphite moderator, the actual pressure boundary is the vessel surrounding the moderator.

3.3 THERMOPHYSICAL PROPERTIES OF PROPOSED GEN-IV REACTOR COOLANTS

In this section, a comparison of the main thermophysical properties of coolants of the investigated GEN-IV reactor systems is made. It is important to note that the properties investigated are presented for a wide range of temperatures (from 250°C to 1,000°C), which covers the range of operating temperatures for GEN-IV reactors. Properties of supercritical and subcritical water, carbon dioxide, and helium-4 were obtained from NIST REFPROP software (2010). Properties of sodium were taken from Kirillov et al. (2007). Other properties were calculated using either original correlations presented in Handbook on Lead-bismuth Eutectic Alloy and Lead Properties (2007) or using correlations recommended by the authors of this book.

Before comparing properties of the coolants, it is reasonable to discuss the desired characteristics of the coolant. Nuclear reactors have certain specific requirements for the coolants, such as:

- high specific heat, thermal conductivity and low viscosity;
- low corrosive and low erosive effects on all the reactor materials;
- high boiling point and low melting point;
- resistance to high temperatures and radiation;
- low neutron absorption cross-section;
- explosion-proof, non-combustible, non-toxic;
- widely available; and
- weak activation.

Pressure – Temperature diagram for PWR, AGR and proposed GEN-IV reactor concepts

is shown in Figure 3.1. It can be seen that the highest coolant pressure is for the SCWR, while the lowest is for the liquid-metal-cooled nuclear reactors.

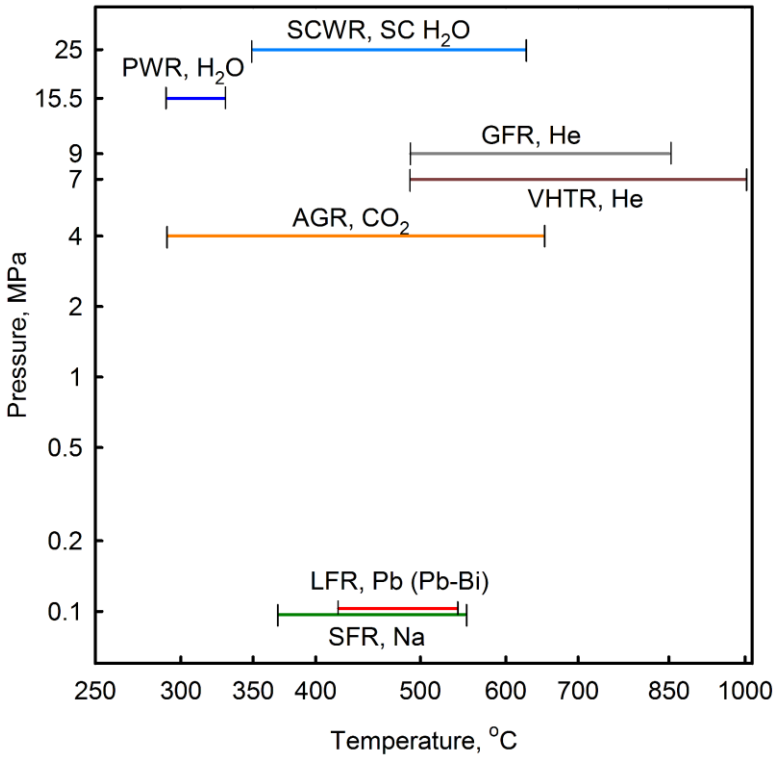

Figure 3.1. Pressure – temperature diagram for PWR, AGR and proposed GEN-IV reactor concepts (pressure assumed to be constant) (Dragunov et al. 2013a).

A density versus temperature diagram is presented in the Figure 3.2. The density drops linearly with the temperature for all the coolants, except SCW. The density of the gases drops significantly, but the density change for liquid metals is insignificant. For SCW, the density drops almost 8 times within the pseudocritical region.

The values of specific heat of He, Na, Pb, and Pb-Bi (Figure 3.3) are nearly constant over the whole range of operational parameters. In the case of CO_2, the specific heat increases linearly and reaches the same value as for Na at ~ 750°C. The specific heat of water goes through a peak (where its value increases almost 8 times) within the pseudocritical region. The specific heats of Pb and LBE are nearly identical and 10 times less than those of Na and CO_2, and almost 40 times less than that of He. At temperatures higher than 450°C, the specific heat of He is higher than that of SCW.

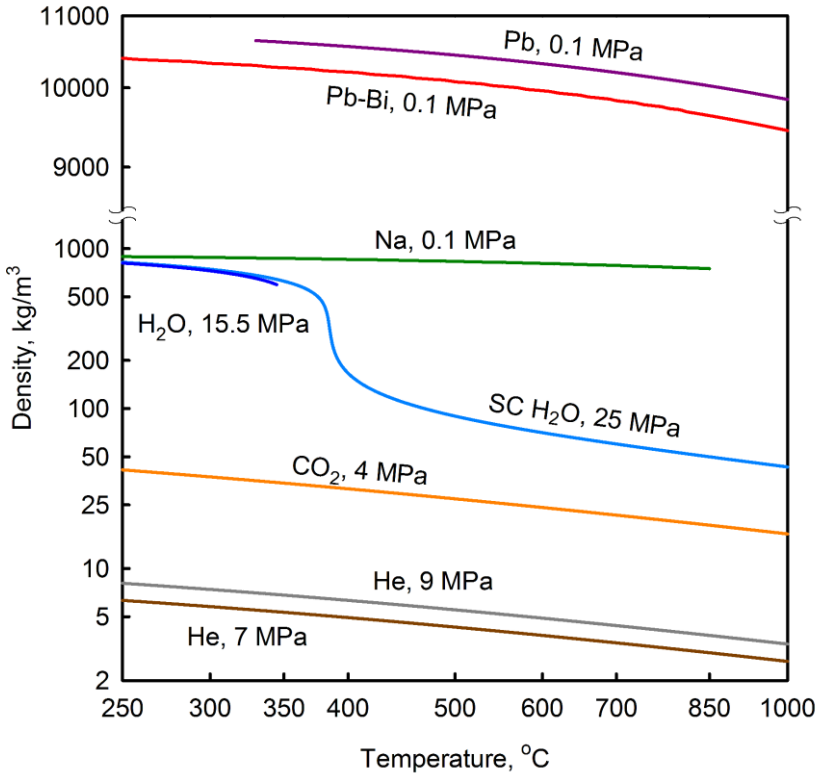

Figure 3.2. Density vs. Temperature (Dragunov et al. 2013a).

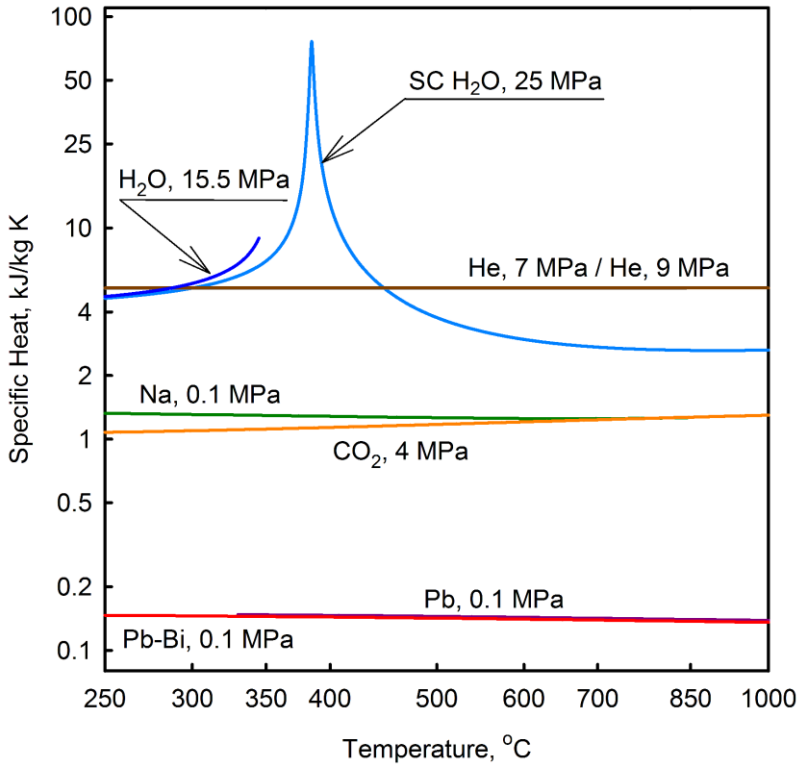

Figure 3.3. Specific Heat vs. Temperature (Dragunov et al. 2013a).

As one would expect, the thermal conductivities of liquid metals are significantly higher than that of gases (Figure 3.4). Thermal conductivity of Na drops slightly, while that for Pb, LBE, He, and CO_2 increases linearly with the temperature. Thermal conductivity behavior of SCW is special – it decreases linearly between 250 – 350°C, then goes through a small peak in the pseudocritical point, before decreasing smoothly from about 0.4 to 0.1 W/m·K. As the temperature increases above 500°C the thermal conductivity increases linearly with values higher than those of CO_2, but lower than those of He.

Dependence of the viscosity of coolants on temperature is shown in Figure 3.5. Viscosity of Na and Pb drop linearly over the whole range of temperature, while the viscosity of Pb-Bi has a slower linear drop up to 600°C. The viscosity then increases for temperatures between 600 and 1,000°C, attaining a value close to that measured at 250°C. The viscosities of gases increase linearly with temperature, and the viscosity of SCW at temperatures beyond the pseudocritical range behave in a similar fashion to that of gases. In general, the shape of a viscosity-temperature curve for SCW is similar to that of thermal conductivity. However, viscosity does not exhibit a peak in the pseudocritical point.

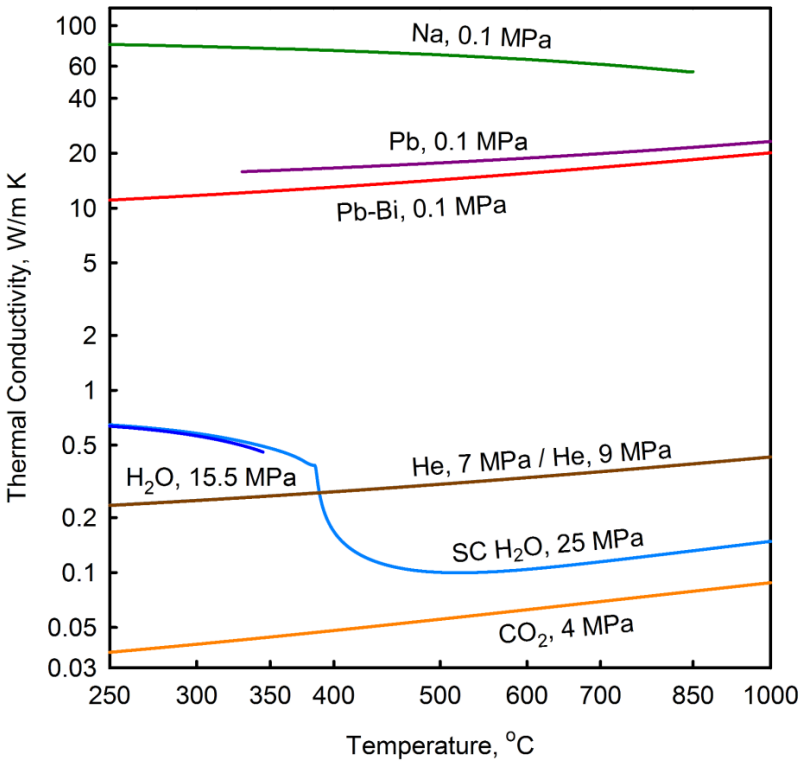

Figure 3.4. Thermal Conductivity vs. Temperature (Dragunov et al. 2013a).

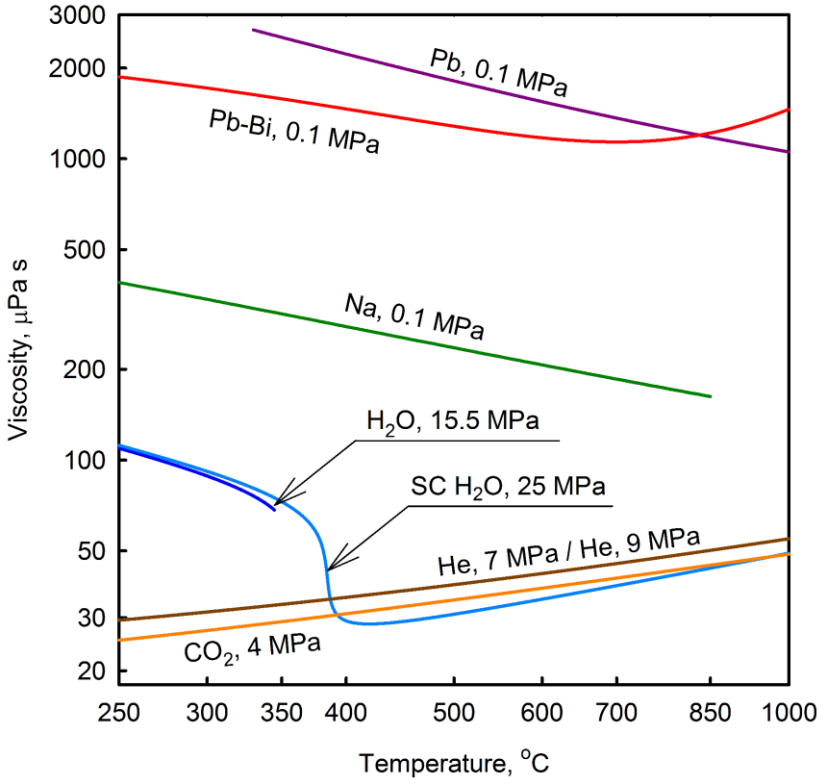

Figure 3.5. Viscosity vs. Temperature (Dragunov et al. 2013a).

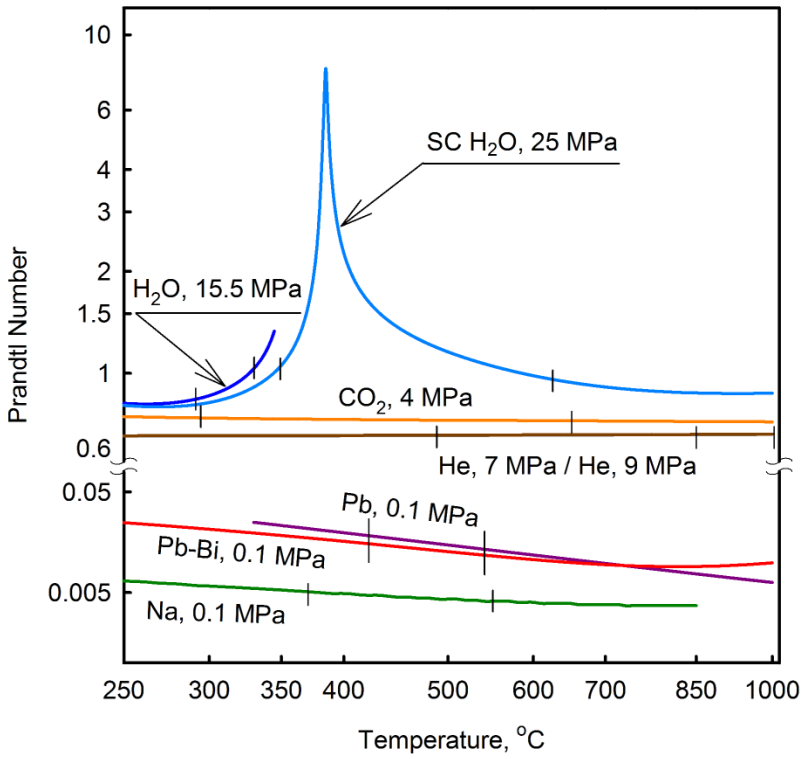

Figure 3.6. Prandtl Number vs. Temperature (Dragunov et al. 2013a).

The dependence of the Prandtl number (Pr) (defined as the ratio of the product of viscosity and specific heat to the thermal conductivity) on temperature for different coolants was plotted and is shown in Figure 3.6. The shape of **Pr** is governed by the more significant change of property of the coolant. We have established that the specific heat is nearly constant for all of the GEN-IV reactor coolants, except for SCW. Therefore, the coolants ratio of viscosity to thermal conductivity will affect the shape of the **Pr**/temperature curve. As we see from Figure 3.6, the changes in viscosity and thermal conductivity of gases are such that they compensate each other, and **Pr** of gases is virtually constant over most of the 750°C temperature span. However, for liquid metals the viscosity drops more significantly than the thermal conductivity increases. As a result, the **Pr** of liquid metals drops almost linearly with temperature. Due to an increase in viscosity of LBE at high temperatures, the corresponding value of Prandtl number of LBE also increases.

Plotted enthalpy increase diagram is shown in Figure 3.7. As higher the value of enthalpy increase, as much heat can be transferred to the coolant for a given mass.

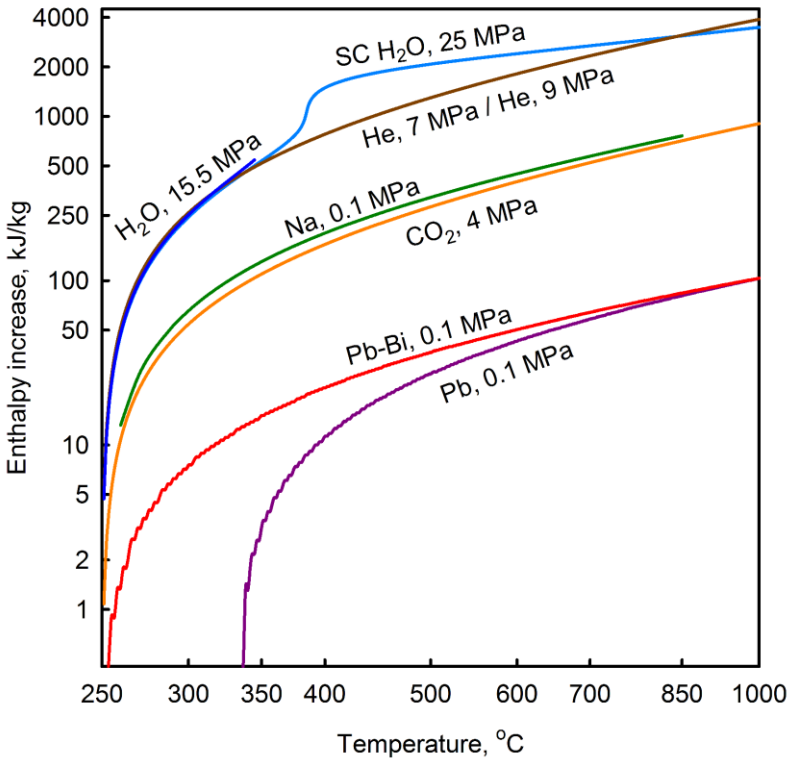

Figure 3.7. Enthalpy increase vs. Temperature (Dragunov et al. 2013a).

Volumetric expansivity of liquid metals is much smaller than that of the remaining coolants (Figure 3.8). Volumetric expansivity of gases drops by a factor 2 in a linear fashion from 250 to 1,000°C. Remarkably, values of volumetric expansivity for SCW at temperatures below the pseudocritical point are close to those of gases. Near the pseudocritical point, volumetric expansivity of SCW peaks. At higher temperatures, the volumetric expansivity of SCW gradually reaches values corresponding to those of gases.

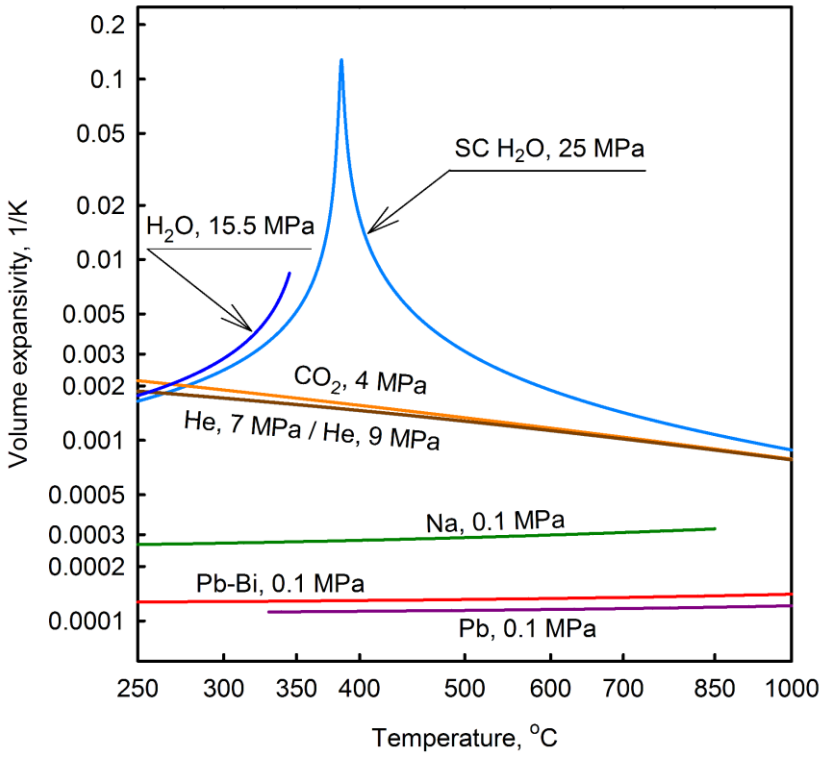

Figure 3.8. Volume Expansivity vs. Temperature (Dragunov et al. 2013a).

To summarize the above, the thermophysical properties of liquid metals and gases experience only minor linear changes with increasing temperature. However, all the properties of SCW at pseudocritical conditions go through very rapid changes.

Another comparison of coolants can be made based on the power required to circulate coolant to achieve a given temperature. Let the circulation power be W, then:

$$W = \frac{\dot{m}}{\rho}\Delta P, \tag{3.1}$$

where ṁ – mass-flow rate of coolant, kg/s; ρ – density of coolant, kg/m^3; and ΔP – hydraulic resistance of the loop, Pa.

The total power $\dot{Q}$, removed by the coolant from the core, can be expressed as:

$$\dot{Q} = < c_p > \dot{m} \Delta T, \tag{3.2}$$

where $< c_p >$ is the average specific heat for a given change of coolant temperature ΔT.

From a thermal-hydraulic point of view, the best coolant would be the one, that will remove the largest amount of power from the core for a given circulation power. Therefore, if we fix thermal resistance of the loop and allowed the temperature of the coolant in the core to increase, then coolants can be compared based on the quantity:

$$a \equiv \frac{\dot{Q} \Delta P}{W \Delta T} = < c_p > \rho \tag{3.3}$$

Consider the temperature range of 350 to 650°C, and compare the coolants based on the circulation power. Results of the calculations are presented in Table 3.2.

Table 3.2. Comparison of coolants based on relative circulation power required to sustain given inlet and outlet temperatures of the coolant.

Coolant	Specific heat, kJ/kg·K	Density, kg/m^3	*a*, Pa/K	$a_{scw}/a_{coolant}$
SCW	6.713	626	4,202.00	1
He, 7MPa	5.189	4.6	23.87	176
He, 9MPa	5.187	5.3	27.49	153
CO_2	1.2	34.2	41.04	102.4
Na	1.4	900	1,260.00	3.3
Pb	0.16	10,500	1,680.00	2.5
Pb-Bi	0.16	10,200	1,632.00	2.6

As seen in Table 3.2, SCW outperforms other coolants greatly in the 350 – 650°C temperature range. Another immediate conclusion is that helium, proposed for both GFR and VHTR concepts, appears to be the most expensive coolant in terms of circulation power (density at T_{ave} is 5.3 kg/m^3).

For better analysis, this comparison should be complemented with considerations of the corrosive properties, size and cost of the machinery for the power conversion side of the plant, and the net-plant efficiency.

3.4 HEAT-TRANSFER-COEFFICIENT CALCULATIONS FOR COOLANTS OF GEN-IV NUCLEAR REACTORS

The heat-transfer coefficients were calculated using MATLAB (2007) software. The developed MATLAB model for heat-transfer coefficient calculations for turbulent flow of sodium in a circular tube is presented in Appendix A.

Heat-transfer calculations were performed under the following conditions:

1. Pressure and temperature range for each coolant were chosen in accordance with Table 3.1;
2. All HTCs were calculated for a bare tube with hydraulic equivalent diameter of 8 mm;
3. Various mass fluxes were investigated: 1000, 4000 and 8000 kg/m^{2}s for applicable coolants. Also, conditions close to the ones in actual reactors were investigated.
4. For calculations of SC H_2O, Pb and Na the value for constant surface heat flux was assumed to be 970 kW/m^2.
5. Steady-state operating conditions were assumed.
6. Pressure of coolant in the reactor was assumed to be constant.

Hydraulic equivalent diameter D_{hy} was chosen according to the following equation:

$$D_{hy} = \frac{4A_{fl}}{P_{wet}} = 8 \cdot 10^{-3}\ m, \tag{3.4}$$

where A_{fl} – flow area of the coolant in m^2 and P_{wet} – wetted perimeter in m.

For each temperature of the coolant in the reactor, the necessary properties of coolants were retrieved from NIST program using the developed MATLAB code (such as enthalpy, dynamic viscosity, thermal conductivity and specific heat). Properties for liquid-metal coolants were calculated using equations presented in the Handbook on Lead-bismuth Eutectic Alloy and Lead Properties (2007). Using G – mass flux (kg/m^2s) and μ - dynamic viscosity of a fluid (Pa·s), the Reynolds number (Re) was calculated:

$$\mathbf{Re} = \frac{G \cdot D_{hy}}{\mu}, \tag{3.5}$$

Turbulent flow is commonly utilized due to the associated higher HTCs. Several applicable correlations were identified for the use in calculations, they presented below.

For H_2O, D_2O, CO_2 and He coolants the Dittus-Boelter equation (Dittus and Boelter,1930) was used to calculate the local Nusselt number (Nu) for fully developed turbulent flow in a smooth circular tube:

$$\mathbf{Nu} = 0.023\, \mathbf{Re}^{0.8} \mathbf{Pr}^{n}, \tag{3.6}$$

where n=0.4 for heating and 0.3 for cooling of the fluid flowing through the tube. This equation has been confirmed experimentally for the range of conditions: $0.6 \le \mathbf{Pr} \le 160$; $\mathbf{Re} \ge 10{,}000$; $L/D \ge 10$ (L – length, m; D – diameter, m) (Incropera et al., 2007).

For liquid-metal coolants, Na and Pb, the Sleicher and Rouse relation (Cengel and Ghajar, 2011) was used to calculate the local Nusselt number for fully developed turbulent flow with constant surface heat flux on a smooth circular tube:

$$\mathbf{Nu} = 6.3 + 0.0167 \mathbf{Re}^{0.85} \mathbf{Pr}_s^{0.93}, \tag{3.7}$$

where the Prandtl number is evaluated at the surface temperature. This equation has been confirmed experimentally for the range of conditions: $0.004 \le \mathbf{Pr} \le 0.01$; $10^4 \le \mathbf{Re} \le 10^6$.

For SCW, the correlation developed by Mokry et al. (2009) was used. This correlation was obtained by analyzing a large set of experimental data obtained in Russia:

$$\mathbf{Nu_b} = 0.0061\,\mathbf{Re_b}^{0.904}\,\overline{\mathbf{Pr}}_{\mathbf{b}}^{0.684}\left(\frac{\rho_w}{\rho_b}\right)^{0.564}, \tag{3.8}$$

where subscripts "w" and "b" mean that properties are evaluated at T_w-wall temperature, T_b – bulk-fluid temperature, and average Prandtl number is to be calculated as:

$$\overline{\mathbf{Pr}}_{\mathbf{b}} = \frac{\mu}{k}\cdot\underbrace{\frac{h_w - h_b}{T_w - T_b}}_{\bar{c}_p} \tag{3.9}$$

This correlation is valid for: pressure 22.8 – 29.4 MPa, constant surface heat flux 70 – 1250 kW/m^2, mass flux 200 – 1500 kg/m^{2}s and hydraulic equivalent diameter 3 – 38 mm. Mokry et al. (2009) correlation has demonstrated a good fit for HTC values (±25%) and wall temperatures (±15) for the analyzed dataset.

Mokry et al. and Sleicher and Rouse correlations require iterations be performed to calculate T_w. Therefore, for the inlet temperatures of the coolants, initial guesses of wall temperature T_w were made, HTCs were calculated from the correlations, and corrected values of wall temperature $T_{w,1}$ were calculated using Newton's cooling law:

$$q'' = htc\cdot\left(T_{w,1} - T_b\right) \Rightarrow T_{w,1} = \frac{q''}{htc} + T_b, \tag{3.10}$$

where q" – constant surface heat flux, assumed to be 970 kW/m^2.

The value of $T_{w,1}$ is compared to T_w. If the absolute value of the difference between these values was higher than 0.1°C, then the value of $T_{w,1}$ was assigned to T_w. and another iteration was performed, starting from redetermining the of heat-transfer coefficient from

the corresponding correlation. The iterations were stopped after the difference of wall temperatures T_w and $T_{w,1}$ became less than 0.1°C. For the next adjacent nodes the initial guess of wall temperature was calculated to be: $T_{w,i+1} = T_{b,i+1} + T_{w,i} - T_{b,i}$.

In Figure 3.9 the HTCs calculated for coolants of GEN-IV, AGR and PWR reactors at nominal operating pressures and mass fluxes ranging from 500 to 8200 kg/m^{2}s are shown. It can be seen that in all cases sodium coolant has the highest HTCs, ranging from 58 – 96 kW/m^{2}K, while CO_2 has the lowest HTCs, ranging from 1 – 4 kW/m^{2}K. The HTC of SCW goes through a peak within the pseudocritical region, where its value increases by almost 2 times, then at temperatures above 450°C drops below 350°C. The HTCs of the gases and lead increase slightly with temperature. The HTC of sodium drops linearly with temperature.

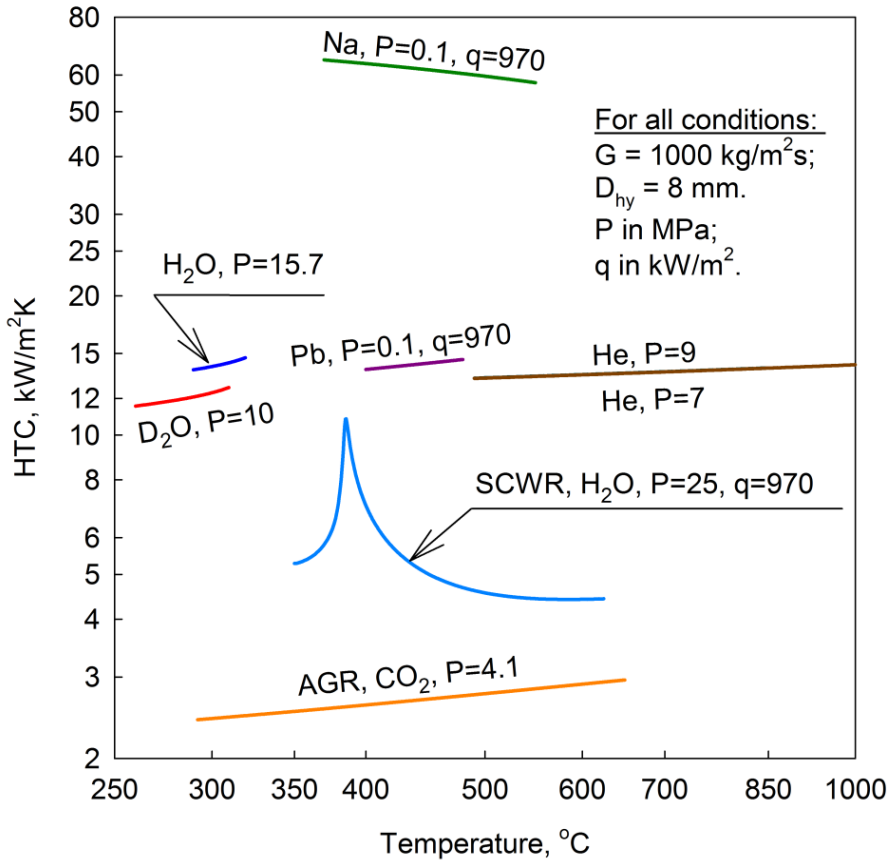

(a) HTCs at mass flux of 1000 kg/m^{2}s

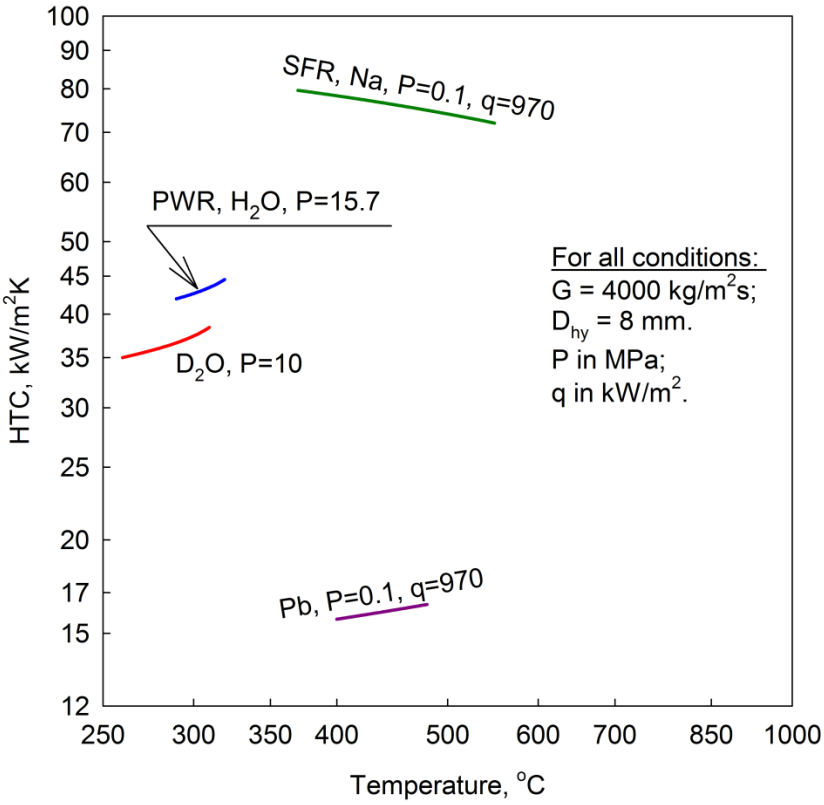

(b) HTCs at mass flux of 4000 kg/m^{2}s

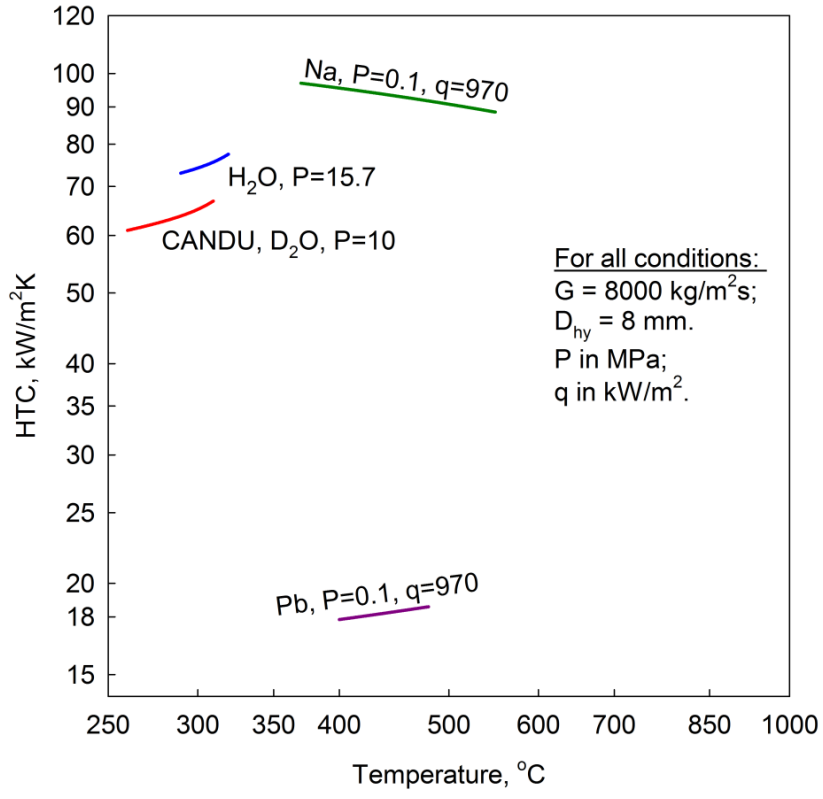

(c) HTCs at mass flux of 8000 kg/m^{2}s

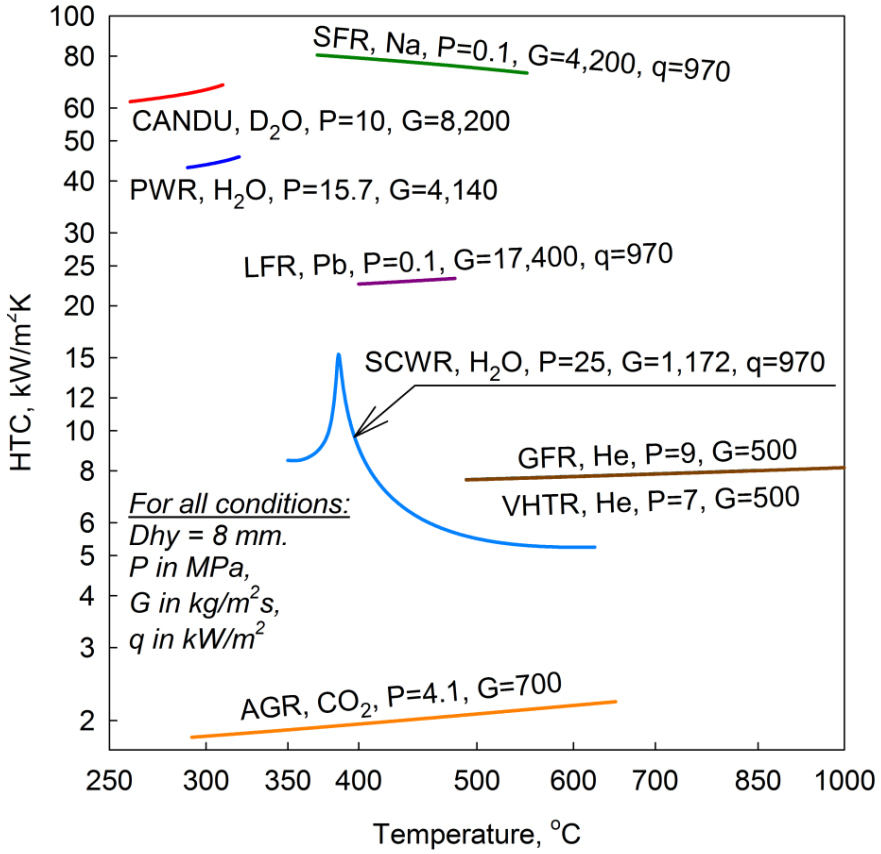

(d) HTCs at mass fluxes, close to actual in the reactors

Figure 3.9. Heat transfer coefficients calculated for a flow of coolants of GEN-IV, AGR and PWR reactors in a bare tube at nominal operating pressures and at various mass fluxes: (a) – 1000 kg/m^{2}s; (b) – 4000 kg/m^{2}s; (c) – 8000 kg/m^{2}s; (d) – at mass fluxes, close to actual mass fluxes in the reactors. For calculations of subcritical H_2O, D_2O, CO_2 and He the value of heat flux wasn't taken into account, while for SC H_2O, Pb and Na value of heat flux was assumed to be 970 kW/m^2. Hydraulic equivalent diameter used in calculations for all the coolants – 8 mm.

In the Figure 3.9d HTCs are shown for close to actual conditions in the reactors. It is reasonable to compare them with HTCs published in the open literature. Typical HTCs for coolant candidates are listed in Table 3.3. It shows that most of the calculated HTCs for conditions close to actual correspond to the typical HTCs presented in the books by Hewitt and Collier (2000) and Pioro (2012). Among the coolants considered, sodium in conditions close to SFR, has the highest HTC of all the proposed coolants (70 – 80 kW/m^{2}K), which corresponds to the data presented in Table 3.3. Conditions achieved in CANDU reactor (added for comparison purposes) allow HTCs above

60 kW/m^{2}K. Calculations also showed that in PWR, the HTCs are about 45 kW/m^{2}K. Lead, as expected, has HTCs around 25 kW/m^{2}K, which is lower than that of another liquid-metal – sodium. HTCs of SCW (5 – 15 kW/m^{2}K) and CO_2 (1.8 – 2.5 kW/m^{2}K) also lie within the typical range of values.

Table 3.3. Typical heat-transfer-coefficient values for coolant candidates (Hewitt and Collier, 2000; Pioro, 2012).

Coolant	Heat transfer coefficient, kW/m^{2}K
SCW	10 – 25
He (rough surface)	10
CO_2 (high pressure)	2 – 5
Na (forced convection)	55 – 85
Pb (forced convection)	25 – 35
Pb-Bi (forced convection)	20 – 30

3.5 NUCLEAR PROPERTIES OF PROPOSED COOLANTS

Water has very appropriate nuclear properties and can be used as both a coolant and a moderator. This feature allows for a simpler core. However, water has very high moderating ratio (Table 3.4), which is a significant disadvantage for fast SCWR concepts. Only weakly moderating materials that maintain a hard-neutron spectrum (which is important for breeding) can be used as a coolant in a fast reactor. This fact has a major impact on the engineering design of fast reactors (IAEA Report, 1985).

Sodium has a relatively small moderating effect compared to water (Table 3.4) and a relatively low neutron-capture cross-section compared to lead and LBE. It is known that neutron irradiation of a liquid metal can produce radionuclides, which increases the radiation dose in the circuit. Neutron capture processes for sodium produces ^{24}Na with a half-life of 15 h, and the primary sodium becomes radioactive while flowing through the core. This activation of sodium in the core leads to a power-plant design with 3 circuits – a primary circuit containing radioactive sodium, a secondary circuit containing non-

radioactive sodium, and a water circuit to produce electricity (IAEA Report, 1985).

Table 3.4. Selected nuclear characteristics of proposed coolants (Lamarsh and Baratta, 2001; Todreas et al. 2004; Neutron Scattering Lengths and Cross-sections website, 2013).

Coolant	Atomic mass (kg/kmol)	Moderating ratio	Neutron scattering cross-section[a], barn	Neutron absorption cross-section, mbarn	
				At 1 MeV	At 0.025 ev
Na	23	1.80	3.2	0.23	530[b]
Pb	207	1	6.4	6.001	699[b]
LBE	~ 208	0.82	6.9	1.492	403[b]
H_2O	18	421	3.5	0.1056	665.3[b]
He	4	0.27	3.7	0.007953	<500[c]

[a] Averaged over fission spectrum (elastic and inelastic).

[b] Data were taken from Neutron Scattering Lengths and Cross-sections website, 2013.

[c] Data were taken from Lamarsh and Baratta, 2001.

Neutron capture by ^{209}Bi results in ^{210}Po, which is an alpha emitter with a half-life of 138 days. Exposure to moisture can result in a volatile polonium hydride producing an airborne hazard.

In general, absorption of thermal neutrons by gas coolants is very low. Table 3.4 shows that helium is one of the most suitable coolants based on its nuclear properties. Although the capture cross-section is very large for helium-3, its content in natural helium is extremely low, about $10^{-7} – 10^{-6}$ %. Helium is most often contaminated with nitrogen and argon, but the presence of contaminants does not cause significant induced activity of helium. The lower values of absorption cross-section lead to an increased fraction of neutrons available for breeding, while the harder neutron spectrum significantly increases the neutron yield per fission (Waltar and Reynolds, 1981). Therefore, helium can have wide application in both thermal- and fast-neutron reactors. Unfortunately, there is a lack of experience in using helium as a coolant in a fast-reactor technology.

3.6 CORROSION BEHAVIOUR OF PROPOSED COOLANTS

Stainless steel is resistant to corrosion in liquid sodium. However, corrosion can occur in the presence of impurities, particularly oxygen in the form of Na_2O. Sodium reacts vigorously with air or water to produce Na_2O and NaOH, both corrosive agents. High concentrations of impurities can lead to increased corrosion and the subsequent detachment of radioactive corrosion products from surfaces in the reactor core, especially from the fuel sheath. These radioactive impurities can be carried-over to the low-temperature parts of the primary coolant circuit (heat exchangers). The accumulation of these radioactive corrosion products is undesirable and should be minimized to avoid future difficulties in maintenance and repair of these components after several years of service (IAEA Report, 1985). Therefore, it is important to maintain the required concentration of impurities, which are mostly comprised of oxygen and carbon. This can be done by cold traps in the bypass of the coolant circuits.

At room temperature lead is resistant to corrosion by air. At temperatures up to 700°C molten lead is protected from oxidation by a dense oxide film. At higher temperatures, the oxide film melts and the oxidation rate increases rapidly (Dragunov et al. 2013a). Hydrogen and nitrogen do not interact with lead up to 600°C. These gases, as well as argon and helium, are used to protect the molten lead from oxidation. Lead contaminated with oxygen, antimony, arsenic, tin, and zinc is more corrosive than non-contaminated. Generally, it is well-known that lead and LBE are more corrosive than sodium.

Helium itself does not cause oxidation of reactor materials. The corrosion of reactor components occurs because He is contaminated with water vapor, oxygen or carbon dioxide. To prevent this, the total content of impurities in He should not exceed 0.01%.

The corrosion of materials in SCW has been reviewed recently (Was et al. 2007; Sun et al. 2009). SCW is highly corrosive, particularly in the presence of oxidizing agents. In the core, radiolysis of water produces oxidants such as H_2O_2 and O_2. Unlike corrosion in sub-critical water, corrosion in SCW appears to proceed by a gaseous oxidation process, probably because of the more gas-like than liquid-like properties of SCW. Ferritic-

Martensitic alloys such as HCM12A follow parabolic oxidation kinetics in SCW, producing a stable, but thick oxide layer that resists spalling (Was et al. 2007). The corrosion rate is high and the volume of the oxide so large that it would fill the void spaces in the reactor core. The addition of chromium to the alloy improves the oxidation resistance. Austenitic stainless steels (304L, 800H) show low corrosion rates, but suffer localized corrosion effects. Thin, coherent oxide films are formed on the surfaces as a result of oxidation in SC water, but the oxide has a tendency to spall leaving the exposed metal susceptible to further localized oxidation (Was et al. 2007). Stress Corrosion Cracking (SCC) has been observed on several of these alloys. The effects of the SC environment on cracking of these alloys are complicated by radiation-induced cracking, which must be considered for several of the candidate austenitic stainless steels. The evaluation of SCC susceptibility is under continuing investigation. Nickel-based alloys are the third nuclear material commonly used, and alloys such as 625, 690, C22 have been investigated. These materials have very low oxidation rates in SCW, but they appear to suffer intergranular attack with chromium depletion from the grain boundaries; SCC and pitting also have been observed (Was et al. 2007). Other materials, including ceramics, are under investigation (Sun et al. 2009). Specialty zirconium alloys are being examined, although zirconium corrodes too rapidly for use in SCW, as are titanium alloys (Was et al. 2007). Long-lived, corrosion resistant materials are needed for the SCWR, and the selection and development of optimal materials is under continuing investigation (Dragunov et al. 2013a).

Currently, subcritical water is the most widely used coolant in nuclear reactors. It is readily available, has low melting point, and has a very high specific heat. Although radiation causes a small amount of chemical decomposition of water, this does not affect its thermal and physical properties appreciably. During NPP operation, the main concern is for the secondary effects of radiolytic water decomposition: corrosion of nuclear materials, formation of highly explosive mixture of oxygen and hydrogen, etc. Sheath corrosion is controlled by systems that carefully maintain specific water chemistry.

3.7 CONCLUSIONS ON PROPERTIES OF WATER, LIQUID-METAL AND GAS COOLANTS

Conclusions on supercritical water

Though quite high outlet temperatures are proposed for SCWR, this will require use of water at a supercritical state and require the highest pressure system (up to 25 MPa) among the rest of GEN-IV reactors. As shown before, all the thermophysical properties of SCW go through very rapid changes in the pseudocritical range, what needs to be taken into account. SCW greatly outperforms other coolants in the 350 – 650°C range in terms of power required to circulate coolant. However, SCW is highly corrosive and requires special materials to be developed, and this can be a problem for a long time. This is one of the major problems associated with the development of SCWR.

Conclusions on helium

As it was shown, helium has low density, which leads to much higher power requirements for pumps. The required high volumetric flow-rates through the reactor complicate the design, and it leads to increased costs of the plant. This can become an economic penalty.

Helium has lower neutron absorption and moderation than other coolants considered. It is far more inert than CO_2; it does not absorb neutrons and cannot become radioactive. However, small amounts of radioactive gas escaping through the fuel sheath and radioactive particles adhering to the fuel channels can be readily carried by helium. In practice, helium being proposed as a coolant for the GFR and VHTR may become radioactive (Lamarsh and Baratta, 2001).

Another difficulty associated with helium is its high diffusivity. Even with the latest technology, systems, sealing, and materials to prevent helium leaks are complicated. Additionally, there are increased acoustic loadings and increased forces across

components associated with the high-pressure drop (Waltar and Reynolds, 1981).

Since helium is operated in a supercritical state far from the critical point, significant interruptions in natural circulation, mechanical damage from flashing coolant, or rapid changes in cooling ability with minor variations in pressure or temperature should not occur (Waltar and Reynolds, 1981).

Conclusions on lead, lead-bismuth and sodium

Before the conclusions on liquid metals will be presented, it should be noted that technically pure sodium, lead or LBE are not exactly the same as the nuclear liquid-metals used as coolants in fast-neutron reactors (Smith, 2010). This is because more stringent requirements are imposed on reactor coolants in terms of corrosion, heat transfer, and possible activation, all of which may be adversely affected by the presence of any impurities. For the purpose of comparing properties, it is assumed that the concentrations of impurities are low enough for the physical properties of both grades of these liquid metals to be the same.

In fast reactors liquid metal coolants have been used for some time, this technology has a long experience. The vapor pressure of liquid metals does not rise rapidly with temperature, this allows liquid metals to be used at high temperatures in the primary circuit at relatively low pressures (0.5 – 0.7 MPa), it increases safety of plants. The availability of bismuth may be a limitation for the use of lead-bismuth eutectic in small power reactors and the use of lead in energy production (Beznosov et al. 2007). Utilizing lead or lead-bismuth increases pressure on necessary reinforcing structures, due to higher density, it means that much thicker structures are required to support the coolant weight and withstand seismic events. For sodium this is not a case, however, an additional circulation circuit should be implemented, as sodium reacts with water and air, with the possibility of an explosion and fire. These factors, together with the installation of electrical-preheating systems for pipes and components of the cooling circuits before the startup of the LMFBR, will lead to an increased cost of the plant.

High thermal conductivities of liquid metals allow for more rapid heat removal from fuel

rods, which is particularly important for fast reactors, where the heat flux from the surface of fuel rods in fast reactors with sodium coolant can be as high as 2.5 MW/m^2 (Dementyev, 1990).

Overall, the relatively low melting point, the excellent heat transfer properties, and a moderate pumping power provide sodium with advantages over other liquid metal coolants. One more important advantage of the sodium-cooled reactor is that it has the lowest fuel sheath temperature for normal operation compared to other coolants, because of the very high heat-transfer coefficient of sodium (calculated and shown in Figure 3.9).

CHAPTER 4. INVESTIGATION OF VARIOUS THERMODYNAMIC CYCLES OF MODERN NUCLEAR AND THERMAL POWER PLANTS

All of the power-conversion cycles for NPPs are based on the Rankine steam cycle, which is also utilized in thermal power plants. The objectives of this chapter are:

- to compare and show alternate cycles and their layouts; and
- to compare thermal performance by plotting figures using NIST software.

In this chapter, steam-cycle arrangements for the CANDU reactor, Pressurized Water Reactor, Sodium–cooled Fast Reactor, Advanced Gas-cooled Reactor, Boiling Water Reactor, Advanced Boiling Water Reactor and Supercritical-pressure ThPP are investigated and compared. Thermodynamic layouts, Temperature–Entropy (T-S) diagrams are plotted; thermodynamic efficiencies of corresponding cycles are calculated and discussed.

T-S diagrams for all the Rankine-steam-cycles, except of the SC-pressure ThPP, were based on the following simplifying assumptions: isentropic compression in a pump and isentropic expansion in a turbine. For the SC-pressure ThPP the actual simplified T-S diagram was plotted.

4.1 INTRODUCTION

All steam-cycle arrangements for CANDU reactor, PWR, SFR, AGR, BWR and ABWR are based on the subcritical Rankine steam cycle. However, these cycles have different parameters at the exit of a steam generator (reactor in BWR and ABWR) / at the inlet to a turbine. Major parameters of these cycles are listed in Table 4.1.

For a CANDU-reactor NPP, a 600-MW_{el} Pickering unit was considered, for a PWR NPP, a VVER-1000-based NPP was considered; for an AGR NPP, Torness Nuclear Power Station (the second generation of AGR) was selected, while for an SFR NPP, which is one of the most efficient NPPs nowadays, a BN-600-based NPP was considered. Also,

among the boiling water reactors, RBMK-1000 and Toshiba ABWR designs were selected. The Tom'-Usinsk thermal power plant (Russia) design layout was selected as a Supercritical-pressure thermal power plant design.

Table 4.1. Major parameters of selected thermal and nuclear power plants (AECL Report, 1969; Grigoryev and Zorin, 1989; Margulova, 1995; Toshiba corporation, 2011; and Nonbel, 1996).

Parameters	Turbine inlet temperature, °C	Turbine inlet pressure, MPa	Reheat
PWR NPP	274	5.9	Using extraction from a steam generator
CANDU-reactor NPP	251	4.0	Using extraction from a steam generator
SFR NPP	505	14.2	Using secondary-loop sodium
AGR NPP	538	16.7	Using extraction from a steam generator
BWR NPP	280	6.46	Using both bleeding from the High Pressure Turbine (HPT) and the main steam
ABWR NPP	287	7	Using both bleeding from the HPT and the main steam
SC-pressure ThPP	600	30	Single-reheat using a steam generator

4.2 STEAM-CYCLE ARRANGEMENTS WITH CORRESPONDING TEMPERATURE-ENTROPY DIAGRAMS

4.2.1 PWR NPP steam-cycle arrangement

The PWR reactor is the most common type of reactors worldwide. General basic features of a VVER-1000 reactor (Russian design of PWR) are: indirect cycle with steam

generator, reactor coolant outlet parameters: pressure 15 – 16 MPa (T_{sat} = 342 – 347°C) and outlet temperature 325°C. Power-conversion cycle in VVER-1000 is subcritical-pressure regenerative Rankine steam-turbine cycle with steam reheat. Turbine steam inlet parameters: saturation pressure of 5.88 MPa and saturation temperature of 274°C (Rassokhin, 1972). The scheme of typical VVER-1000 reactor is shown in Figure 4.1.

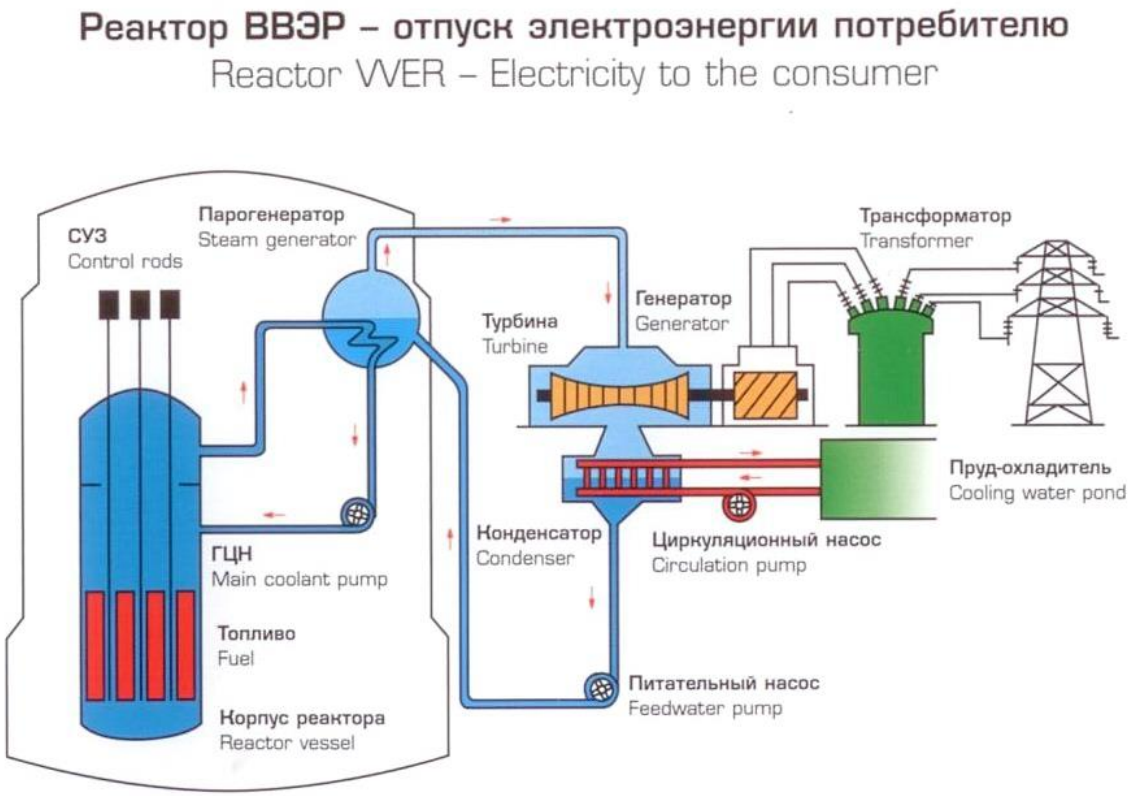

Figure 4.1. Scheme of a typical PWR (Russian VVER) NPP (ROSENERGOATOM, 2004) (courtesy of ROSENERGOATOM)

The thermodynamic layout of the 1000-MW_{el} VVER-1000-reactor NPP is shown in Figure 4.2. The corresponding T-S diagram for the 1000-MW_{el} VVER-1000-reactor NPP is shown in Figure 4.3. Steam with inlet parameters of 5.88 MPa and 274°C expands in HPT. In order to reduce the moisture content in the Low Pressure Turbine (LPT), the wet steam after significant pressure and temperature drop in HPT goes through a set of moisture separators. Then, the dry steam is reheated once to the temperature of 250°C, at which it enters LPT, to improve thermal efficiency of the cycle.

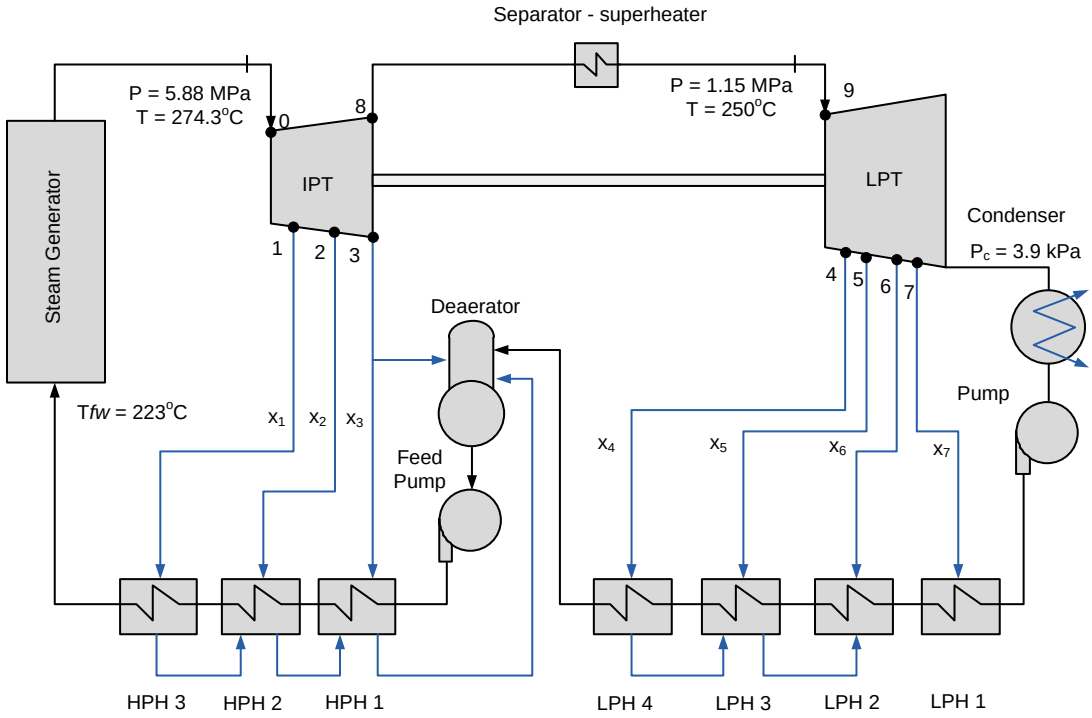

Figure 4.2. Thermodynamic layout of 1000-MW_{el} VVER-1000 PWR NPP (Based on schematics from Grigoryev and Zorin, 1989).

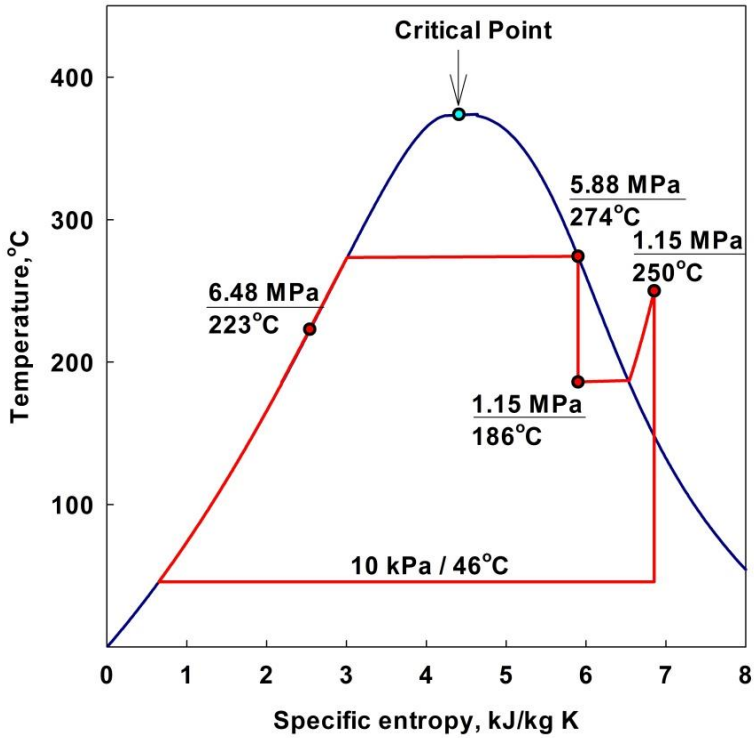

Figure 4.3. Simplified T–S diagram for a VVER-1000 turbine cycle (plotted using NIST software).

4.2.2 CANDU-reactor NPP steam-cycle arrangement

General features of the CANDU reactor at the Pickering nuclear generation station (courtesy of AECL): indirect cycle with steam generator; power-conversion cycle is a subcritical-pressure regenerative Rankine steam-turbine cycle with steam reheat. The turbine steam inlet parameters are: saturation pressure of 4.03 MPa and saturation temperature of 251°C.

The corresponding T-S diagram for the Pickering 600-MW_{el} CANDU-reactor NPP is shown in Figure 4.4 (Pickering unit). The steam with a mass flow-rate of 751.6 kg/s exits the boiler in a saturated state with a steam quality of 99.78% at a pressure of 4.03 MPa and a temperature 251°C and enters the HPT. After it expands in the HPT, wet steam with quality of 89.2% enters a moisture separator. Then, dry steam with a quality of 99.5% is reheated to 230°C by steam from the boiler and enters three LPTs where it expands. Then, steam is condensed in the condenser and goes through the set of feedwater heaters. The corresponding layout of the Pickering 600-MW_{el} CANDU-reactor NPP is shown in Figure 4.5.

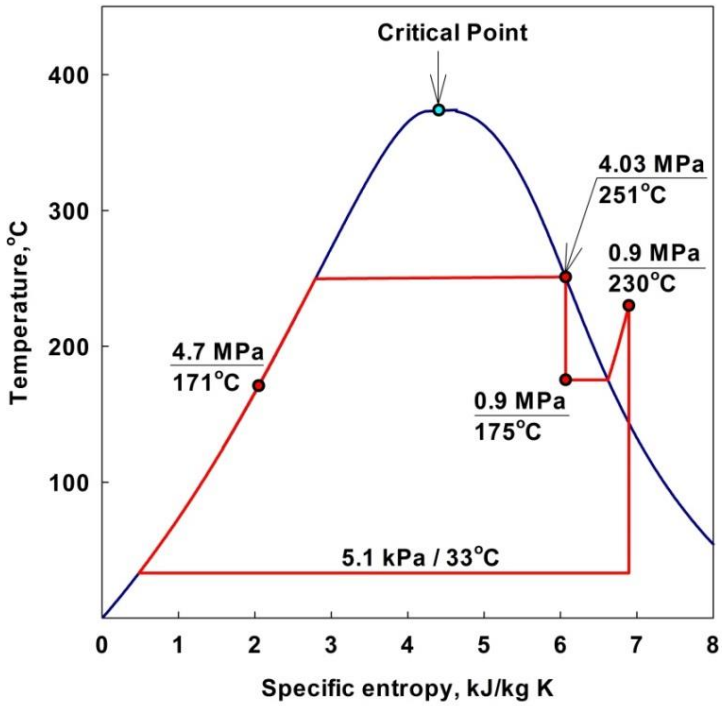

Figure 4.4. Simplified T–S for the Pickering 600-MW_{el} NPP turbine cycle.

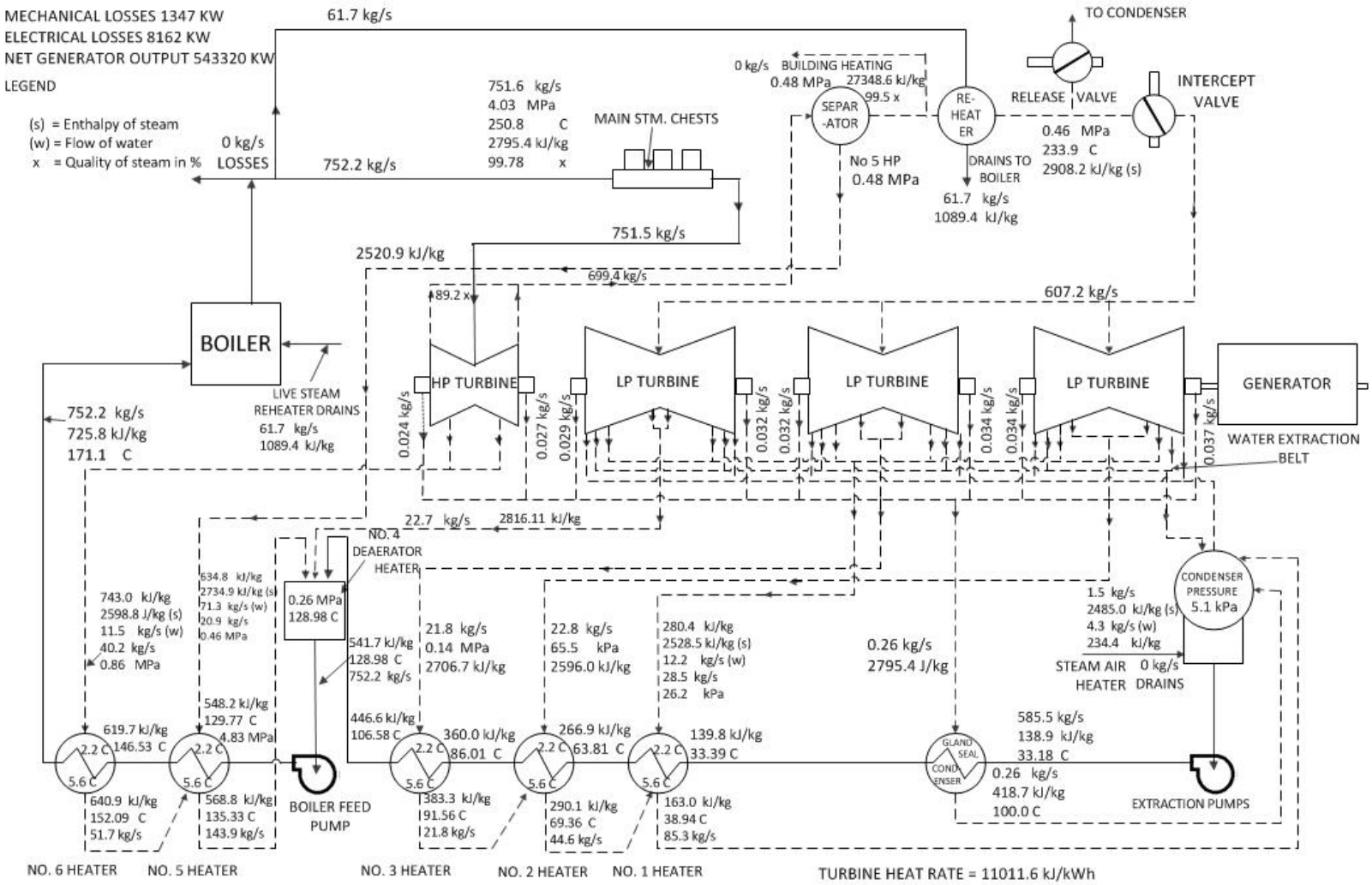

Figure 4.5. Detailed layout of the 600-MW_{el} CANDU-reactor NPP (redrawn, based on schematics from AECL Report, 1969).

4.2.3 SFR NPP steam-cycle arrangement

On Figure 4.6 the schematic of electricity generation in a BN-600 SFR (Russian design of SFR) is presented. For safety reasons this reactor has 2 sodium loops: primary – radioactive and secondary – non-radioactive. From the schematic, it is clear that the temperature of water in the steam generator depends on the outlet temperature of the secondary sodium. As the outlet temperature of primary sodium is 550°C, the outlet of secondary sodium is 520°C, and the steam temperature is 505°C. It is seen that 45°C is lost due to the exchange of heat between primary/secondary sodium and water in the power-conversion cycle. The steam temperature at the SG exit is 505°C at 14.2 MPa, which is higher than the saturation temperature (338°C). Thus, superheated steam enters the HPT, where expands and has a significant pressure and temperature drop to 2.45 MPa (T_{sat} = 223°C) and 245°C. As the steam is in the superheated state, it does not need to go through the moisture separators as in the case of PWR or CANDU reactor. To increase the thermal efficiency of the cycle, the steam is reheated by the secondary-loop sodium up to 505°C.

The corresponding layout of the power-conversion cycle of the 600-MW_{el} BN-600-reactor NPP is presented in Chapter 5 (Figure 5.1).

The corresponding T-S diagram for 600-MW_{el} BN-600 SFR NPP is shown in Figure 4.7.

Figure 4.6. Scheme of a Russian BN-600 NPP (ROSENERGOATOM, 2004) (courtesy of ROSENERGOATOM).

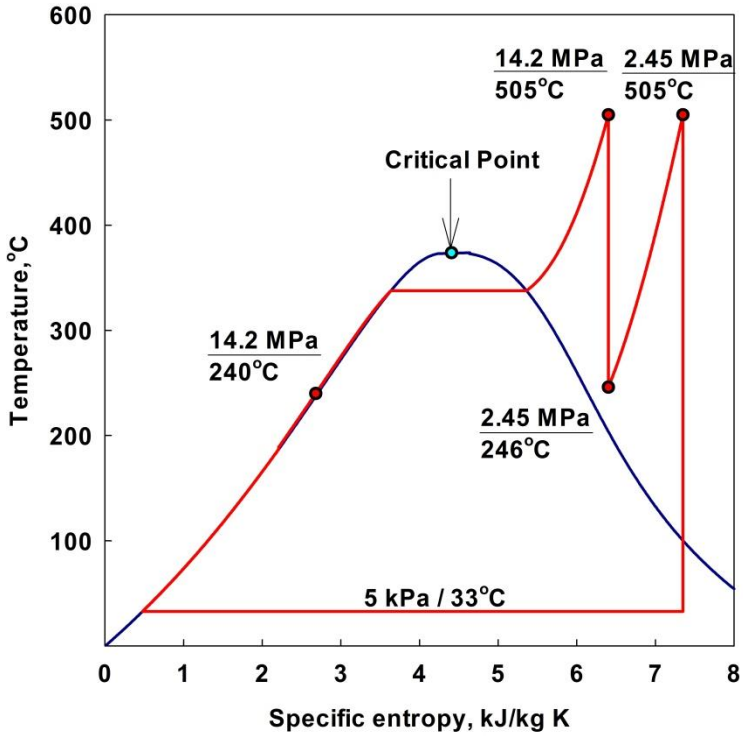

Figure 4.7. Simplified T–S diagram for the 600-MW_{el} BN-600 SFR NPP turbine cycle (plotted using NIST software).

4.2.4 AGR NPP steam-cycle arrangement

As mentioned in chapter 3, the AGR is the most efficient reactor in the world. It has very specific design futures in terms of the power-conversion: the heat exchanger is contained within the steel-reinforced concrete-combined pressure vessel and radiation shield, as seen in the Figure 4.8. The mean inlet CO_2 coolant temperature in the boiler is 619°C (20°C lower than at the outlet of the reactor), and it allows steam to achieve the temperature 541°C at 17.3 MPa in the superheater. On the way to the HPT, the superheated steam has a pressure and temperature drop of 0.6 MPa and 3°C respectively, entering the HPT at 538°C and 16.7 MPa. The corresponding layout of the turbine cycle of AGR Torness NPP (second generation of AGR reactors) is shown in Figure 4.9. As it seen from the schematic, Torness NPP has four low-pressure feedwater heaters and no high pressure feedwater heaters.

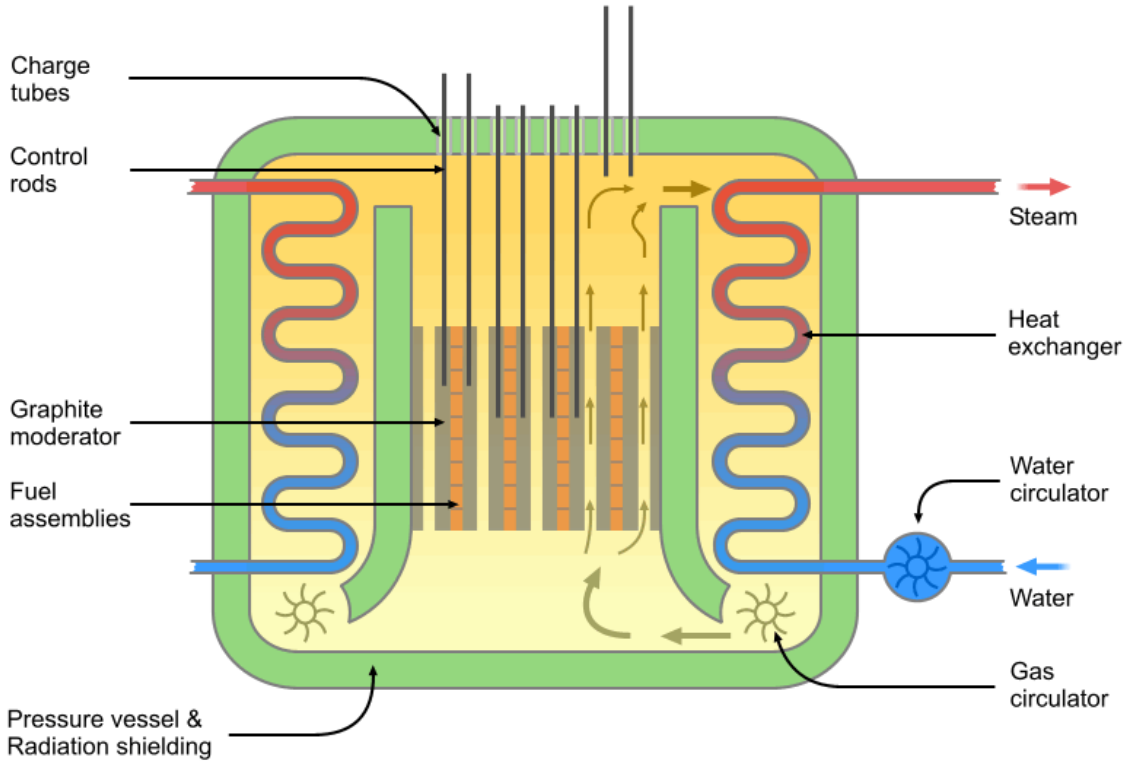

Figure 4.8. Schematic of Advanced Gas-cooled Reactor (Wikimedia Commons, 2013).

The plotted T-S diagram for the AGR Torness NPP is shown in Figure 4.10.

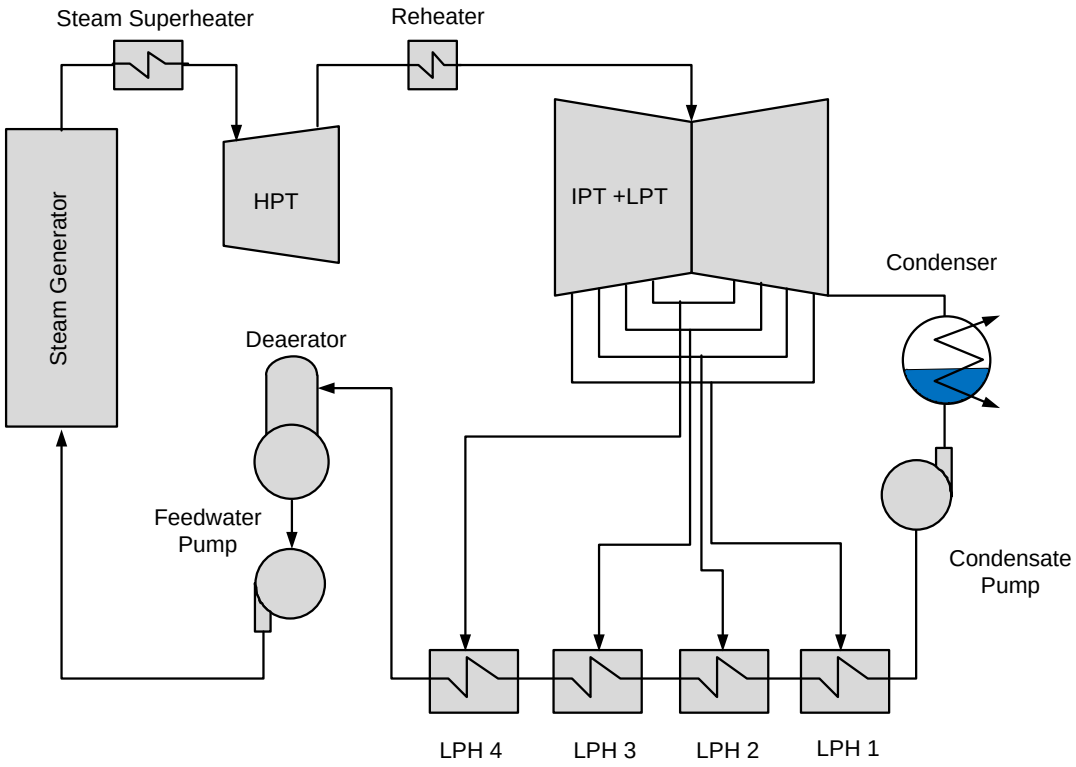

Figure 4.9. Thermodynamic layout of AGR Torness NPP (Based on schematics from Nonbel, 1996).

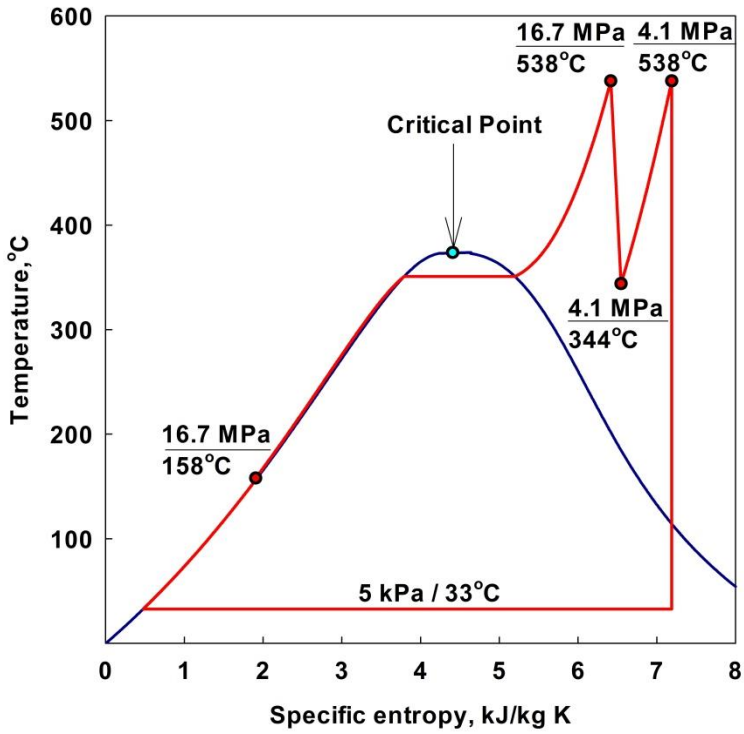

Figure 4.10. Simplified T–S diagram for the AGR Torness NPP turbine cycle.

4.2.5 BWR NPP steam-cycle arrangement

The corresponding schematic of the RBMK-1000 (Russian BWR) NPP is shown in Figure 4.11 with the corresponding thermodynamic layout in Figure 4.12. The NPP is a direct cycle system: steam from a nuclear reactor is fed directly to the turbine. This design eliminates the need for expensive and complex steam generators. The steam temperatures and pressures are the same as in the reactor, and it results in higher thermal efficiency of the cycle. As can be seen from Figure 4.13, steam after expansion in the HPT is wet and, in order to reduce the moisture content, it goes through a set of moisture separators. The steam is reheated twice: by the steam extracted from the HPT and directly by the main steam from the steam drum. It should be noted that steam extraction for LPH4 is taken at the point between the exit of the HPT and the moisture separators. Feedwater in HPH1 is heated by the steam extractions from the HPT. After the deaerator feedwater with a temperature of 168°C is fed back to the steam drum. The plotted T-S diagram for the RBMK-1000 NPP is shown in Figure 4.13.

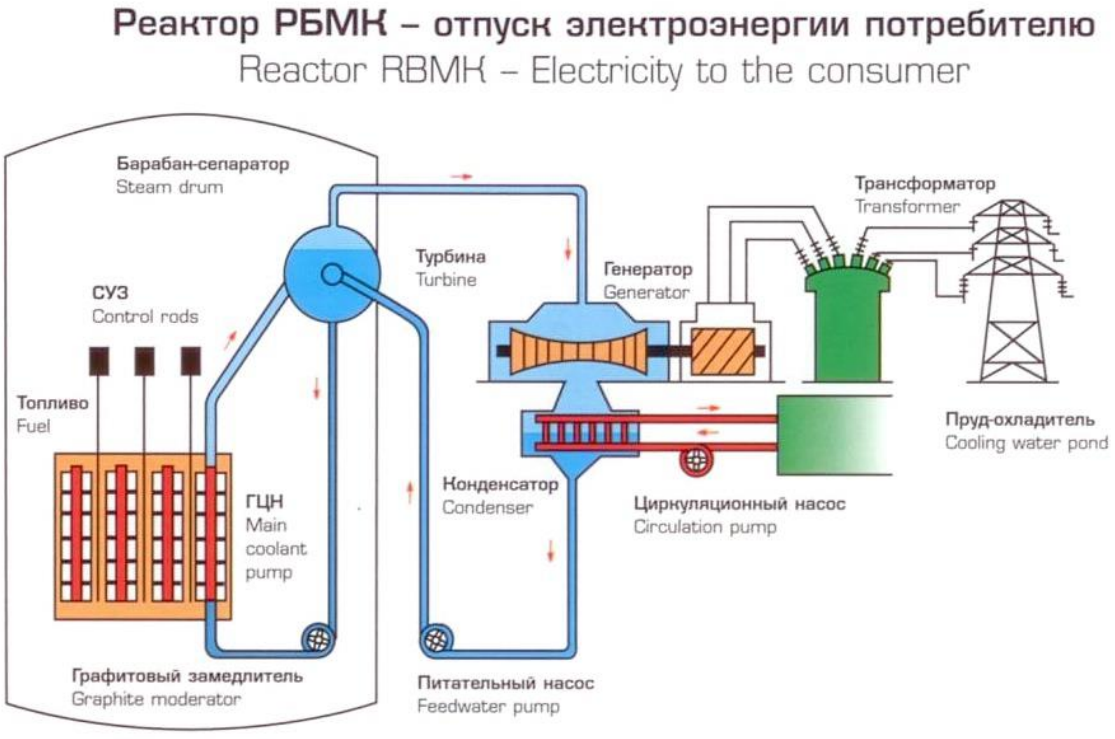

Figure 4.11. Schematic of a Russian RBMK-1000 NPP (ROSENERGOATOM, 2004) (courtesy of ROSENERGOATOM).

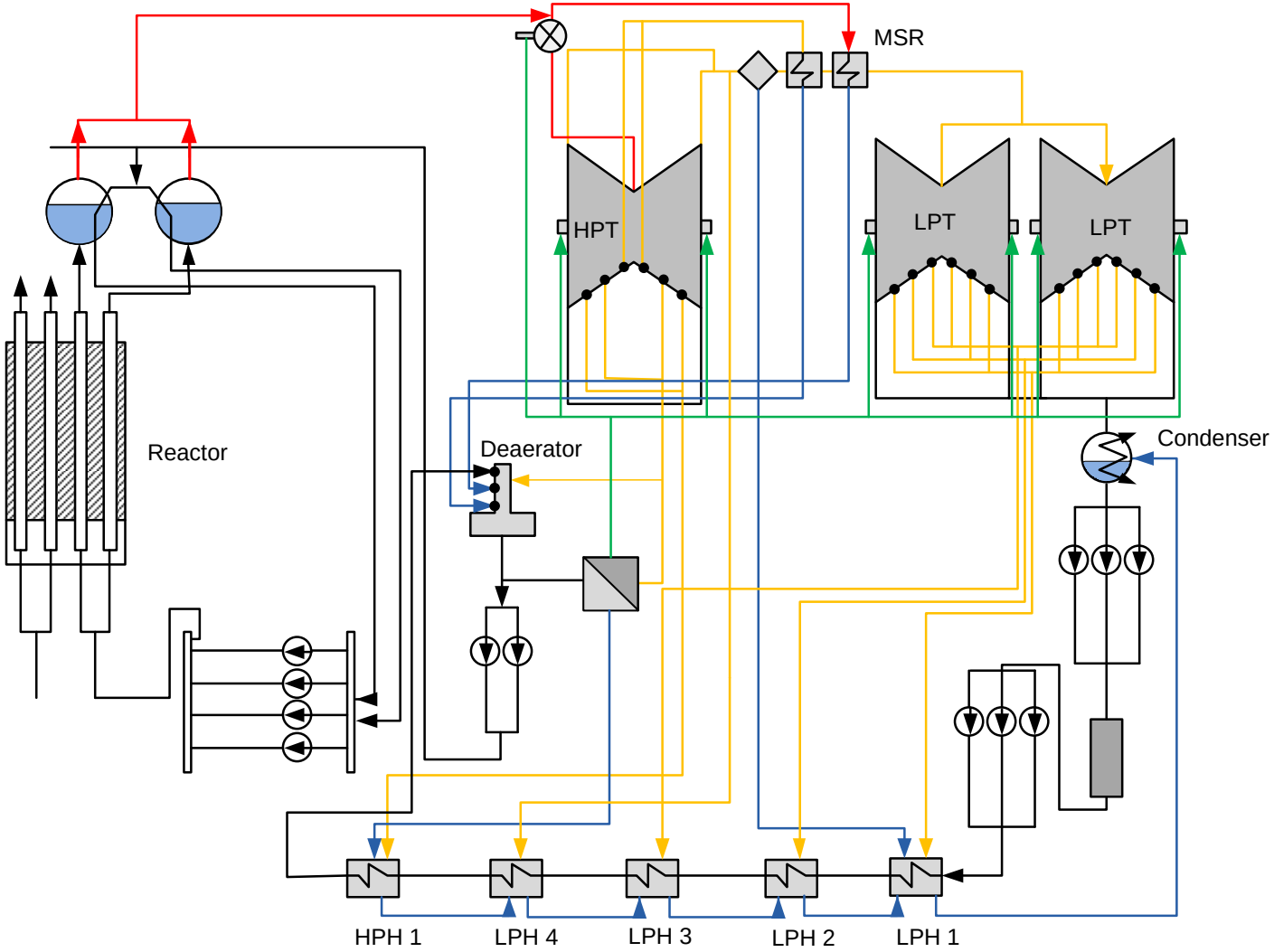

Figure 4.12. Thermodynamic layout of RBMK-1000 NPP (Simplified version based on schematics in Abramov et al., 2006).

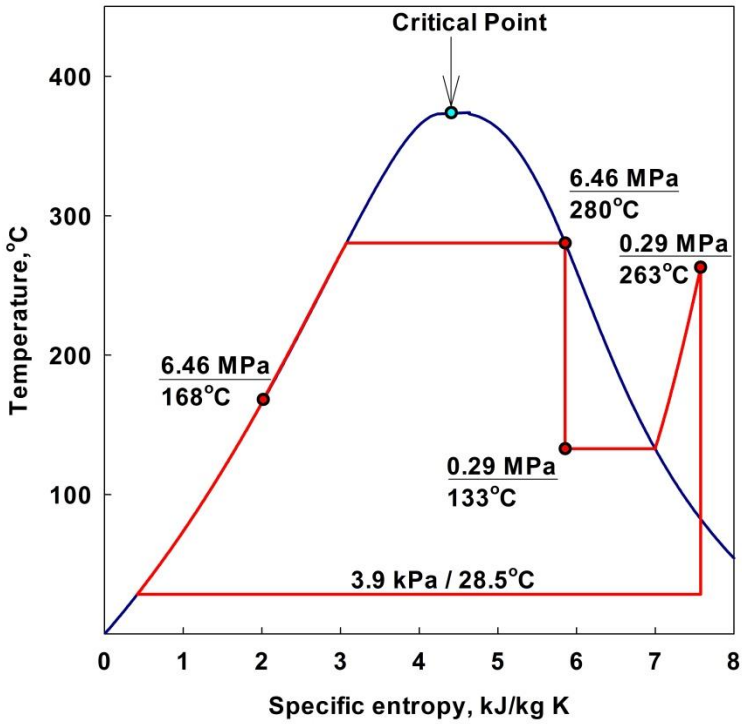

Figure 4.13. Simplified T–S diagram for the RBMK-1000 NPP turbine cycle.

4.2.6 ABWR NPP steam-cycle arrangement

Toshiba's ABWR is a reactor that has been in operation since 1996 when unit 6 at Kashiwazaki - Kariwa NPP was started as the world's first ABWR plant. In 1997 and 2005 another ABWRs started their operation. The ABWR reactor designs were based on experience gained from the technologies of BWRs around the world.

The layout of an ABWR NPP is presented in Figure 4.14. The feedwater heater's high pressure drain water is transferred to the reactor feedwater pump inlet by the drain pump, while the low-pressure drain water is transferred to the condensate demineralizer inlet and, to the outlet of the condensate filter by the drain pump. This contributes to enhanced thermal efficiency of the turbine cycle. Furthermore, the system enables downsizing of the condenser, the condensate pumps and the condensate filter and demineralizer.

An important feature in the ABWR is that the condenser plays the role of a deaerator. As

seen from the layout of the Toshiba ABWR NPP, there is no deaerator on the secondary side. The system consists of the main deaerating condenser connected to an air ejector and off-gas treatment system.

There is one HPT with steam inlet parameters of 287°C at 6.97 MPa and three LPTs with moisture separators and steam reheat implemented between HPT and LPTs. The feedwater system consists of four low-pressure feedwater heaters and two high pressure feedwater heaters.

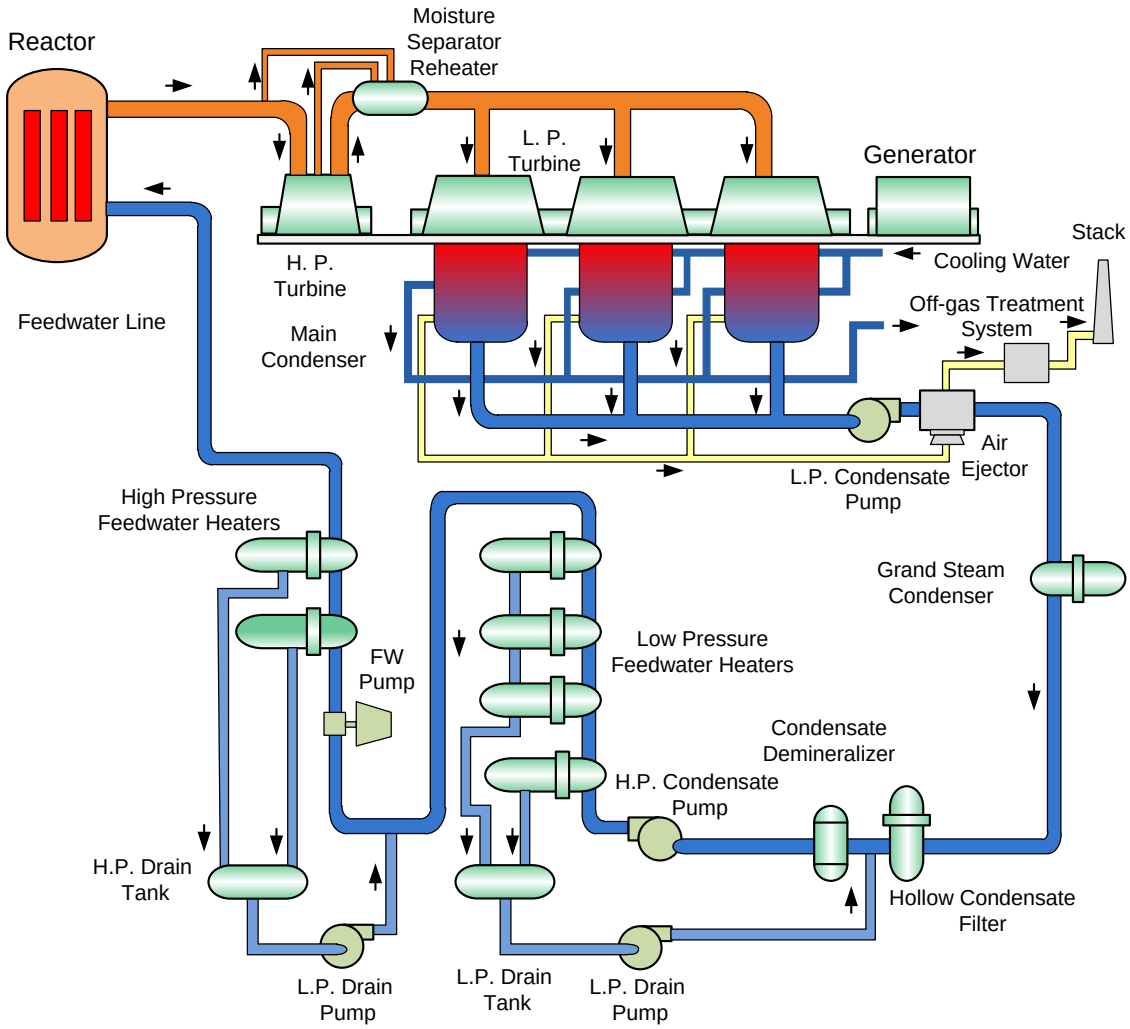

Figure 4.14. Layout of ABWR NPP (Simplified version based on schematics in Toshiba Corporation, 2011).

T-S diagram of the Toshiba ABWR NPP is shown in Figure 4.15. Note that the reheat pressure was assumed to be 1/4 of the main steam pressure as it is the average value for the reheat pressure for most of the NPPs. On the graph, the known parameters are presented in bold, while unknown (assumed) parameters are in a regular font.

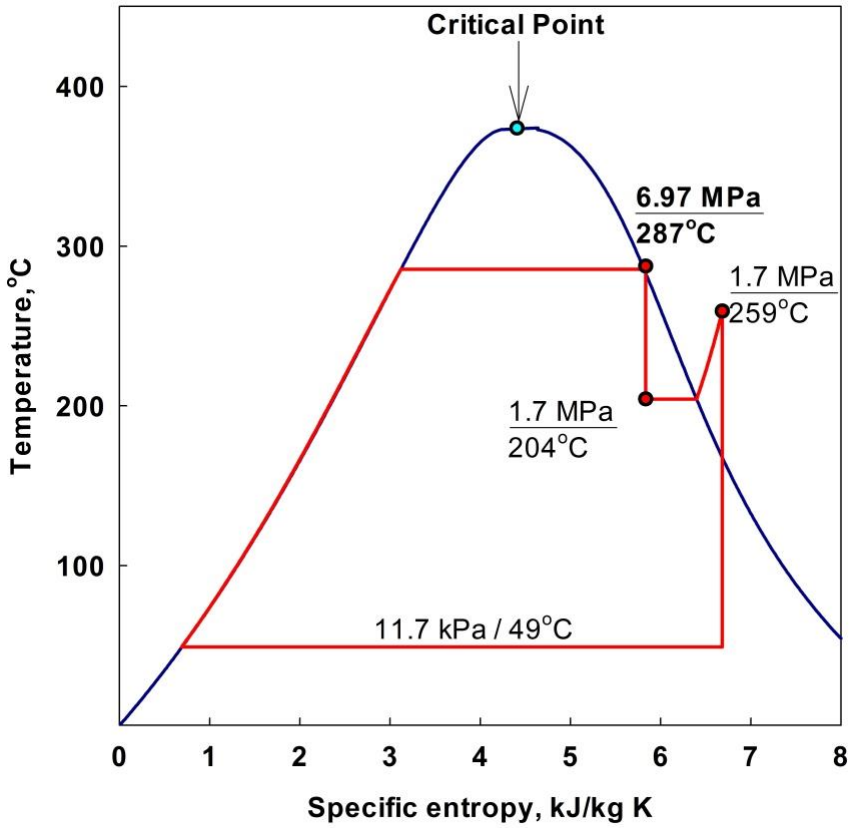

Figure 4.15. Simplified T–S diagram for ABWR NPP turbine cycle (reheat pressure was assumed to be 1/4 of the main steam pressure).

4.2.7 Supercritical-pressure single-reheat regenerative cycle design for a 600-MW_{el} Tom'-Usinsk thermal power plant in Russia

Nowadays, there are more than 500 operating supercritical fossil power plants around the world. Most of them have single-reheat cycle turbines. Supercritical-pressure Tom'-Usinsk thermal power plant design consists of one high pressure turbine, one intermediate pressure turbine and two low-pressure turbines. The HPT "steam" inlet parameters of this

cycle are: pressure - 30 MPa and temperature - 600°C. The HPT superheated steam with a temperature of 321°C at 5 MPa is fed back to the steam generator. The reheat subcritical-pressure steam is 620°C at 4.8 MPa. Steam with these parameters enters IPT. Interesting to note that the reheat temperature is higher than the main "steam" temperature by 20°C. Inlet parameters of the LPT are: pressure 0.32 MPa (T_{sat} = 136°C) and temperature 241°C. There are a total of 8 feedwater heaters and one deaerator utilized in the scheme. A T-S diagram of the supercritical-pressure Tom'-Usinsk thermal power plant design is shown in Figure 4.16. Pressure, temperature, mass flow-rate and specific enthalpy values are given for each major point of the cycle in the Figure 4.17.

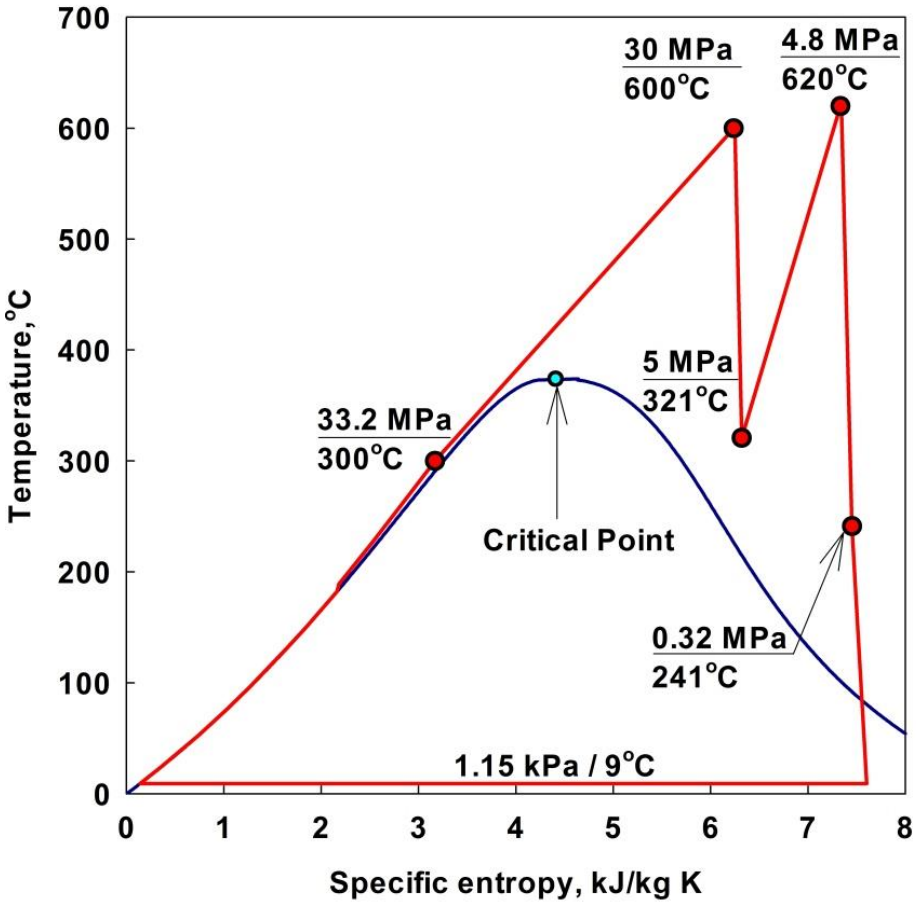

Figure 4.16. Actual T–S diagram for a Tom'-Usinsk thermal power plant turbine cycle.

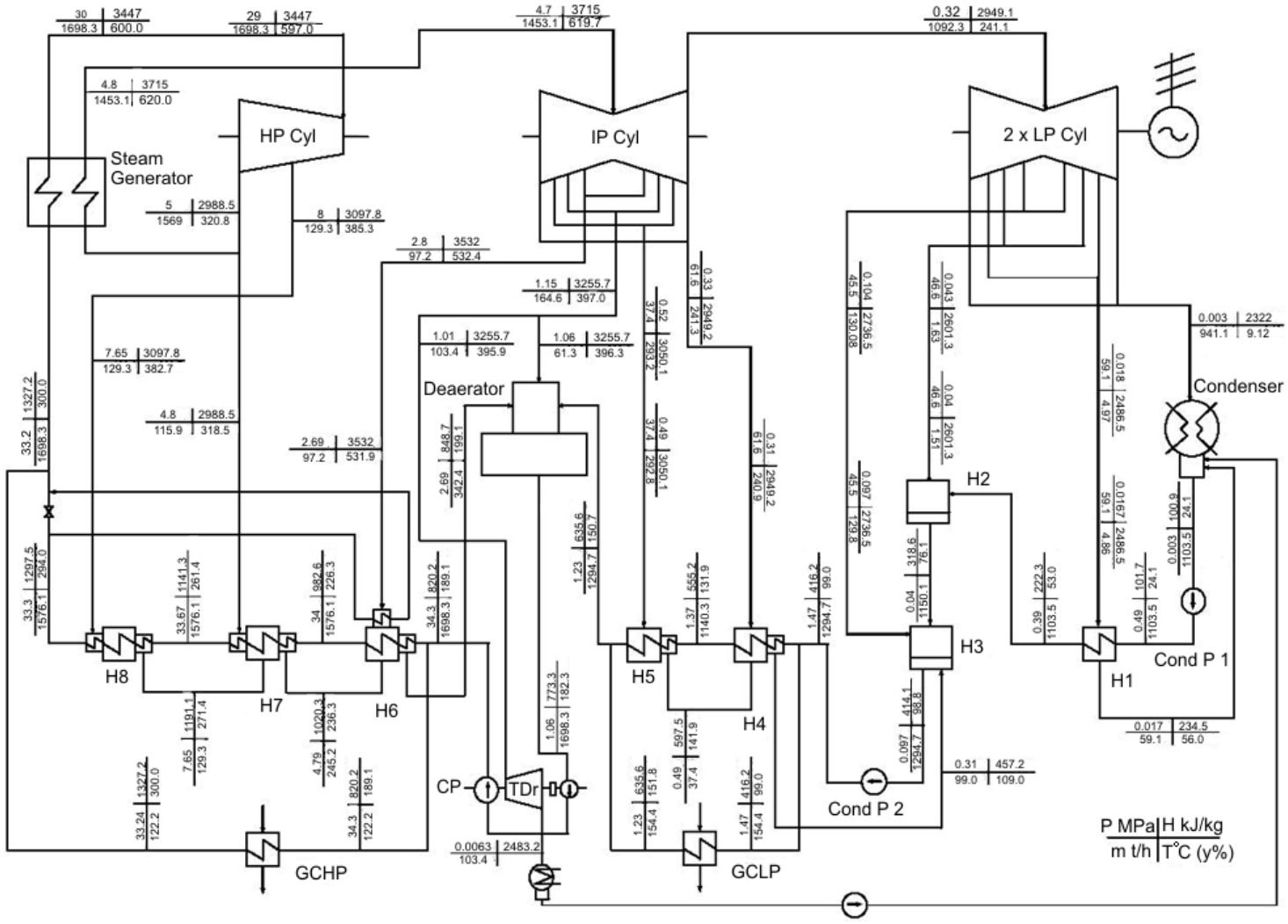

Figure 4.17. Supercritical-pressure single-reheat regenerative cycle 600-MW_{el} Tom'-Usinsk ThPP (Russia) layout (Simplified version based on schematics in Kruglikov et al., 2009).

4.3 ANALYSIS, COMPARISON AND DISCUSSION OF THE CORRESPONDING CYCLES AND T-S DIAGRAMS

A comparison of T–S diagrams for the thermodynamic cycles of a CANDU reactor and a VVER-1000 NPPs is shown in Figure 4.18. As both are pressurized water reactors, it is reasonable to compare their thermal performance in one graph. It is seen that the turbine cycle of a VVER-1000 NPP outperforms the turbine cycle of a Pickering CANDU reactor NPP due to the higher temperature and pressure of steam to the turbine. Also, both turbine cycles are of a single-reheat type with reheat temperatures lower than the temperatures of main steam due to the fact that reheat is made by extraction from a steam generator. Both cycles have moisture separators after the high pressure turbines as the steam is wet.

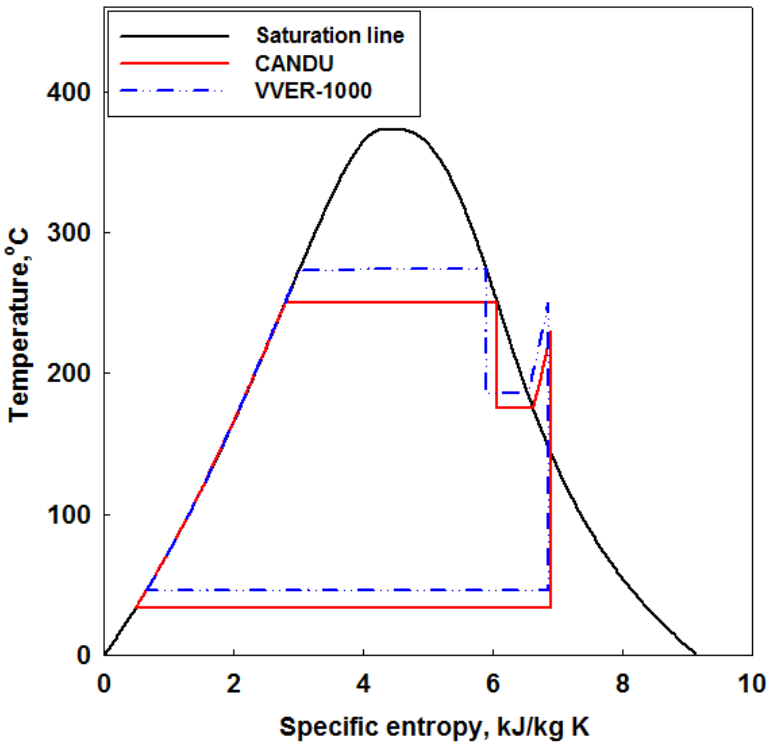

Figure 4.18. T–S diagrams for CANDU reactor and VVER-1000 NPPs' turbine cycles.

A T–S diagram comparison of the thermodynamic cycles for BWR RBMK-1000 and

Toshiba's ABWR NPPs is shown in Figure 4.19. The high pressure turbine inlet parameters for Toshiba's ABWR are higher than that of BWR and it lead to a higher efficiency. Although it is not reasonable to compare the reheat behaviour since the reheat pressure was assumed for ABWR design, it can be stated that both of these thermodynamic cycles are of a single-reheat type. For economic reasons it was unreasonable to implement double-reheat in these NPPs.

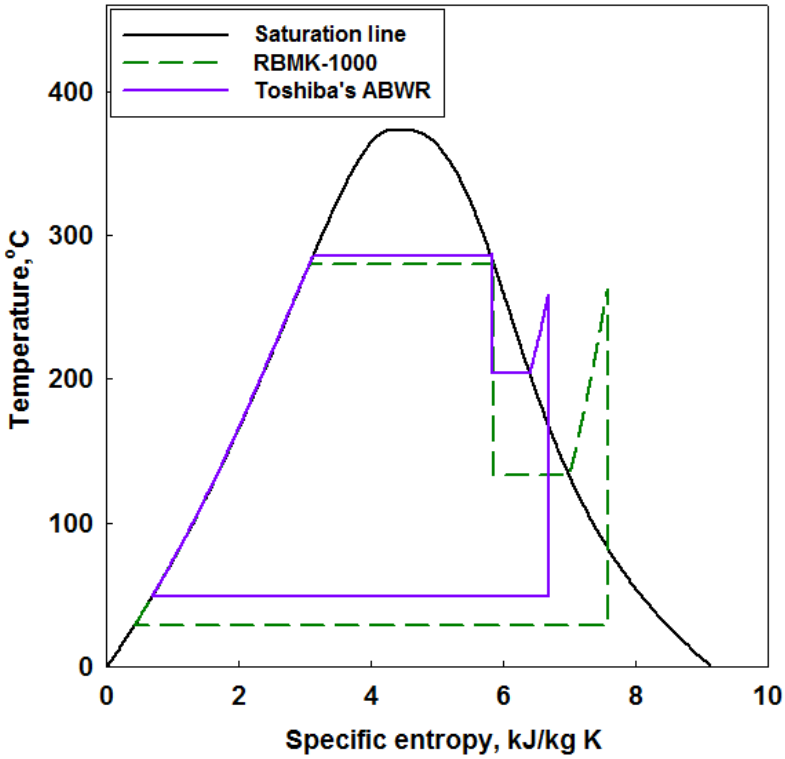

Figure 4.19. T–S diagrams for the RBMK-1000 and Toshiba's ABWR NPPs' turbine cycles.

A comparison of the T–S diagrams for the BN-600 and AGR NPPs is shown in Figure 4.20. Although these reactors are of different types, their turbine cycles are very close to each other due to the high coolant outlet temperatures in the reactor and consequent high turbine inlet parameters. Both of the cycles are double-reheat regenerative cycles. It is interesting to note that reheat temperatures are the same as the main steam temperatures, which increases the thermal efficiency of the cycle. From Figure 4.20 it is seen that the AGR reactor outperforms BN-600 reactor in terms of the thermal efficiency due to the higher turbine inlet parameters. Turbine inlet temperature for AGR NPP is 538°C which

is higher than the 505°C for BN-600 SFR NPP. It will be shown later that the thermal efficiency of the AGR NPP is higher than that of the BN-600 SFR NPP.

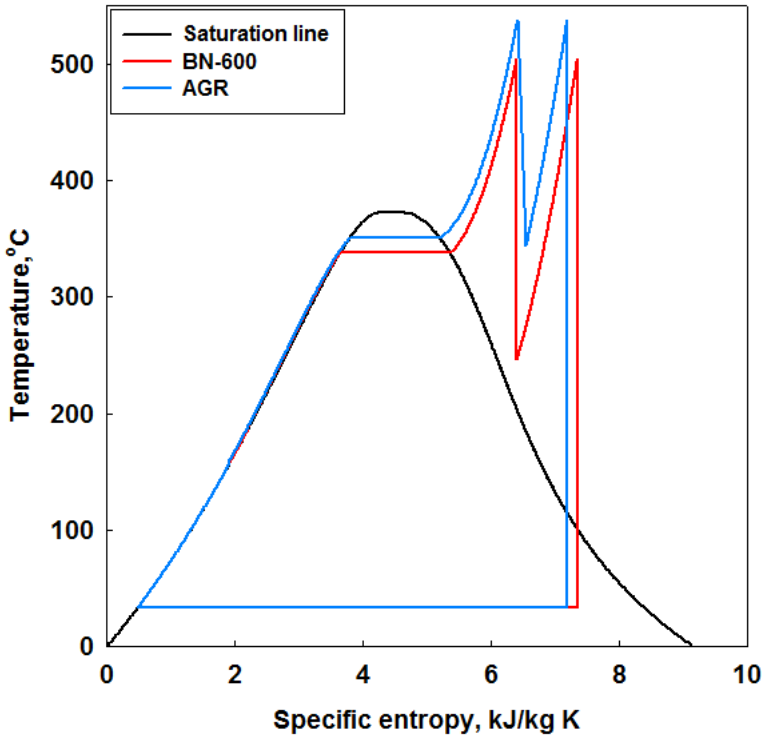

Figure 4.20. T–S diagrams for the BN-600 and AGR NPPs' turbine cycles.

Table 4.2 shows the thermal efficiencies based on the Carnot cycle for the nuclear and thermal power plants considered, but within the ranges of temperatures:

1. reactor inlet to a turbine temperature and environment $T = 10$°C;
2. reactor inlet to a turbine temperature and environment $T = 20$°C;
3. reactor inlet to a turbine temperature and environment $T = 30$°C.

Table 4.2 is shown to illustrate this approach by using the theoretical efficiency η, calculated as $\eta = (T_2\text{-}T_1)/T_2$, where T_2 is turbine inlet temperature and T_1, a condenser temperature (in K), is considered as a sink temperature (10°C, 20°C, 30°C).

Thermal efficiencies of the considered thermal and nuclear power plants and their corresponding turbine cycles are listed in Table 4.3. It is seen that the best theoretical efficiency can be achieved for a SC-pressure ThPP due to the high temperatures of

"steam". Also, with regards to nuclear power plants, the maximum theoretical thermal efficiency was achieved for the AGR and BN-600 NPPs, and it varied from 61-65%. The lowest possible thermal efficiency was achieved for the CANDU reactor of the Pickering design; efficiency clearly depends on the sink temperature and varies from 42-44%. The next group of NPPs lies in the middle of the table: BWR, PWR, VVER and ABWR with thermal efficiencies for the Carnot cycle of around 43-47%.

Table 4.2. The Carnot cycle thermal efficiencies for the temperatures of power-conversion cycles of considered nuclear and thermal power plants.

Reactor / PP	Turbine inlet T, K (°C)	Thermal efficiency of the Carnot cycle, %		
		T_{sink} = 283K	T_{sink} = 293K	T_{sink} = 303K
VVER	547 (274)	48.3	46.4	44.6
CANDU	524 (251)	46.0	44.1	42.2
SFR	778 (505)	63.6	62.3	61.1
AGR	811 (538)	65.1	63.9	62.6
BWR	553 (280)	49.2	47.0	45.2
ABWR	560 (287)	49.5	47.7	45.9
SCP ThPP	870 (597)	67.5	66.3	65.2

For T–S diagrams for CANDU-reactor and VVER-1000 NPPs there is a 6% increase in overall thermal efficiency if the steam generator exit temperature is increased by 20°C and the pressure by 1.85 MPa. Regarding the BN-600 NPP, due to high temperature of the reactor coolant (550°C), steam in the power-conversion cycle can be superheated up to 505°C at a pressure of 14.2 MPa, which gives about an 8% increase in thermal efficiency for the plant compared to the VVER-1000 NPP.

In the Table 4.3 all known efficiencies for the considered NPP turbine cycles with the corresponding thermal efficiencies of the whole NPPs are presented in ascending order from left to right. The lowest NPP thermal efficiency as expected has the CANDU reactor at Pickering Generating Station (29%), while the highest thermal efficiency has the

second generation AGR reactor at the Torness NPP (40.7%). The BN-600 SFR NPP thermal efficiency is slightly lower (40.0%) than that of the Torness AGR NPP.

Table 4.3. Thermal efficiencies of the considered NPP cycles.

Parameter	Nuclear Power Plants					
	CANDU	**RBMK-1000**	**VVER-1000**	**ABWR**	**BN-600**	**AGR**
Thermal efficiency of turbine cycle	33%[1]	36%[2]	~35%[2]	N/A	49%*	N/A
Thermal efficiency of NPP	29%[1]	31.3%[2]	32%[2]	~38%[3]	40%[4]	40.7%[5]

[1] AECL Report, 1969;

[2] Grigoryev and Zorin, 1989;

[3] Toshiba Corporation, 2011;

[4] Margulova, 1995;

[5] Nonbel, 1996;

* Was calculated for an idealized cycle in Dragunov et al., 2012.

Plotted T-S diagrams showed thermal performance of one cycle over another, as the thermal efficiency of the cycle is very important and affects the net efficiency of a plant. Comparison of thermodynamic cycles of six types of NPPs showed that implementation of the steam reheat by the reactor coolant or by an intermediate liquid-sodium coolant (in the case of BN-600 NPP) rather than by partially extracted working fluid, i.e., saturated steam (as in CANDU and VVER-1000 reactor NPPs) allows a drastic increase in the cycle thermal efficiency (up to 8%). For PHWR NPPs, where the core consists of individual channels, nuclear steam reheat may be implemented by passing a high-pressure-turbine exhaust through a number of channels. In general, the efficiency of BN-600 NPP is higher than the water-cooled NPPs, because of much higher temperatures of the steam in the power-conversion cycle (505°C compared to 274°C and 251°C).

CHAPTER 5. STUDY ON VARIOUS POWER-CONVERSION CYCLES FOR SODIUM-COOLED FAST REACTORS

The evolution of nuclear-power engineering in the last 50 years demonstrated its vitality and usability and the possibility of providing safe and competitive power to the consumers, notwithstanding a certain risk of the environment contamination. It is obvious that a further development of a nuclear industry is possible only after creating environmentally clean, safe and more efficient NPPs (Dragunov et al. 2012).

One of the current engineering challenges is to design GEN-IV NPPs with significantly higher thermal efficiencies (43 – 55%) compared to those of current NPPs and to match or at least to be close to the thermal efficiencies reached at fossil-fired power plants (55 – 62%). The SFR is one of the six concepts considered under the GIF initiative.

The BN-600 reactor is a sodium-cooled fast-breeder reactor built at the Beloyarsk NPP in Russia. This concept is the only one from the GEN-IV nuclear-power reactors that is actually in operation (since 1980). On the power-conversion side, it uses a subcritical-pressure Rankine-steam cycle with heat regeneration. Steam extractions are taken from High-Pressure (HP), Intermediate-Pressure (IP) and Low-Pressure (LP) turbines. The reactor generates electrical power in the amount of 600 MW_{el}. The reactor core dimensions are 0.75 m (height) by 2.06 m (diameter). The UO_2 fuel enriched to between 17 and 26% is used in the core, while depleted uranium is used in the blanket.

There are two loops (circuits) for sodium flow. For safety reasons, sodium is used both in the primary and the intermediate circuits. A sodium-to-sodium heat exchanger is used to transfer heat from the primary to the intermediate sodium. In the section 5.1 major parameters of the BN-600 reactor are listed. The actual scheme of the power-conversion heat-transport system is presented, and the results of the calculation of thermal efficiency of this scheme are analyzed in section 5.2. Details of the heat-transport system, including parameters of the sodium-to-sodium heat exchanger and main coolant pump, are presented in the next sections.

In general, there are three possibilities for an SFR in terms of the secondary cycle:

1. Subcritical-pressure Rankine-"steam"-cycle through a heat exchanger (current approach used in Russian and Japanese power reactors).

2. Supercritical-pressure Rankine-"steam"-cycle through a heat exchanger (new approach proposed by some countries).

3. Supercritical-pressure CO_2 Brayton-gas-turbine-cycle through a heat exchanger (US approach).

In this chapter all three possibilities for the SFR in terms of the power-conversion cycle are presented, compared and investigated.

The basic method of increasing the thermal efficiency of power plants is to increase the operating pressure and temperature. With the advent of modern super alloys, the Rankine-"steam"-cycle has progressed into the supercritical region of the coolant and is generating net efficiencies into the mid 50% range. Calculations of thermal efficiency for a secondary sub- and supercritical-pressure Rankine-"steam"-cycle with heat regeneration are presented in the section.

Carbon dioxide is becoming an important working fluid due to its low toxicity and environmental impact. According to GIF, the Brayton gas-turbine cycle is under consideration for future nuclear power reactors. The supercritical CO_2 cycle is a new approach in the Brayton-gas-turbine cycle. Carbon dioxide has a critical pressure of 7.38 MPa and a critical temperature of 31.0°C, which is significantly less than that of water (22.064 MPa and 373.95°C). Liquid sodium is more compatible with SC CO_2 than with water. In addition, the high fluid density of supercritical CO_2 greatly reduces the size of a turbine and compressors, resulting in significant reductions in the size and capital cost of the turbomachinery. Therefore, the thermal efficiency of SC CO_2 cycle is calculated, and the dependence of the thermal efficiency on inlet parameters of the gas turbine is investigated.

5.1 BN-600 SFR DESIGN

One of the distinctive features of the SFR reactor is the possibility of breeding fuel. This requires using a coolant that has low moderating power over the whole spectrum of neutron energies, which is a characteristic of liquid metals. Liquid sodium has been used in numerous experimental reactors, in a number of power reactors (for example, Monju reactor in Japan) and is currently being used in BN-600 reactor in Russia.

The sodium coolant has the melting point at 98°C and high boiling point at 892°C. It has very attractive thermal properties, and the best thermal conductivity among the nuclear reactor coolants considered in this thesis (see Figure 3.4). The high boiling point of sodium allows attaining high coolant outlet temperatures, which leads to thermal efficiency of ~40% for the NPP.

The relatively high specific heat (≈ 1.25 – 1.28 kJ/kg·K) allows moderate coolant velocities within the fuel elements – around 5-8 m/s for BN-600 (Grigoryev and Zorin, 1989). As a consequence, low pumping power is required. Very high thermal conductivity (60 – 70 W/m·K) allows achieving very appropriate conditions for natural convection in the reactor core during reactor shutdown and any kind of emergency cooling conditions (see Figure 3.4). Another important advantage is the low fuel cladding temperature in normal operation of sodium-cooled reactors because of the very high heat-transfer coefficient values (55 – 85 $kW/m^2 \cdot K$).

However, sodium is chemically active and reacts with air and water even at room temperatures. The sodium interaction with water requires an intermediate loop to prevent the potential for an explosion. An additional challenge in the design of any fast reactor is associated with the development of core materials, which not only have to satisfy requirements typical for thermal reactors, but also have to withstand much harder neutron fluxes than those in thermal reactors.

The BN-600 Reactor design and operating parameters are listed in Table 5.1.

Table 5.1. Main design and operating parameters of the BN-600 reactor (Grigoryev and Zorin, 1989).

Parameter	Value
Thermal power, MW	1,470
Electrical power, MW	600
Maximal coolant's temperature (primary/secondary loop),^{o}C	550/520
Turbine inlet pressure, MPa	14.2
Turbine inlet temperature,^{o}C	505
Feedwater temperature,^{o}C	240
Number of fuel enrichment zones	3
Core height, m	0.75
Top/bottom blanket height, m	0.4/0.4
Blanket thickness, m	0.4
Breeding ratio	0.9 – 1.3
Linear heat flux, kW/m: core max./blanket max./core average	53/43/36
Power density, MW/m^{3}	350
Volumetric ratios of core components: fuel/Na/other	0.45/0.33/0.22
Lattice design of driver and blanket	Hexagonal bundles in triangular lattice
Fuel sheath material	Cr16Ni15Mo3Nb
Fuel sheath outer diameter (core/blanket), mm	6.9/14.2
No of fuel rods per bundle (core/blanket)	127/37
Reactor vessel diameter/height, m	13.8/12.8 (Oshkanov and Govorov, 2009)
Primary coolant flow rate, kg/s	6.05
Primary coolant temperature (inlet/outlet), ^{o}C	380/550
Secondary coolant temperature (inlet/outlet), ^{o}C:	320/520

Sodium as the reactor coolant has the advantage that it can be heated to 550-600°C without being pressurized, so the reactor does not need a massive pressure vessel. The reactor also has a very specific safety feature in that it can maintain cooling by natural convection, should the cooling pumps fail (Inside WANO, 2004).

Primary sodium is separated into two regions by a number of thermal shields. In the first "hot" region, sodium enters six Intermediate Heat exchangers (IHX) that are connected by pairs to 3 circulation circuits of the secondary sodium. In the second "cold" region, 3 main circulation pumps are used to pump the cold primary sodium exiting the IHX to the core. Argon is used as a cover gas above the free surface of sodium to prevent contact with air (Grigoryev and Zorin, 1989).

Primary sodium is heated in the core from 365 °C to 550 °C. In 6 IHXs, it releases heat to the secondary sodium, the latter being heated from 320 °C to 518 °C. The main parameters of BN-600 circulation pumps are given in Table 5.2.

Table 5.2. Main parameters of BN-600 circulation pumps (Grigoryev and Zorin, 1989).

Parameters	**Values**	
	Primary loop	**Secondary loop**
Pumped fluid	Na	Na
Pump head, MPa	0.87	0.57
Pumping rate, m^3/s	172.8	158.4
Efficiency, %	76	80
Pumped fluid temperature,°C	380	320
Gas pressure, MPa	0.14	0.3
Type of inner space sealing	Mechanical sealing with electric motor	
Pump location	Submersible, on the cold leg of the loop	Cold leg of the loop

Secondary sodium is then fed into three Steam Generators (SGs). Each of the SGs has 8

sections comprised of the evaporator, main steam-reheater and intermediate steam-reheater. These are vertical heat exchangers (HXs) with straight tubes and linear thermal expansion compensators. Water and steam are passed upwards inside the tubes of the evaporator and main steam-reheater, in the direction opposite to the sodium flow. Secondary sodium is first passed through the main- and intermediate steam-reheater, and then passed through the evaporator. Exhaust from the high pressure turbine is passed downwards through the intermediate steam-reheater (Oshkanov and Govorov, 2009).

Three serial K-210-130 turbines (manufactured at "LMZ" - the largest Russian manufacturer of power turbines for electric power stations) are connected to the reactor. The turbines were designed with a steam-reheat option in order to increase the thermal efficiency of the cycle and to reduce the amount of moisture in the last stages of the turbine (Dragunov et al. 2012). Major parameters of this turbine are listed in Table 5.3.

Table 5.3. Parameters of K-210-130 Russian turbine (Grigoryev and Zorin, 1989).

Parameters	K-210-130
Power / max power, MW_{el}	210/215
Main steam pressure, MPa	14.2
Main steam temperature, °C	505
Reheated steam pressure, MPa	2.45
Reheated steam temperature, °C	505
Max flow rate through HP turbine, t/h	670
Number of steam extractions	7
Outlet pressure, kPa	5
Cooling-water temperature, °C	10
Cooling-water flow rate, m^3/h	25,000
Feedwater Temperature, °C	240
Total mass, t	560
Total length, m	20
Total length with generator, m	33

It should be noted that thermal-cycle efficiencies calculated in this chapter based on reversible thermodynamic cycles and did not account for any major irreversibilities that would occur in an actual turbine-cycle. Calculations of thermal efficiencies of the Rankine-steam-cycles were based on the following simplifying assumptions:

- no mechanical losses (e.g., bearing losses);
- no steam turbine packing leakage or gland steam-system losses;
- no turbine exhaust losses;
- no generator losses;
- no piping heat losses;
- no steam-generator heat losses; and
- no pump work.

5.2 SUBCRITICAL-PRESSURE SINGLE-REHEAT RANKINE-STEAM-CYCLE WITH HEAT REGENERATION

The objective of this section is to show the subcritical-pressure Rankine-"steam"-cycle used in the BN-600 SFR and to calculate thermal efficiency of this cycle in order to compare it to other cycles.

The thermodynamic layout, which is currently used at the BN-600 SFR in Russia, principally corresponds to the subcritical-pressure Rankine-steam-cycle configuration.

The actual simplified cycle of the BN-600 reactor is shown in Figure 5.1. The regenerative feedwater-heating system consists of four Low Pressure Heaters (LPHs), three High Pressure Heaters (HPHs), and one deaerator. Water enters the SG at 240°C, where its temperature is raised to 505°C and the resulting superheated steam enters the HP turbine at a pressure of 14.2 MPa. Steam is extracted twice from the HP turbine in order to heat the feedwater flowing through HPH2 and HPH3. Steam exiting the HP

turbine steam is reheated once in an intermediate reheater section of the SG, with outlet pressure of 2.45 MPa and temperature of 505°C. The Intermediate Pressure Turbine (IPT) supplies extraction steam for the HPH1 and a fraction of the steam is diverted to heat the water in the deaerator. The IPTs and LPTs also supply steam extractions for the LPH1, LPH2, LPH3, and LPH4. The condensate from the LPH1 is fed back to the condenser. The condensate from the HPH1 is fed back to the deaerator (Dragunov et al. 2012).

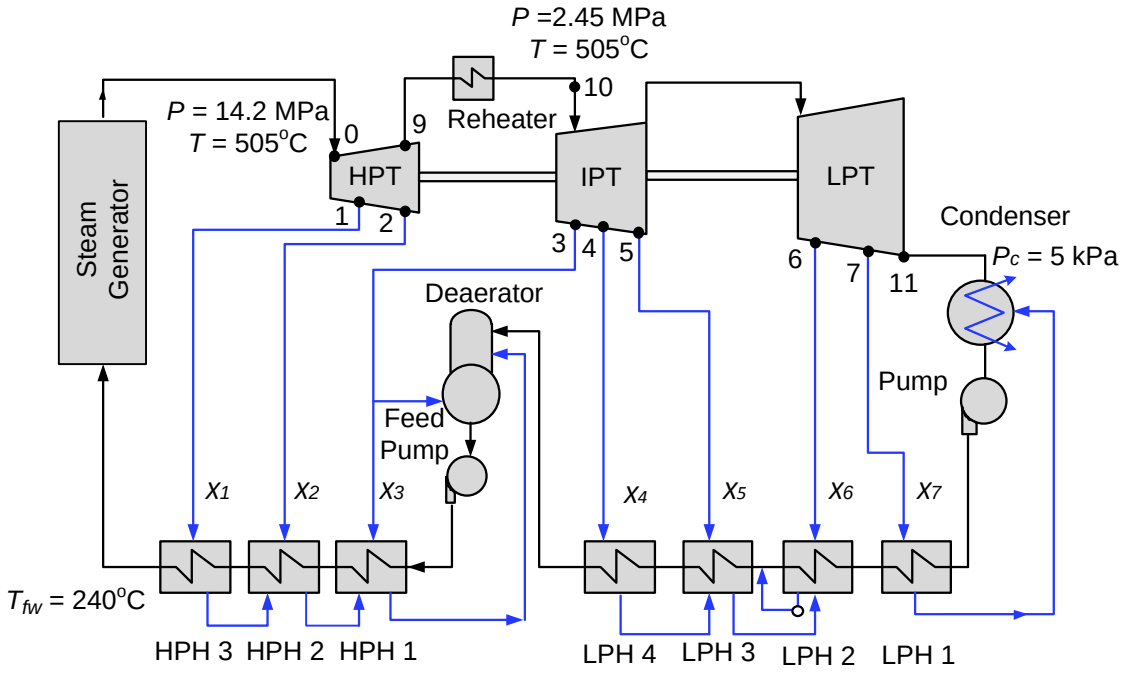

Figure 5.1. Layout of the ideal BN-600 reactor NPP operating on a single-reheat subcritical-pressure Rankine-steam-cycle with heat regeneration (Dragunov et al., 2013b).

The turbine K-210-130 has 7 steam extractions from HP, LP, and IP turbines for regeneration. Parameters of these steam extractions are presented in Table 5.4. It should be noted that the relative steam consumptions were calculated as solutions of heat-balance equations for LP and HP feedwater heaters.

Table 5.4. Parameters of steam extractions of K-210-130 turbine (Kostyuk and Frolov, 2001).

Steam Extractions	Pressure, MPa	Temperature, °C	Enthalpy, kJ/kg	Relative steam consumption α, %
1	3.855	403	3224	4.9
2	2.520	347	3119	7.4
3	1.187	477	3427	3.5
4	0.627	393	3255	3.7
5	0.270	289	3048	4.1
6	0.125	207	2888	3.0
7	0.026	78	2643	3.4

Generally, the efficiency of the Rankine-steam-cycle without pump work is the turbine work output divided by the heat input in the Steam Generator:

$$\eta_{th} = \frac{H_0}{q_1} \tag{5.1}$$

In our case, heat regeneration and steam reheat need to be taken into account. The turbine consists of a HPT, an IPT and an LPT:

$$\eta_{th} = \frac{{H_0}^{HPT} + {H_0}^{IPT+LPT}}{q_1} \tag{5.2}$$

Enthalpy of the main steam is found using NIST REFPROP software:

$$h_0 = f(P_0, T_0) = 3335 \ \frac{\text{kJ}}{\text{kg}} \tag{5.3}$$

Enthalpy of the feedwater is found as a function of $P_{fw} = 18.4$ MPa and $T_{fw} = 240°C$:

$$h_{fw} = f(P_{fw}, T_{fw}) = 1040 \ \frac{\text{kJ}}{\text{kg}} \tag{5.4}$$

Then, the heat added in the SG:

$$q_1 = h_0 - h_{fw} = 2295 \ \frac{\text{kJ}}{\text{kg}} \tag{5.5}$$

To find relative steam consumptions ${\alpha_j}^{SE}$ and corresponding enthalpies ${h_j}^{SE}$, data listed in Table 5.4 was used. Then, the power generated by the high pressure turbine can be written as:

$$\begin{gathered} {H_0}^{HPT} = (h_0 - {h_1}^{SE}) + \left({h_1}^{SE} - {h_2}^{SE}\right) \cdot (1 - {\alpha_1}^{SE}) + \\ + \left({h_2}^{SE} - h_9\right) \cdot (1 - {\alpha_1}^{SE} - {\alpha_2}^{SE}) = 365.6 \ \frac{\text{kJ}}{\text{kg}}, \end{gathered} \tag{5.6}$$

where: ${\alpha_j}^{SE}$ – the relative consumption of steam in each steam extraction; h_9 – the enthalpy at the point 9 (exit of the HPT); values ${\alpha_j}^{SE}$ were calculated as the solutions of heat balance equations for HPHs and LPHs (the Table 5.4); ${h_j}^{SE}$ – enthalpy of the steam in each steam extraction.

To find α_k – the relative consumption of steam in the condenser*:*

$$\alpha_k = 1 - \sum_{\text{j=1}}^{\text{n}} \alpha_j = 0.701 \tag{5.7}$$

Calculate the work out for IP and LP turbines was calculated in the same way as for the HPT:

$$H_0{}^{IPT+LPT} = 759.6\ \frac{\text{kJ}}{\text{kg}} \tag{5.8}$$

It follows that the thermal efficiency of the ideal BN-600 SFR subcritical–pressure Rankine – "steam" – regenerative-cycle without pump work is:

$$\eta_{th} = \frac{H_0{}^{HPT} + H_0{}^{IPT+LPT}}{q_1} = 49.1\% \tag{5.9}$$

Developed MATHCAD code is presented in Appendix B for calculation of thermal efficiency of a Rankine-steam cycle. An immediate conclusion of the calculations presented here is that the thermal efficiency of the ideal BN-600 SFR NPP turbine cycle is closely approaching that of current supercritical water thermal power plants, and application of supercritical steam leads to higher thermal efficiencies (Dragunov et al. 2012).

5.3 SUPERCRITICAL-PRESSURE RANKINE-"STEAM"-CYCLE WITH HEAT REGENERATION

Steam turbines in NPPs have the same theoretical thermal-efficiency limit as coal-fired power plants. Currently, NPPs operate at temperatures and pressures significantly lower than coal-fired power plants, i.e., the NPP turbine inlet – saturated steam at 286°C and 7 MPa compared to thermal power plants turbine inlet – supercritical "steam" at 625°C and 25 MPa.

The Rankine cycle can be greatly improved by operating in the supercritical region of the coolant (Hough, 2009). Most modern thermal power plants employ the SuperCritical Rankine-"steam"-cycle which raises the thermal efficiency of the plant (Grigoryev and

Zorin, 1989). The steam-cycle configuration of the SC cycle is very similar to that of the subcritical cycle in modern fossil-fueled power plants. Steam is usually reheated once in a boiler after passing through the HP turbine to achieve higher efficiency. The regenerative feedwater-heating system consists of LP and HP feedwater heaters and a deaerator. Typically, SC "steam" cycles involve 8 to 10 stages of feedwater heating, while subcritical-steam cycles usually involve 6-8 stages. Based on the review in the previous section on subcritical Rankine cycle, it follows that for an SFR to be matched with modern SC turbines, the reactor has to be operating on a single-reheat cycle with the same temperature (505ºC) at the heat exchanger and the reheater outlets. This possible option, in terms of the secondary thermodynamic side, has to be considered. The objective of this section is to analyze possible supercritical Rankine-"steam"-cycle arrangement and to evaluate conceptually its complexity and adaptability to the current SFR concept.

The scheme considered in this section is used in thermal power plants in Russia and corresponds to the SC-pressure Rankine-"steam"-regenerative-cycle configuration. Steam extractions are taken from HP, IP and LP turbines (Figure 5.2).

The K-1200-240 turbine, a standard for thermal power plants, is utilized in the reactor. The turbine was designed with a steam-reheat option in order to increase the thermal efficiency of the cycle and to reduce the amount of moisture in the last stages of the turbine. Major parameters of this turbine are listed in Table 5.5.

As shown in Table 5.6, the K-1200-240 turbine has 9 steam extractions from HP, IP and LP turbines for heat regeneration. Parameters of these steam extractions are listed in Table 5.6.

Table 5.5. Parameters of K-1200-240 Russian turbine (Grigoryev and Zorin, 1989).

Parameters	K-1200-240
Power/Max Power, MW_{el}	1200/1380
Main Steam Pressure, MPa	23.54
Main Steam Temperature,°C	505
Reheat Steam Pressure, MPa	3.51
Reheat Steam Temperature,°C	505
Max Flow Rate Through HP Turbine, t/h	3950
Number of Steam Extractions	9
Outlet Pressure, kPa	3.58
Cooling Water Temperature,°C	12
Cooling Water Flow Rate, m^3/h	108,000
Feedwater Temperature,°C	274
Total Mass, t	1900
Total Length, m	47.9
Total Length with Generator, m	78.1

Table 5.6. Parameters of steam extractions of K-1200-240 turbine (Kostyuk and Frolov, 2001).

Steam Extraction	Pressure, MPa	Temperature, °C	Enthalpy, kJ/kg	Relative steam consumption α, %
1	6.29	354	3047	9.0
2	3.90	295	2951	6.4
3	1.82	450	3360	5.0
4	0.90	355	3170	0.4
5	0.49	280	3023	2.3
6	0.26	218	2904	2.1
7	0.13	150	2774	1.9
8	0.05	80	2643	1.8
9	0.02	60	2505	2.1

A simplified SC Rankine cycle for an SFR is shown in Figure 5.2. Steam is reheated once after passing through the HP turbine to achieve higher efficiency. The regenerative feedwater-heating system consists of five LPH, three HPH and one deaerator.

The water flows through the steam generator, being heated from 274°C to 505°C and enters the HP turbine at pressure of 23.54 MPa. Steam is extracted twice from the HP turbine in order to heat the feedwater flowing through HPH2 and HPH3. After passing through the HP turbine, steam to achieve higher efficiency, this steam is reheated once in an intermediate reheater at the output pressure of 3.51 MPa and the same temperature of 505°C.

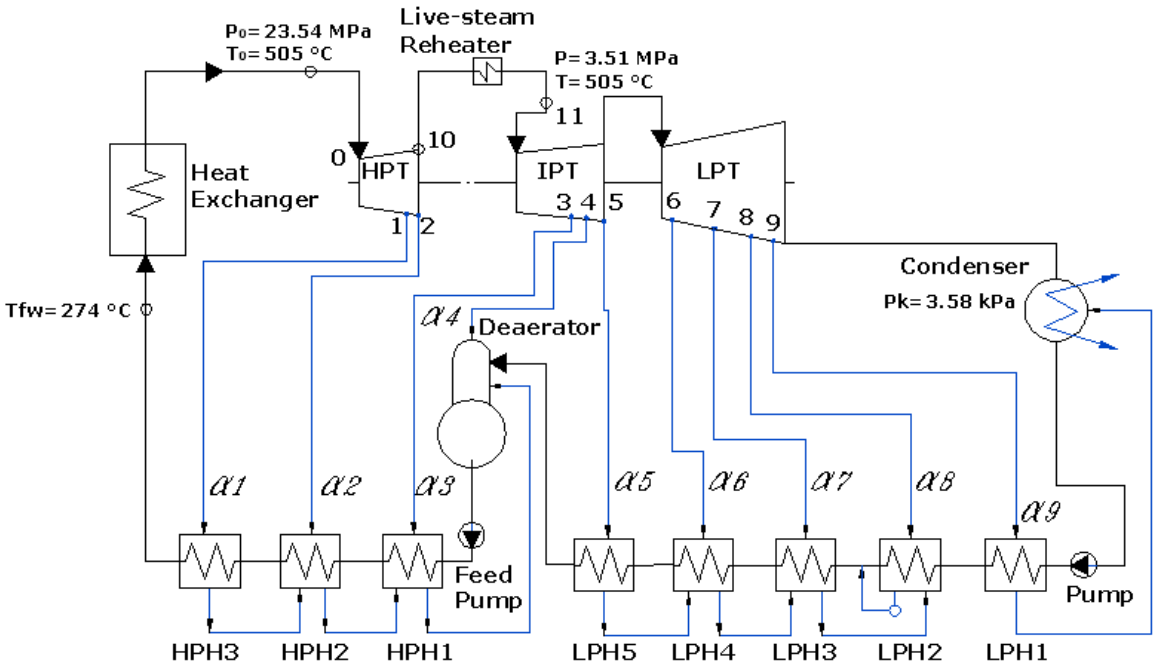

Figure 5.2. Ideal single-reheat supercritical-pressure Rankine-"steam"-cycle with heat regeneration (Dragunov et al., 2012).

Calculation of the thermal efficiency of the SC-pressure Rankine-"steam"-cycle, which can be used in SFRs, was performed. As shown in Eq. (5.2), the efficiency of the Rankine cycle with heat regeneration without pump work is the turbine work out divided by the heat input in the heat exchanger. In calculations, a similar procedure and same notation as in the previous section is used.

It follows that the thermal efficiency of the ideal SC-pressure Rankine-"steam"-regenerative cycle without the pump work is:

$$\eta_{th} = \frac{{H_0}^{HPT} + {H_0}^{IPT+LPT}}{q_1} = 52.7\% \tag{5.10}$$

As the calculations suggest, the basic method of increasing the thermal efficiency of steam-power plants is to increase the operating pressure. The Rankine-"steam"-cycle has progressed into the SC region of the coolant and is generating higher thermal efficiencies. As a result, the thermal efficiency of the SC-pressure Rankine-"steam"-cycle is higher than that of subcritical pressure for the BN-600 SFR by 7.3%.

SC "steam" is considered as a working fluid for power-conversion systems in order to reach high levels of performance on thermal efficiency, safety and reliability. With innovations to reduce capital cost, the SFR can be more competitive in the area of producing electricity. And SC-pressure Rankine-"steam"-cycle has the potential to provide high thermal efficiencies if this turbine cycle is connected the nuclear power plant. From the latest news, in the Russian lead-cooled "BREST-OD-300" reactor similar turbine cycle is planned to be used.

5.4 SUPERCRITICAL-PRESSURE CO_2 BRAYTON-GAS-TURBINE CYCLE

The major safety concern associated with using water as the working fluid is the possible failure of a sodium-to-water HX. Sodium reacts with water to release gaseous hydrogen and large amounts of heat, which may lead to the failure of the HX. To improve safety, a secondary sodium system acts as a buffer between the radioactive sodium in the first loop and the steam (or water) in the third loop. This serves as a reason to search for alternative fluids to be used in the power conversion side of an NPP with SFR. Carbon dioxide, which does not undergo through auto-combustion below 500°C when in contact with sodium (Simon et al. 2007), may be used in a supercritical Brayton cycle. The idea of

using a Brayton cycle coupled with liquid-metal cooled reactors has recently become very attractive.

5.4.1 Ideal cycle

In the analysis of the ideal SC CO_2 Brayton cycle the main assumptions were as follows:

- Gas Turbine (GT) efficiency is 100%;
- compressor efficiency is 100%;
- no mechanical losses;
- no heat losses to the surroundings; and
- all heat exchangers have 100% effectiveness.

The layout of a simple ideal SC CO_2 Brayton-gas-turbine closed-cycle is shown in Figure 5.3 and the cycle consists of a compressor, a recuperator, a heater, a gas turbine, and a cooler. CO_2 leaves the cooler in a supercritical state.

In the compressor a fraction of the SC fluid is compressed from 7.7 MPa to 20 MPa (point 2, Figure 5.3). The fluid enters recuperator where waste heat from the turbine exhaust stream heats the compressed CO_2 to 287°C. The fluid then enters the Na-to-CO_2 heat exchanger (point 3) at a temperature of 287°C, where heat addition to the cycle takes place. The fluid leaves the heater (point 4) at the highest temperature of 505°C (the same as the inlet temperature for the steam in actual BN-600 SFR NPP). The SC CO_2 turbine operating conditions are: P_3 = 20 MPa, T_3 = 505°C. SC fluid expansion takes place in the turbine and generates rotational energy. After leaving the turbine (point 5), the fluid is at $T_5 = 384°C$ and $P_5 = 7.7$ MPa and goes into a recuperator, where heats the fluid from the compressor. The fluid enters the cooler at the temperature of 60°C. Then fluid finishes the cycle entering compressor at a temperature 32°C.

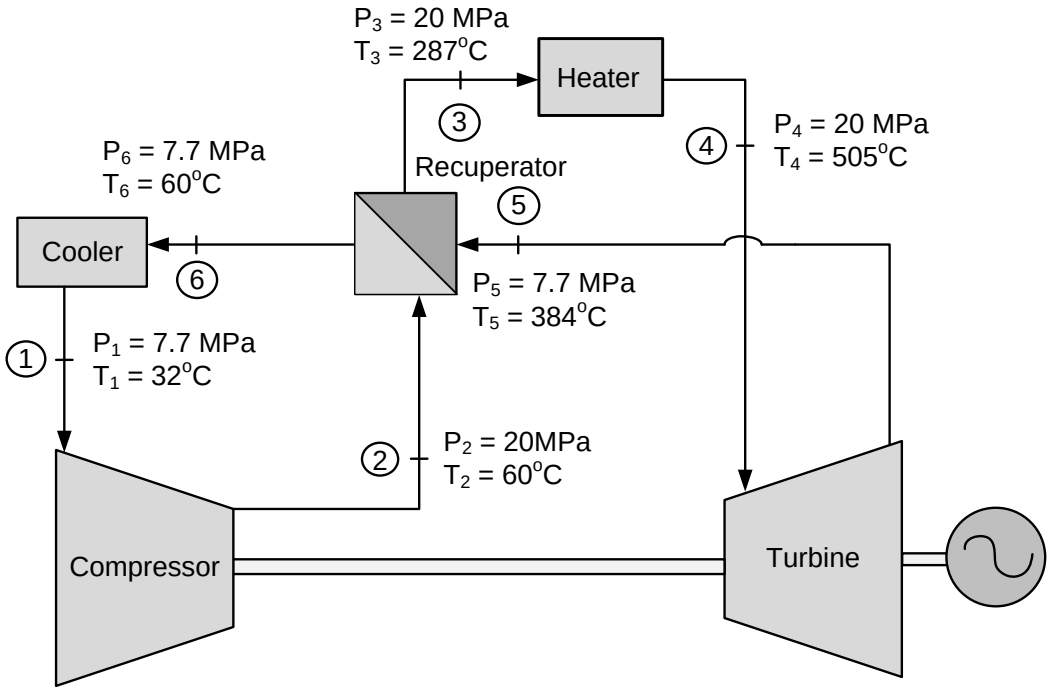

Figure 5.3. Ideal supercritical-pressure CO_2 Brayton-gas-turbine cycle (Dragunov et al., 2013b).

Parameters of state points of the cycle are listed in Table 5.7.

Table 5.7. State points of the ideal SC CO_2 Brayton-gas-turbine cycle.

Point	Pressure, MPa	Temperature, °C	Specific enthalpy, kJ/kg	Specific entropy, kJ/kg·K
1	7.7	32	306.2	1.346
2	20	60	324.5	1.346
3	20	287	711.5	2.267
4	20	505	979.5	2.671
5	7.7	384	849.3	2.671
6	7.7	60	462.3	1.840

It is seen that the heat addition to the cycle is:

$$q_{add} = h_4 - h_3 = 268 \ \frac{\text{kJ}}{\text{kg}} \tag{5.11}$$

Assuming that the potential- and kinetic-energy losses are negligible, the turbine work calculated as the SC CO_2 enthalpy change in the turbine:

$$H_{GT} = h_4 - h_5 = 130.13 \ \frac{\text{kJ}}{\text{kg}} \tag{5.12}$$

The compressor work is:

$$H_{comp} = h_2 - h_1 = 18.3 \ \frac{\text{kJ}}{\text{kg}} \tag{5.13}$$

It follows that the overall thermal efficiency of the ideal SC CO_2 Brayton-gas-turbine cycle in terms of enthalpies becomes:

$$\eta_{th} = \frac{H_{\text{GT}} - H_{\text{Comp}}}{q_{\text{add}}} = 42\% \tag{5.14}$$

Major parameters of the cycle are listed in Table 5.8.

The recuperator captures the waste heat from the turbine exhaust stream to preheat the compressor discharge CO_2 before the latter enters the heater. Use of heat regeneration greatly improves the thermal efficiency of the cycle. Analysis of a simple ideal Brayton cycle showed that only 17% of thermal efficiency is attained when there is no recuperator used (Dragunov et al. 2012). It was shown that if the SC CO_2 gas-turbine inlet temperature is more than 500-550℃, it becomes competitive with SC Rankine-"steam"-cycle (Dostal et al. 2004).

A further improvement in the thermal efficiency of the cycle can be achieved by adding more stages of reheat, as well as an additional stage of compression. In investigations it was shown that the recompression cycle has potential to improve the thermal efficiency (Dostal and Kulhanek, 2009).

Table 5.8. Major parameters of the SC CO_2 Brayton-gas-turbine cycle.

Parameters	SC CO_2 Brayton cycle
Pressure ratio	2.6
Heat addition to the cycle, kJ/kg	268
Turbine work, kJ/kg	130.1
Compressor work, kJ/kg	18.3
Thermal efficiency, %	42
Highest pressure, MPa	20
Highest temperature, °C	505
Lowest pressure, MPa	7.7
Lowest temperature, °C	32

The highest and lowest pressures and temperatures discussed above correspond to those for the reference layout of BN-600. It is reasonable to analyze the effect of changing of the highest pressure and temperature on the efficiency of the cycle. For this reason, the inlet pressure to the turbine was varied from 16 to 24 MPa in steps of 2 MPa, and the inlet temperature was varied from 505°C to 550°C. The lowest pressure and temperature were unchanged. The results of calculations are presented in the Table 5.9.

From the Table 5.9, it can be seen that higher thermal efficiencies were achieved at higher operating temperatures. The highest thermal efficiency was 45.5%, achieved for a turbine inlet temperature of 550°C. This is fairly competitive with the traditional Rankine-steam cycle now utilized in BN-600. Moreover, assuming that this Rankine-steam cycle utilizes 8 stages of regeneration and 1 stage of reheat, while the ideal SC CO_2 Brayton-gas-turbine cycle has just one recuperator, we can state that Brayton layout has much more potential for improve. For example, one stage of recompression can give as a minimum 1% thermal efficiency profit, which is significant.

Table 5.9. Parameters of various ideal SC CO_2 Brayton-gas-turbine cycles by temperature and pressure.

Turbine inlet temperature, °C	Turbine inlet pressure, MPa	Pressure ratio	Heat addition to the cycle, kJ/kg	Turbine work, kJ/kg	Compressor work, kJ/kg	Thermal efficiency, %
505	**16**	2.17	231.62	101.73	12.64	38.5
505	**18**	2.33	251.29	116.94	15.48	40.4
505	**20**	2.60	267.96	130.13	18.27	41.8
505	**22**	2.86	282.66	142.06	21.01	42.8
505	**24**	3.12	295.50	152.65	23.71	43.6
520	**16**	2.17	233.85	103.96	12.64	39.1
520	**18**	2.33	253.82	119.47	15.48	40.9
520	**20**	2.60	270.91	133.08	18.27	42.4
520	**22**	2.86	285.82	145.22	21.01	43.5
520	**24**	3.12	298.93	156.08	23.71	44.3
535	**16**	2.17	236.09	106.20	12.64	39.6
535	**18**	2.33	256.43	122.08	15.48	41.6
535	**20**	2.60	273.72	135.89	18.27	42.9
535	**22**	2.86	288.99	148.39	21.01	44.1
535	**24**	3.12	302.37	159.52	23.71	44.9
550	**16**	2.17	238.23	108.34	12.64	40.2
550	**18**	2.33	258.95	124.60	15.48	42.1
550	**20**	2.60	276.56	138.73	18.27	43.6
550	**22**	2.86	292.14	151.54	21.01	44.7
550	**24**	3.12	305.71	162.86	23.71	45.5

5.4.2 Non-ideal cycle

In the analysis of the non-ideal SC CO_2 Brayton cycle main assumptions were as follows:

- turbine efficiency is 90%;
- compressor efficiency is 90%;
- no mechanical losses;
- no any additional losses to the surroundings; and
- the lowest temperature difference in the recuperator is 10 °C.

The layout of a simple non-ideal SC CO_2 Brayton-gas-turbine closed-cycle is shown in Figure 5.4 and consists of the same components as the layout for ideal cycle.

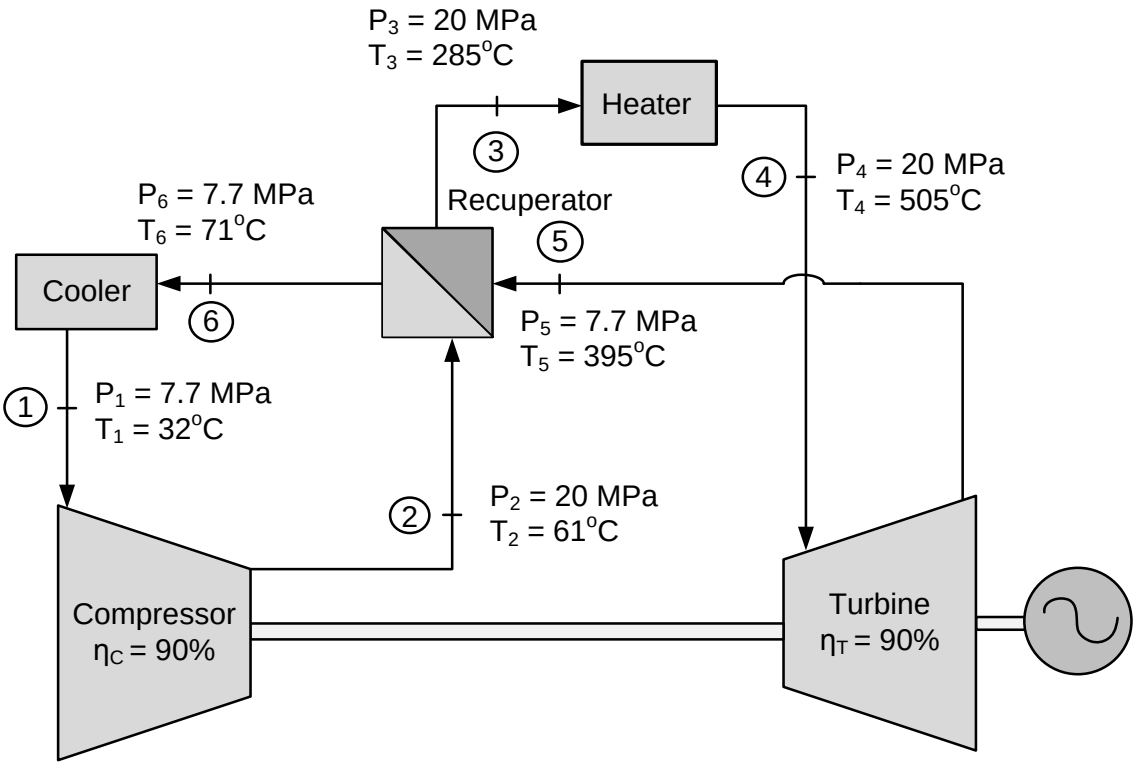

Figure 5.4. Non-ideal supercritical-pressure CO_2 Brayton-gas-turbine cycle (Dragunov et al., 2013b).

Parameters of state points of the cycle are listed in Table 5.10.

Table 5.10. State points of the non-ideal SC CO_2 Brayton-gas-turbine cycle.

Point	Pressure, MPa	Temperature, °C	Specific Enthalpy, kJ/kg	Specific Entropy, kJ/kg·K
1	7.7	32	306.2	1.346
2	20	61	326.5	1.352
3	20	285	708.2	2.262
4	20	505	979.5	2.671
5	7.7	395	862.3	2.691
6	7.7	71	480.6	1.901

Major parameters of the cycle are listed in Table 5.11.

Table 5.11. Major parameters of the SC CO_2 Brayton-gas-turbine cycle.

Parameters	Non-ideal SC CO_2 Brayton cycle
Pressure ratio	2.6
Heat addition to the cycle, kJ/kg	271
Turbine work, kJ/kg	117.1
Compressor work, kJ/kg	20.3
Thermal efficiency, %	36

It follows that the overall thermal efficiency of the non-ideal SC CO_2 Brayton-gas-turbine cycle in terms of enthalpies becomes:

$$\eta_{th} = \frac{H_{\mathrm{GT}} - H_{\mathrm{Comp}}}{q_{\mathrm{add}}} = 36\% \tag{5.21}$$

It can be seen that although the efficiency of a Brayton cycle is lower, than that of Rankine cycles, utilizing SC CO_2 in the power conversion cycle increases the safety of the NPP, what should be taken into account.

Now let's consider the effect of variation of pressure (ranging from 16 MPa to 24 MPa) and temperature (ranging from 505°C to 550°C) on thermal efficiency of the same non-ideal SC CO_2 Brayton-gas-turbine cycle with regeneration layout. The results of calculations are given in the Table 5.12 below.

Table 5.12. Parameters of various non-ideal SC CO_2 Brayton-gas-turbine cycles by temperature and pressure.

Turbine inlet temperature, °C	Turbine inlet pressure, MPa	Pressure ratio	Heat addition to the cycle, kJ/kg	Turbine work, kJ/kg	Compressor work, kJ/kg	Thermal efficiency, %
505	**16**	2.17	256.2	91.56	14.04	30.3
505	**18**	2.33	256.8	105.2	17.20	34.3
505	**20**	2.60	271.2	117.1	20.30	35.7
505	**22**	2.86	284.0	127.9	23.34	36.8
505	**24**	3.12	295.2	137.4	26.34	37.6
520	**16**	2.17	258.2	93.56	14.04	30.8
520	**18**	2.33	259.1	107.5	17.20	34.8
520	**20**	2.60	273.9	119.8	20.30	36.3
520	**22**	2.86	286.9	130.7	23.34	37.4
520	**24**	3.12	298.3	140.5	26.34	38.2
535	**16**	2.17	260.2	95.58	14.04	31.3
535	**18**	2.33	261.4	109.9	17.20	35.4
535	**20**	2.60	276.4	122.3	20.30	36.9
535	**22**	2.86	289.7	133.6	23.34	38.0
535	**24**	3.12	301.4	143.6	26.34	38.9
550	**16**	2.17	262.1	97.51	14.04	31.8
550	**18**	2.33	263.7	112.1	17.20	36.0
550	**20**	2.60	279.0	124.9	20.30	37.5
550	**22**	2.86	292.5	136.4	23.34	38.6
550	**24**	3.12	304.4	146.6	26.34	39.5

5.4.3 Discussion of the ideal and non-ideal SC CO_2 Brayton-gas-turbine cycles

Results of calculations of thermal efficiencies for ideal and non-ideal SC CO_2 Brayton cycle are presented in Tables 5.9 and 5.12, respectively. As one would expect, in both cases the higher pressures and temperatures led to higher efficiencies for the cycles. The highest efficiency of the non-ideal cycle was achieved at P_{max} = 24 MPa and T_{max} = 550°C and was equal to 39.5%. This value lies between 39.1% and 39.6%, which are efficiencies of the ideal cycles with P_{max} = 16 MPa, for both cases, and T_{max} = 520°C and 535°C, respectively. The increase of 8 MPa is required to compensate only for inefficiencies of the major components of the cycle.

The lowest efficiency of the ideal cycle for 20 MPa corresponds approximately to the efficiency of the AGR, which has the highest thermal efficiency among all operating NPPs (Pioro, 2012), and the lowest efficiency of the non-ideal cycle corresponds to the efficiency of the existing PHWRs. The dependence of cycle efficiency on T_{max} is shown on Figure 5.5.

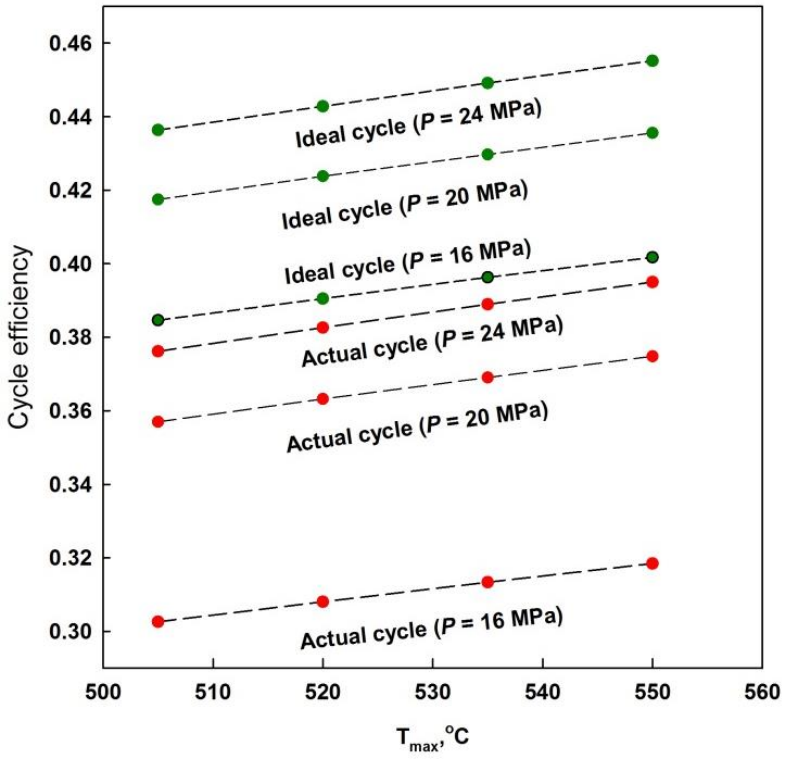

Figure 5.5. Effect of temperature on the efficiency of the cycle.

Since the highest temperature of the SC CO_2 is significantly limited in an SFR, there is need to strive for the highest possible efficiency at reasonable pressures. Therefore, a further investigation on possible advances of SC CO_2 (e.g., with additional compression and reheat stages) is necessary.

5.5 COMPARISON OF THE POWER-CONVERSION CYCLES FOR SODIUM-COOLED FAST REACTORS

Before comparing the efficiency of the cycles, it is important to note that the cycles are compared based on their thermal efficiencies, not net efficiencies, which depend on all nuclear power plant loads. Also, all main assumptions previously stated for all the cycles needs to be taken into account.

A comparison of the thermodynamic cycles is shown in Table 5.13.

Table 5.13. Thermodynamic comparison of the cycles with the same turbine inlet temperature of 505°C as in BN-600 SFR.

Cycle	**Ideal Subcritical - pressure Rankine - "steam" – regenerative - cycle**	**Ideal SuperCritical - pressure Rankine - "steam" – regenerative - cycle**	**Ideal SuperCritical CO_2 Brayton – gas - turbine cycle**
Turbine pressure (inlet), MPa	14.2	23.5	24.0
Working fluid	Subcritical-pressure steam	SC "steam"	SC carbon dioxide
Thermal efficiency, %	49.1	52.7	43.6

The thermal efficiency of the ideal subcritical-pressure Rankine-"steam"-cycle utilized in the BN-600 SFR, is 49.1%. This is approaching that of supercritical water thermal power plants, and is considerably higher than that of current water-cooled reactors.

The basic method of increasing the thermal efficiency of steam-power plants is by increasing the turbine operating pressure and temperature. As seen in Table 5.13, the thermal efficiency of the SC-pressure Rankine-“steam”-cycle is higher than that of subcritical pressure BN-600 SFR by 7.3%. The SC-pressure Rankine-“steam”-cycle has the potential to provide higher thermal efficiencies if this turbine cycle can be connected a nuclear power plant. Moreover, considered “steam” turbines are standard ones for the thermal-power industry, are a good fit for an SFR NPP.

The highest calculated thermal efficiency of the ideal SC CO_2 Brayton-gas-turbine cycle is 43.6% (achieved for the turbine inlet temperature of 505°C at 24 MPa), which is lower, but competitive with the traditional Rankine-steam cycle, currently utilized in the BN-600 SFR NPP.

A further improvement in the thermal efficiency of the considered cycles can be achieved by adding one more stage of reheat to the Rankine cycle or an additional stage of compression to the Brayton cycle.

Regarding the SC CO_2 Brayton-gas-turbine cycle, it is important to note that SC carbon dioxide closed-cycle gas turbines are not yet manufactured, but they are currently under development. If successful, then turbines can affect some possible changes in net efficiency.

CHAPTER 6. CONCLUSIONS

The investigation reported in Chapter 3 showed that sodium coolant has very appropriate thermal and nuclear properties important for fast reactors, that provides sodium with advantages over other liquid metal coolants. Using MATLAB (2007) software, a code was developed to calculate heat-transfer coefficients for the GEN-IV nuclear reactor coolants. It was shown that sodium, due to the highest thermal conductivity among the considered coolants, appeared to have the highest heat transfer coefficients for a bare tube among the considered nuclear reactor coolants. This will allow for more rapid heat removal from fuel rods, which is particularly important for fast reactors. The high boiling point of sodium allows the reactor to operate at low pressures (less than 1 MPa) and achieve high coolant outlet temperatures, which leads to thermal efficiency for a BN-600 SFR NPP of 40%.

The temperature – entropy diagram for the actual subcritical Rankine-steam cycle used in the BN-600 SFR NPP was plotted and compared to other diagrams of NPPs in Chapter 4. As expected, the high temperatures for the sodium coolant led to the high values for the parameters of the working fluid in the power-conversion cycle. Comparing the thermodynamic cycles of six types of NPPs showed that implementing steam reheat by an intermediate liquid-sodium coolant (in the case of BN-600 NPP) rather than by partially extracted working fluid, i.e., saturated steam (as in CANDU and VVER-1000 reactor NPPs) allows a drastic increase in the cycle thermal efficiency (up to 8%). It was shown that reheat temperatures of steam used in the BN-600 NPP are the same and not lower than the main steam temperatures, which increased the thermal efficiency of the cycle. The BN-600 SFR NPP turbine cycle appeared to be the most efficient turbine cycle among those considered (with exception for an AGR, but they will not be built anymore). Although the thermal-performance of the BN-600 power-conversion cycle outperforms most of the other cycles, and the thermal efficiency of the BN-600 NPP is 40%, because one of the goals of GEN-IV reactor concepts is to increase thermal efficiency and safety, it was reasonable to investigate different options for the power-conversion side for an SFR.

Nowadays, SCW and SC CO_2 are considered as the most promising working fluids for power conversion in an SFR which would allow high-level performance in both thermal efficiency and safety. Research was conducted on the thermodynamic analysis of different power-conversion cycle layouts for an SFR with the same turbine inlet temperatures. Three possible solutions for the power-conversion cycle for the SFR were investigated. For the given core outlet temperatures of the BN-600 reactor, the thermal efficiencies of the subcritical Rankine-steam cycle, SC Rankine -"steam" - cycle, and the supercritical ideal and non-ideal CO_2 Brayton gas-turbine cycles were calculated. The codes in MATHCAD program were developed to calculate thermal efficiencies for all the cycles. It was shown that the thermal efficiency of the ideal BN-600 SFR NPP turbine cycle (49.1%) is closely approaching that of current supercritical water thermal power plants, while the calculated thermal efficiency of the SC-pressure Rankine-"steam"-cycle (52.7%) is higher than that of the subcritical pressure cycle for the BN-600 SFR by 7.3%. SC-pressure Rankine-"steam"- cycle layout, provided in this thesis, is utilized at SC ThPPs in Russia. If it can be connected to an SFR, it would provide higher thermal efficiencies. From the latest news, in the Russian lead-cooled "BREST-OD-300" reactor, a similar turbine cycle is planned to be used.

With regards to the ideal SC CO_2 Brayton gas-turbine cycle, it appears to provide a lower thermal efficiency (43.6% achieved for turbine inlet P=24 MPa and T=505°C), compared to the Rankine cycles. However, using a SC CO_2 Brayton gas-turbine cycle there is no possible reaction of sodium with water in the heat exchanger, thereby improving the safety of the reactor. A further improvement in the thermal efficiency of the SC CO_2 Brayton gas-turbine cycle can be achieved by adding an additional stage of compression to the Brayton cycle.

The thermal efficiencies of ideal and non-ideal CO_2 Brayton gas-turbine cycles were optimized by varying CO_2 pressures from 16 to 24 MPa and temperatures from 505°C to 550°C at the outlet of Na-CO_2 heat exchanger. It was shown, that since the highest temperature of the SC CO_2 is significantly limited in an SFR, there is need to strive for the highest possible efficiency at reasonable pressures (24 MPa and possibly higher).

Overall, coupling the SFR with a SC-pressure Rankine-“steam”- cycle will increase the overall thermal efficiency of a NPP, making these reactors competitive alternatives to ThPPs, while utilizing SC CO_2 Brayton gas-turbine cycle will increase the safety of a NPP, providing competitive efficiencies.

CHAPTER 7. FUTURE WORK

Future work on this topic may be devoted to the development of more complex and advanced power-conversion cycles for an SFR. This would require investigation to determine an optimal number of reheat stages for Rankine steam cycles and the number of recompression stages for the SC CO_2 Brayton-gas-turbine cycle.

Regarding the SC CO_2 Brayton-gas-turbine cycle, future work may be devoted to the development of the design issues of the SC CO_2 closed-cycle gas turbines, as they are currently under development.

Also, part of the future work might be devoted to the development of a design of the nuclear steam reheat in water-cooled nuclear power reactors by passing a high-pressure-turbine exhaust through a number of channels.

REFERENCES

Abramov, M.A., Avdeev, V.I., Adamov E.O. and others, 2006. Channel-Type RBMK Nuclear Power Reactor (in Russian), Joint Stock Company "NIKIET", Moscow, Russia, 632 pages.

AECL Report, 1969. Pickering Generation Station. Design Description. Report prepared by Atomic Energy of Canada Limited.

Beznosov, A.V., Dragunov, Yu.G. and Rachkov, V.I. 2007. Heavy-liquid metal coolants in nuclear engineering. Moscow, IzdAt Publishing House, Moscow, Russia, 434 pages. (in Russian).

Cengel, Yu.A. and Boles, M.A., 2011. Thermodynamics. An Engineering Approach, McGraw-Hill, New York, NY, USA, 1023 pages.

Cengel, Yu.A. and Ghajar, A.J., 2011. Heat and Mass Transfer. Fundamentals& Applications, McGraw-Hill, New York, NY, USA, 924 pages.

Dementyev, B.D., 1990. Nuclear Power Reactors. Energoatomizdat Publishing House, Moscow, Russia, 352 pages.

Department of Energy (DOE). Office of Nuclear Energy. Generation IV reactor concepts. http://nuclear.energy.gov/genIV/neGenIV4.html

Dittus, F.W. and Boelter, L.M.K., 1930. Heat Transfer in Automobile Radiators of the Tubular Type, University of California, Berkeley, Publications in Engineering, Vol. 2, No. 13, pp. 443-461 (or Int. Communications in Heat and Mass Transfer, 1985, Vol. 12, pp. 3-22).

Dostal, V., Driscoll, M.J., Hejzlar, P. 2004. A Supercritical Carbon Dioxide Cycle for Next Generation Nuclear Reactors, MIT-ANP-TR-100. Massachusetts Institute of Technology, Dept. of Nuclear Engineering. Boston, USA.

Dostal, V., Kulhanek, M. 2009. Research on the Supercritical Carbon Dioxide Cycles in the Czech Republic, Proceedings of the S-CO_2 Cycle Symposium, ASME, Rensselaer Polytechnic Institute, Troy NY, April 29-30.

Dragunov, A., Saltanov, Eu., Bedenko, S. and Pioro, I., 2012. A Feasibility Study on Various Power-Conversion Cycles for a Sodium-Cooled Fast Reactor, Proceedings of the 20th International Conference On Nuclear Engineering (ICONE-20), ASME, July 30–August 3, Anaheim, California, USA, Paper #55130, 10 pages.

Dragunov, A., Saltanov, Eu., Pioro, I., and Pioro, I., Ikeda, B., Miletic, M. and Zvorykina, A., 2013a. Investigation of Thermophysical and Nuclear Properties of Prospective Coolants for Generation-IV Nuclear Reactors, Proceedings of the 21st International Conference on Nuclear Engineering (ICONE–21), ASME, July 29 - August 2, Chengdu, China, Paper #16020, 11 pages.

Dragunov, A., Saltanov, Eu., Pioro, I., Harvel, G. and Ikeda, B., 2013b. Study on Primary and Secondary Heat-Transport Systems for Sodium-Cooled Fast Reactor, Proceedings of the 21st International Conference on Nuclear Engineering (ICONE–21), ASME, July 29 - August 2, Chengdu, China, Paper #16014, 9 pages.

GIF – Generation IV International Forum, 2002. A Technology Roadmap for Generation IV Nuclear Energy Systems, Issued by the Generation IC International Forum and the U.S. DOE Nuclear Energy Research Advisory Board, 97 pages.

Gerasimov, V.V. and Monachov, A.S., 1982. Materials of nuclear technology, Energoatomizdat Publishing House, Moscow, Russia (In Russian).

Grigoryev, V.A. and Zorin, V.M., 1989. Thermal and Nuclear Power Plants, (In Russian), Energoatomizdat Publ. House, Moscow, Russia, 608 pages.

Handbook on Lead-bismuth Eutectic Alloy and Lead Properties, 2007. Materials Compatibility, Thermal-hydraulics and Technologies, 2007 Edition, Nuclear science.

Hejzlar, P., Dostal, V., Driscoll, M., Dumaz, P., Poullennec, G., and Alpy, N., 2005. Assessment of gas cooled fast reactor with indirect supercritical CO 2 cycle. Proceedings of the American Nuclear Society - International Congress on Advances in Nuclear Power Plants, ICAPP'05. Seoul, South Korea, May 15- 19, volume 1, pages 436-446.

Hewitt, G.F. and Collier, J.G, 2000. Introduction to Nuclear Power, 2nd edition, Taylor and Francis Publishing Office, USA, 304 pages.

http://www.burningcutlery.com/solar

http://www.environment.nationalgeographic.com

http://www.ieso.ca/imoweb/marketdata/genEnergy.asp

http://www.wiki.windpower.org/index.php/variations_in_energy

IAEA (1985) Status of liquid metal-cooled fast reactors. Technical report series No. 246, IAEA, Vienna.

Incropera, E.P., Dewitt, D.P., Bergman, T.L. and Lavine, A.S., 2007. Fundamentals of Heat and Mass Transfer, Sixth Edition, John Wiley & Sons., Hoboken, N.J., pp 514 - 515. Inside WANO, 2004. The Magazine of the World Association of Nuclear Operators (WANO): Volume 12 – Number 3, page 20.

Kindzierski, W., 2007. EPCOR Genesee Generating Station Phase 3. Project Background. CIV E 240 Technical Communications., Dept. Civil & Environmental Engineering.

Kirillov, P., Terent'eva, M., and Deniskina, N., 2007, Thermophysical Properties of Nuclear Engineering Materials (in Russian), 2nd ed., IzdAT Publishing House, Moscow, Russia.

Kostyuk, A.G. and Frolov, V.V., 2001. Turbines of Thermal and Nuclear Power Plants, (In Russian). MEI Publ. House, Moscow, Russia, 488 pages.

Kruglikov, P.A., Smolkin, Yu.V. and Sokolov, K.V., 2009. Development of engineering solutions for the thermal scheme of power unit of thermal power plant with supercritical parameters of steam, (In Russian), Proc. Int. Workshop "Supercritical Water and Steam in Nuclear Power Engineering: Problems and Solutions", Moscow, Russia, October 22–23, 6 pages.

Lamarsh, J., Baratta, A., 2001. Introduction to Nuclear Engineering (3rd Edition), Prentice-Hall, ISBN-10: 0201824981.

Lizon-A-Lugrin, L., Teyssedou, A. and Pioro, I., 2012. Appropriate Thermodynamic Cycles to Be Used in Future Pressure-Channel Supercritical Water-Cooled Nuclear Power Plants, Nuclear Engineering and Design, Vol. 246, pp. 2‑11.

Margulova, T.Ch., 1995. Nuclear Power Plants, (in Russian), Izdat Publishing House, Moscow, Russia, 289 pages.

MATLAB version 7.4, R2007a, computer software, The MathWorks, Inc., Natick, Massachusetts, USA.

Mokry, S., Gospodinov, Ye., Pioro, I. and Kirillov, P., 2009. Supercritical Water Heat-Transfer Correlation for Vertical Bare Tubes, Proceedings of the 17th International Conference on Nuclear Engineering (ICONE-17), ASME, Brussels, Belgium, July 12-16, Paper # 76010, 8 pages.

Naidin, M., Mokry, S., Baig, F., Gospodinov, Ye., Zirn, U., Pioro, I. and Naterer, G., 2009. Thermal-Design Options for Pressure-Channel SCWRs with Co-Generation of Hydrogen, J. of Engineering for Gas Turbines and Power, Volume 131, January, 8 pages.

National Institute of Standards and Technology, 2010. NIST Reference Fluid Thermodynamic and Transport Properties-REFPROP. NIST Standard Reference Database 23, Ver. 9.0. Boulder, CO, U.S.: Department of Commerce.

Neutron Scattering Lengths and Cross-sections website, 2013. Source: www.ncnr.nist.gov/resources/n-lengths/elements.

Nonbel, E., 1996. Description of the Advanced Gas Cooled Type of Reactor (AGR). Risoe National Laboratory. Roskilde, Denmark, 88 pages.

Nuclear News, 2011, March, A Publication of the American Nuclear Society (ANS), pp. 45-78.

Nuclear News, 2013, March, A Publication of the American Nuclear Society (ANS), pp. 47-78.

Oshkanov N.N., Govorov P.P., 2009. Liquid-metal-cooled reactor BN-600 – Major specifics and experience of operation (in Russian). Izvestiya Vuzov, Nuclear Energy issue 2, pp. 7-20.

Pioro I., Zirn U., Duffey R., Naidin M., Mokry S., Gospodinov Ye. and Baig F., 2008. Supercritical water-cooled nuclear reactors: thermodynamic cycles options, 6th International Conference on Heat Transfer. Fluid Mechanics and Thermodynamics (HEFAT2008), ASME, Pretoria, South Africa, 30 June - 2 July, 9 pages.

Pioro, I.L. and Duffey, R.B., 2007. Heat Transfer and Hydraulic Resistance at Supercritical Pressures in Power Engineering Applications, ASME Press, New York, NY, USA, 328 pages.

Pioro, I. and Mokry, S., 2011. Thermophysical Properties at Critical and Supercritical Conditions, Chapter in book *Heat Transfer. Theoretical Analysis, Experimental Investigations and Industrial Systems*, Editor: A. Belmiloudi, INTECH, Rijeka, Croatia, pp. 573–592; free download from: www.intechopen.com.

Pioro, I., 2011. The Potential Use of Supercritical Water-Cooling in Nuclear Reactors. Chapter in *Nuclear Energy Encyclopedia: Science, Technology, and Applications*, Editors: S.B. Krivit, J.H. Lehr and Th.B. Kingery, J. Wiley & Sons, Hoboken, NJ, USA, pp. 309–347.

Pioro, I., 2012. Nuclear Power as a Basis for Future Electricity Production in the World, Chapter in book: *Current Research in Nuclear Reactor Technology in Brazil and Worldwide*, Editors: A.Z. Mesquita and H.C. Rezende, INTECH, Rijeka, Croatia, pp. 211–250; free download from: www.intechopen.com.

Rassokhin, N.G., 1972. Steam generating units for nuclear power plants, (in Russian), Atomizdat Publishing House, Moscow, Russia, 385 pages.

ROSENERGOATOM, 2004. Russian Nuclear Power Plants. 50 Years of Nuclear Power, Moscow, Russia, 120 pages.

Ryzhov, S.B., Mokhov, V.A., Nikitenko, M.P. et al., 2010. Advanced Designs of VVER Reactor Plant, Proceedings of the 8th International Topical Meeting on Nuclear Thermal-Hydraulics, Operation and Safety (NUTHOS-8), Shanghai, China, October 10 – 14.

Shane Hough, 2009. Supercritical Rankine Cycle. A synopsis of the cycle, it's background, potential applications and engineering challenges, ME-517.

Shultis, J.K. and Faw, R.E., 2008. Fundamentals of Nuclear Science and Engineering, 2nd ed., CRC Press, Boca Raton, FL, USA, 591 pages.

Simon, N., Latge, C., and Gicquel, L., 2007. Investigation of Sodium – Carbon Dioxide Interactions With Calorimetric Studies, Proceedings of ICAPP, ASME, May 13 – 18, Nice, France, Paper #7547, 8 pages.

Smith, C., 2010. Lead-Cooled Fast Reactor (LFR) Design: Safety, Neutronics, Thermal Hydraulics, Structural Mechanics, Fuel, Core, and Plant Design. A Compendium of Reactor Technology.

Sun, C., Hui, R., Qu, W. and Yick, S., 2009. Progress in corrosion resistant materials for supercritical water reactors. Corrosion Science vol. 51, pp. 2508-2523.

Todreas, N.E., MacDonald, P.E., Heizlar P., Buongiorno, J. and Loewen, E., 2004. "Medium-power Lead-Alloy Reactors: Missions for this Reactor Technology", Nuclear Technology, Vol. 147, No. 3, 305.

Toshiba Corporation, 2011. Leading innovation. Advanced Boiling Water Reactor (ABWR). Booklet, Toshiba.

Waltar, A.E. and Reynolds A.B., 1981. Fast breeder reactors, Pergamon Press, USA, 700 pages.

Was, G.S., P. Ampornrat, G. Gupta, S. Teysseyre, E.A. West, T.R. Allen, K. Sridharan, L. Tan, Y. Chen, X. Ren and C. Pister, 2007. Corrosion and stress corrosion cracking in supercritical water, Journal of Nuclear Materials vol. 371, pp. 176-21.

Wikimedia Commons, 2012a. Username: Lcolson. Shevchenko BN350 nuclear fast reactor. http://upload.wikimedia.org/wikipedia/commons/c/cb/Shevchenko_BN350.gif

Wikimedia Commons, 2012b. Username: Nife. Monju Nuclear Power Plant. http://upload.wikimedia.org/wikipedia/commons/b/b8/Monju.JPG

Wikimedia Commons, 2013. AGR reactor schematic. http://upload.wikimedia.org/wikipedia/commons/e/e1/AGR_reactor_schematic.svg

World Nuclear Association, 2012. Information Library. Supply of Uranium. Source: http://www.world-nuclear.org/info/Nuclear-Fuel-Cycle/Uranium-Resources/Supply-of-Uranium/.

World Nuclear Association, 2013. The WNA. Uranium: Sustaining the Global Nuclear Renaissance. Source: http://www.world-nuclear.org/WNA/Publications/WNA-Position-Statements/Uranium--sustaining-the-Global-Nuclear-Renaissance/.

Yatchew, A., and Baziliauskas, A., 2011. Ontario Feed-in-Tariff Programs, Energy Policy, Vol. 39, Issue 7, pp. 3885-3893.

APPENDIX A. DEVELOPED MATLAB PROGRAM FOR HEAT-TRANSFER-COEFFICIENT CALCULATIONS FOR TURBULENT FLOW OF SODIUM COOLANT IN A CIRCULAR TUBE

```
clear all;

% Temperature in K, pressure in kPa, mass flux in kg/m^2s, heat flux in W/m^2,

% specific enthalpy in J/kg, specific heat capacity in J/(kg*K),

% dynamic viscosity in (Pa*s), thermal conductivity in W/(m*K)

D_hy=8*10^-3;

T_in=370+273.15;

G=4200;

q=970*10^3;


m=1;

T_bf(m,1)=T_in;

T_sh(m,1)=T_in;

sum=0;

for i=1:360

%   evaluation of properties (T_bulk fluid):

%   thermal conductivity in W/m-K

k_bf=104-(0.047*T_bf(m,i));
```

```
%     Dynamic viscosity in Pa-s

v_bf=exp((556.835/T_bf(m,i))-(0.3958*log(T_bf(m,i)))-6.4406);

%     Cp in J/kg-K

Cp_bf=1658-(0.8479*T_bf(m,i))-
(3.001*10^6/T_bf(m,i)^2)+(4.454*T_bf(m,i)^2/10000);


%     Calculation of Reynolds number

Re=G*D_hy/v_bf;


eps=1;

if i==1

T_w(m,i)=T_bf(m,i)+20;

else

T_w(m,i)=T_bf(m,i)+T_w(m,i-1)-T_bf(m,i-1);

end;


while abs(eps)>=0.1

%   evaluation of properties (T_wall):

v_w=exp((556.835/T_w(m,i))-(0.3958*log(T_w(m,i)))-6.4406);

k_w=104-(0.047*T_w(m,i));
```

```
Cp_w=1658-(0.8479*T_w(m,i))-(3.001*10^6/T_w(m,i)^2)+
+(4.454*T_w(m,i)^2/10000);

%   Prandtl number (T_wall):

Pr_w=v_w/k_w*Cp_w;


%  Sleicher and Rouse correlation:

Nu=6.3+(0.0167*Re^0.85*Pr_w^0.93);


%  HTC calculations:

htc(m,i)=Nu*k_bf/D_hy;


T_w1 = q/htc(m,i) + T_bf(m,i);

eps=T_w1-T_w(m,i);

T_w(m,i)=(T_w1+T_w(m,i))/2;

end;


T_bf(m,i+1)= T_bf(m,i)+0.5;

end;


out=T_bf'-273.15;
```

```
save T_bf.txt out -ascii

out=T_w'-273.15;

save T_w.txt out -ascii

out=htc'/1000;

save htc.txt out -ascii
```

APPENDIX B. CALCULATION OF THERMAL EFFICIENCY OF A BN-600 SFR SUBCRITICAL-PRESSURE RANKINE STEAM CYCLE USING MATHCAD SOFTWARE

The corresponding points in the following calculations of thermal efficiency of a BN-600 SFR Subcritical-pressure Rankine steam cycle are based on the figure Figure 5.1 (presented in chapter 5).

POINT 0 (After SG):

T_0:=505°C

P_0:=14.2*10^6 Pa

S_0:=6.40215 kJ/kg K

H_0:=3335.57*10^3 J/kg

POINT 0’ (at the entrance of HPT):

ΔP:= P_0*0.05=7.1*10^5 Pa

$P_{0'}$:=P_0 – ΔP= 13.49*10^6 Pa

$H_{0'}$:=3336*10^3 J/kg

POINT 9 (After HPT):

T_9:=273°C

P_9:=2.46*10^6 Pa

H_9:=2943.28*10^3 J/kg

POINT 10 (Before IPT):

T_{10}:=505°C

P_{10}:=2.45*10^6 Pa

H_{10}:=3475.61*10^3 J/kg

POINT 2t:

H_{2t}:=2248.835*10^3 J/kg

POINT 2 (After LPT):

T_2:=33°C

P_2:=0.005*10^6 Pa

H_2:=2494.2*10^3 J/kg

CONDENSER:

T_k:=32.9°C

P_k:= 0.005*10^6 Pa

Steam enthalpy:

H_k:= H_{2t} =2248.835*10^3 J/kg

Liquid enthalpy:

$H_{k'}$:=137*10^3 J/kg

FEEDWATER PARAMETERS (SG entrance):

T_{fw}:=240°C

P_{fw}:=1.3* P_0=18.46*10^6 Pa

H_{fw}:=1039.81*10^3 J/kg

Parameters of steam extractions for HPT:

T_{SE1}:=403°C T_{SE2}:=347°C

P_{SE1}:= 3.855*10^6 Pa P_{SE2}:= 2.52*10^6 Pa

H_{SE1}:=3224*10^3 J/kg H_{SE2}:=3119*10^3 J/kg

Take next as solutions of heat balance equations:

σ_{SE1}:= 0.0487 σ_{SE2}:= 0.0739

Then:

H_{HPT} :=$(H_0 - H_{SE1})+(H_{SE1} - H_{SE2})(1 - \sigma_{SE1})+(H_{SE2} - H_9)(1 - \sigma_{SE1} - \sigma_{SE2})$ = 365.6*10^3 J/kg

Parameters of steam extractions for IPT and LPT:

H_{SE3}:=3427*10^3 J/kg

H_{SE4}:=3255*10^3 J/kg

H_{SE5}:=3048*10^3 J/kg

H_{SE6}:=2888*10^3 J/kg

H_{SE7}:=2643*10^3 J/kg

Take next as solutions of heat balance equations:

σ_{SE3}:= 0.0351

σ_{SE4}:= 0.0368

σ_{SE5}:= 0.0409

σ_{SE6}:= 0.0296

σ_{SE7}:= 0.0337

Then:

$H_{IPT\_LPT} := (H_{10} - H_{SE3})(1 - \sigma_{SE1} - \sigma_{SE2}) + (H_{SE3} - H_{SE4})(1 - \sigma_{SE1} - \sigma_{SE2} - \sigma_{SE3}) + (H_{SE4} - H_{SE5})(1 - \sigma_{SE1} - \sigma_{SE2} - \sigma_{SE3} - \sigma_{SE4}) + (H_{SE5} - H_{SE6})(1 - \sigma_{SE1} - \sigma_{SE2} - \sigma_{SE3} - \sigma_{SE4} - \sigma_{SE5}) + (H_{SE6} - H_{SE7})(1 - \sigma_{SE1} - \sigma_{SE2} - \sigma_{SE3} - \sigma_{SE4} - \sigma_{SE5} - \sigma_{SE6}) + (H_{SE7} - H_2)(1 - \sigma_{SE1} - \sigma_{SE2} - \sigma_{SE3} - \sigma_{SE4} - \sigma_{SE5} - \sigma_{SE6} - \sigma_{SE7}) = 761*10^3$ J/kg

THERMAL EFFICIENCY OF THE CYCLE WITHOUT PUMP WORK:

$H_T := H_{HPT} + H_{IPT\_LPT} = 1127*10^3$ J/kg

$q_0 := H_0 - H_{fw} = 2296*10^3$ J/kg

$\eta_{th} := H_T/q_0 = 0.491$

APPENDIX C. PUBLISHED PAPERS, CONFERENCES ATTENDED AND AWARDS

In total: papers published in refereed proceedings of international/national conferences/symposiums – 7; major technical reports – 1.

Papers published in refereed proceedings of international and national conferences and symposiums

1. Pioro, I., Mokry, S., Gupta, S., Saltanov, Eu., **Dragunov, A.**, Draper, Sh., and Mann, D., 2013. Heat Transfer at Supercritical Pressures in Power-Engineering Applications, Proceedings of the 13th UK Heat Transfer Conference (UKHTC2013), Imperial College London, UK, September 2–3, 8 pages.

2. **Dragunov, A.**, Saltanov, Eu., Pioro, I., and Pioro, I., Ikeda, B., Miletic, M. and Zvorykina, A., 2013. Investigation of Thermophysical and Nuclear Properties of Prospective Coolants for Generation-IV Nuclear Reactors, Proceedings of the 21th International Conference on Nuclear Engineering (ICONE–21), July 29 - August 2, Chengdu, China, Paper #16020, 11 pages.

3. **Dragunov, A.**, Saltanov, Eu., Pioro, I., Harvel, G. and Ikeda, B., 2013. Study on Primary and Secondary Heat-Transport Systems for Sodium-Cooled Fast Reactor, Proceedings of the 21th International Conference on Nuclear Engineering (ICONE–21), July 29 - August 2, Chengdu, China, Paper #16014, 9 pages.

4. Miletić, M., Fukač, R., Pioro, I. and **Dragunov, A.**, 2013. Development of experimental setup of High Temperature Helium Loop and preparation for In-Pile Operation, Proceedings of the 21st International Conference on Nuclear Engineering (ICONE-21), July 29 - August 2, Chengdu, China, Paper #16715, 10 pages.

5. **Dragunov, A.**, Saltanov, E., Higgins, A. and Pioro, I., 2013. Investigation of Various Thermodynamic Cycles for Modern Nuclear Power Plants, Proceedings of the 34th Canadian Nuclear Society (CNS) and 37th Student Conference of the CNS and CNA, Toronto, Canada, June 9-12, 6 pages.

6. **Dragunov, A.**, Bedenko, S. and Pahtousov A., 2012. Investigation of the thermal and hydrodynamic characteristics of steam generator PGV-1000, Proceedings of the annual conference of scientific papers «Knowledge of young nuclear scientists to Nuclear Power Plants", October 26, Moscow, Russia.

7. **Dragunov, A.**, Saltanov, Eu., Bedenko, S. and Pioro, I., 2012. A Feasibility Study on Various Power–Conversion Cycles for a Sodium–Cooled Fast Reactor, Proceedings of the 20th International Conference on Nuclear Engineering (ICONE–20), July 30 – August 3, Anaheim, California, USA, Paper #55130, 9 pages.

Major technical reports

1. Saltanov, Eu., **Dragunov, A.**, Pioro, I. and Lang, P., 2013. Cermet Fuels, Technical Report for FEDDEV Applied Research and Commercialization Initiative "UNITHERM Nuclear Reactor Design and Technology Evaluation Project", Ver. 1, UOIT, Oshawa, ON, Canada, March – April, 20 pages.

Conferences attended with paper presentation:

1. 20th International Conference On Nuclear Engineering (ICONE-20), Anaheim, California, USA, July 30 – August 3, 2012.

2. 34st Canadian Nuclear Society (CNS) and 37th Student Conference of the CNS and CNA, Toronto, Canada, June 9-12, 2013.

3. 21st International Conference On Nuclear Engineering (ICONE-21), Chengdu, China, July 29 – August 2, 2013.

Awards and honors:

1. **Winner** in the ICONE-20 (International Conference On Nuclear Engineering) Student Best Poster Competition for the paper/poster "A Feasibility Study on Various Power–Conversion Cycles for a Sodium–Cooled Fast Reactor".

2. **Winner** in the ICONE-21 Student Best Poster Competition for the paper/poster "Investigation of Thermophysical and Nuclear Properties of Prospective Coolants for Generation-IV Nuclear Reactors".

3. **Winner** in the annual conference of scientific papers «Knowledge of young nuclear scientists to Nuclear Power Plants", with paper "Investigation of the thermal and hydrodynamic characteristics of a steam generator PGV-1000", October 26, 2012, Moscow, Russia.